REPORT DOCUMENTATION PAGE

Form Approved
OMB No 0704-0188

1a REPORT SECURITY CLASSIFICATION
UNCLASSIFIED

1b RESTRICTIVE MARKINGS

2a SECURITY CLASSIFICATION AUTHORITY

2b DECLASSIFICATION / DOWNGRADING SCHEDULE

3 DISTRIBUTION / AVAILABILITY OF REPORT
Approved for public release; distribution unlimited.

4 PERFORMING ORGANIZATION REPORT NUMBER(S)

5 MONITORING ORGANIZATION REPORT NUMBER(S)

6a NAME OF PERFORMING ORGANIZATION
Naval Postgraduate School

6b OFFICE SYMBOL (If applicable)
3A

7a NAME OF MONITORING ORGANIZATION
Naval Postgraduate School

6c. ADDRESS (City, State, and ZIP Code)
Monterey, CA 93943-5000

7b ADDRESS (City, State, and ZIP Code)
Monterey, CA 93943-5000

8a NAME OF FUNDING / SPONSORING ORGANIZATION

8b OFFICE SYMBOL (If applicable)

9 PROCUREMENT INSTRUMENT IDENTIFICATION NUMBER

8c. ADDRESS (City, State, and ZIP Code)

10 SOURCE OF FUNDING NUMBERS

PROGRAM ELEMENT NO	PROJECT NO	TASK NO	WORK UNIT ACCESSION NO

11 TITLE (Include Security Classification)
EFFECTS OF SURFACE-BASED DUCTS ON ELECTROMAGNETIC SYSTEMS

12 PERSONAL AUTHOR(S)
Cairns-McFeeters, Eugenia, L.

13a TYPE OF REPORT
Master's Thesis

13b TIME COVERED
FROM ________ TO ________

14 DATE OF REPORT (Year, Month, Day)
September 1992

15 PAGE COUNT
139

16 SUPPLEMENTARY NOTATION The views expressed in this thesis are those of the author and do not reflect the official policy or position of the Department of Defense or the U.S. Gov't.

17 COSATI CODES

FIELD	GROUP	SUB-GROUP

18 SUBJECT TERMS (Continue on reverse if necessary and identify by block number)

19 ABSTRACT (Continue on reverse if necessary and identify by block number)

A study of the effect the atmosphere has on anomalous propagation is performed on an active radar fire control/guidance system operating around 13 GHZ and a passive Electroni Support Measure (ESM) countermeasure (CM) system designed to detect signals in the 600 MHZ range. Atmospheric conditions for three different areas of the world were examined: the Persian Gulf, the Indian Ocean and the Caribbean. Also demonstrated were the different effects horizontally homogeneous and inhomogeneous atmospheric profiles can have on electromagnetic (EM) systems. A comparison with a standard atmosphere was done for both the radar and the ESM system to illustrate the effect ducting conditions have on extended signal strength.

20 DISTRIBUTION / AVAILABILITY OF ABSTRACT
☐ UNCLASSIFIED/UNLIMITED ☒ SAME AS RPT ☐ DTIC USERS

21 ABSTRACT SECURITY CLASSIFICATION
Unclassified

22a NAME OF RESPONSIBLE INDIVIDUAL
Kenneth L. Davidson

22b TELEPHONE (Include Area Code)
(408) 646-2309

22c OFFICE SYMBOL
MR/DS

T257748

Approved for public release; distribution is unlimited.

Effects of Surface-Based Ducts on Electromagnetic Systems

by

Eugenia L. Cairns-McFeeters
Lieutenant, United States Navy
B.A., University of Mississippi

Submitted in partial fulfillment
of the requirements for the degree of

MASTER OF SCIENCE IN SYSTEMS ENGINEERING
(ELECTRONIC WARFARE)
from the

NAVAL POSTGRADUATE SCHOOL
September 1992

ABSTRACT

A study of the effect the atmosphere has on anomalous propagation is performed on an active radar fire control/guidance system operating around 13 GHZ and a passive Electronic Support Measure (ESM) countermeasure (CM) system designed to detect signals in the 600 MHZ range. Atmospheric conditions for three different areas of the world were examined: the Persian Gulf, the Indian Ocean and the Caribbean. Also demonstrated were the different effects horizontally homogeneous and inhomogeneous atmospheric profiles can have on electromagnetic (EM) systems. A comparison with a standard atmosphere was done for both the radar and the ESM system to illustrate the effect ducting conditions have on extended signal strength.

33

TABLE OF CONTENTS

I. INTRODUCTION 1

II. BACKGROUND 3

A. "GENERIC ESM SYSTEM" (Systems ESM a and ESM b) 6

B. "GENERIC FIRE CONTROL SYSTEM" (System FCS) . . 8

III. ATMOSPHERIC PROPAGATION 11

A. REFRACTIVITY 11

B. DUCTING CONDITIONS 13

1. Formation 13

C. SPECIAL FEATURES OF SURFACE-BASED DUCTS 16

1. Minimum Frequency 16

2. Skip Zones and Coverage 18

IV. EM PROPAGATION MODELS 21

A. INTRODUCTION 21

1. EMPE (Electromagnetic Parabolic Equation) . 21

2. EREPS (Engineer's Refractive Effects Prediction System) 24

V. ASSESSMENT OF HORIZONTALLY HOMOGENEOUS PROFILES . 26

A. INTRODUCTION 26

1. Overview 26

2. Outputs 30

3. System Parameters 32

4. Environments 32

B. CASE STUDIES 33

1. Case 0 - Standard Atmosphere 33

a. Standard Profile 33

b. Case 0 Results 34

(1) Signal Strength Results. 34

2. Case 1 - Persian Gulf 37

a. Abu Dhabi Profile 37

b. Case 1 Results 38

(1) Signal Strength Results. 38

(2) EREPS and EMPE Loss Predictions. . . 45

3. Case 2 - Indian Ocean 52

a. Diego Garcia Profile 52

b. Case 2 Results 53

(1) Signal Strength Results. 53

(2) EREPS and EMPE Loss Predictions. . . 58

4. Case 3 - Caribbean 64

a. Curacao Profile 64

b. Case 3 Results 65

(1) Signal Strength Results. 65

(2) EREPS and EMPE Loss Predictions. . . 71

C. SUMMARY 77

VI. ASSESSMENT OF HORIZONTALLY INHOMOGENEOUS PROFILES 79
  A. INTRODUCTION 79
  B. CASE STUDIES 79
    1. Case 4 - Persian Gulf 87
      a. Persian Gulf Profile 87
      b. Case 4 Results 88
        (1) Signal Strength Results. 88
        (2) EMPE Loss Predictions. 90
    2. Case 5 - Indian Ocean 92
      a. Indian Ocean Profile 92
      b. Case 5 Results 93
        (1) Signal Strength Results. 93
        (2) EMPE Loss Predictions. 96
    3. Case 6 - Caribbean 98
      a. Caribbean Profile 98
      b. Case 6 Results 98
        (1) Signal Strength Results. 98
        (2) EMPE Loss Predictions. 100
  C. SUMMARY 102

VII. SUMMARY 104

APPENDIX A 106
  A. INDEX OF REFRACTION PROPERTIES 107

APPENDIX B 111

APPENDIX C 114
A. RADIOSONDE 114
B. LIDAR (Light Detection and Ranging) 115
C. AMR (Airborne Microwave Refractometer) . . . 117

LIST OF REFERENCES 120

LIST OF TABLES

TABLE I ANTENNA SUMMARY FOR SYSTEM ESM-a, 600 MHZ AT 300 FEET. 7
TABLE II ANTENNA SUMMARY FOR SYSTEM ESM-b, 600 MHZ AT 50 FEET. 8
TABLE III ANTENNA SUMMARY FOR SYSTEM FCS, 13 GHZ AT 60 FEET. 10
TABLE IV MINIMUM DUCT THICKNESS REQUIRED FOR TRAPPING DETERMINED BY RADAR FREQUENCY BAND (From Cook, 1987, p. 9). 18
TABLE V SUMMARY OF HOMOGENEOUS CASES. 33
TABLE VI SUMMARY OF RANGE DEPENDENT CASES. 81

LIST OF FIGURES

Figure 1 Profiles for modified-refractivity-versus-height for (a) an elevated duct; (b) a surface-based duct; and (c) an evaporation duct (From Hitney, 1988, p. 18). 15

Figure 2 Trapping Requirements of Frequency vs. Duct Height (From Hoipkemeier, 1980, p. 52). 17

Figure 3 Illustrations of (a) a EREPS (PROPR) Graph (System ESM-a); (b) a EREPS (PROPR) Graph (System FCS); and (c) a EMPE Transmission Loss Graph (System ESM-b). 29

Figure 4 EMPE Signal Strength Prediction for a Standard Atmosphere for System ESM-a, 600 MHZ at 300 Feet (dB is relative to FS). 31

Figure 5 EMPE Signal Strength Prediction for a Standard Atmosphere for System ESM-b, 600 MHZ At 50 Feet (dB is relative to FS). 35

Figure 6 EMPE Signal Strength Prediction for a Standard Atmosphere for System FCS, 13 GHZ At 60 Feet (100 nmi; dB is relative to FS). 36

Figure 7 EMPE Signal Strength Prediction for a Standard Atmosphere for System FCS, 13 GHZ At 60 Feet (10 nmi; dB is relative to FS). 37

Figure 8 Geographical Locations Of The Persian Gulf Sites. 39

Figure 9 EMPE Signal Strength Prediction for Abu Dhabi, 25 September 1987 (System ESM-a, 600 MHZ At 300 Feet; dB is relative to FS). 40

Figure 10 EMPE Signal Strength Prediction for Abu Dhabi, 25 September 1987 (System ESM-b, 600 MHZ At 50 Feet; dB is relative to FS). 41

Figure 11 EMPE Signal Strength Prediction for Abu Dhabi, 25 September 1987 (System FCS, 13 GHZ At 60 Feet; 100 nmi). dB is relative to FS. 43

Figure 12 EMPE Signal Strength Prediction for Abu Dhabi, 25 September 1987 (System FCS, 13 GHZ At 60 Feet; 10 nmi). dB is relative to FS. 44

Figure 13 EREPS (PROPR) Prediction for Abu Dhabi, 25 September 1987 (System ESM-a operating). 47

Figure 14 EREPS (PROPR) Prediction for Abu Dhabi, 25 September 1987 (System ESM-b operating). 48

Figure 15 EREPS (PROPR) Prediction for Abu Dhabi, 25 September 1987 (System FCS operating). 49

Figure 16 EMPE Transmission Loss Prediction for Abu Dhabi, 25 September 1987 (System ESM-a operating). 50

Figure 17 EMPE Transmission Loss Prediction for Abu Dhabi, 25 September 1987 (System ESM-b operating). 51

Figure 18 EMPE Transmission Loss Prediction for Abu Dhabi, 25 September 1987 (System FCS operating). . 52

Figure 19 Geographical Locations Of The Indian Ocean Sites. 54
Figure 20 EMPE Signal Strength Prediction for Diego Garcia, Spring 1982 (System ESM-a, 600 MHZ At 300 Feet). dB is relative to FS. 55
Figure 21 EMPE Signal Strength Prediction for Diego Garcia, Spring 1982 (System ESM-b, 600 MHZ At 50 Feet). dB is relative to FS. 56
Figure 22 EMPE Signal Strength Prediction for Diego Garcia, Spring 1982 (System FCS, 13 GHZ At 60 Feet; 100 nmi). dB is relative to FS. 57
Figure 23 EMPE Signal Strength Prediction for Diego Garcia, Spring 1982 (System FCS, 13 GHZ At 60 Feet; 10 nmi). dB is relative to FS. 58
Figure 24 EREPS (PROPR) Prediction For Diego Garcia, Spring 1982 (System ESM-a operating). 59
Figure 25 EMPE Transmission Loss Prediction for Diego Garcia, Spring 1982 (System ESM-a operating). . . . 60
Figure 26 EREPS (PROPR) Prediction for Diego Garcia, Spring 1982 (System ESM-b operating). 61
Figure 27 EMPE Transmission Loss Prediction for Diego Garcia, Spring 1982 (System ESM-b operating). . . . 62
Figure 28 EREPS (PROPR) Prediction for Diego Garcia, Spring 1982 (System FCS operating). 63
Figure 29 EMPE Transmission Loss Prediction for Diego Garcia, Spring 1982 (System FCS operating). 64

Figure 30 Geographical Locations Of The Caribbean Sites. 66

Figure 31 EMPE Signal Strength Prediction for Curacao, December 1985 (System ESM-a, 600 MHZ At 300 Feet). dB is relative to FS. 67

Figure 32 EMPE Signal Strength Prediction for Curacao, December 1985 (System ESM-b, 600 MHZ At 50 Feet). dB is relative to FS. 68

Figure 33 EMPE Signal Strength Prediction for Curacao, December 1985 (System FCS, 13 GHZ At 60 Feet; 100 nmi). dB is relative to FS. 69

Figure 34 EMPE Signal Strength Prediction for Curacao, December 1985 (System FCS, 13 GHZ At 60 Feet; 10 nmi). dB is relative to FS. 70

Figure 35 EREPS (PROPR) Prediction for Curacao, December 1985 (System ESM-a operating). 72

Figure 36 EMPE Transmission Loss Prediction for Curacao, December 1985 (System ESM-a operating). 73

Figure 37 EREPS (PROPR) Prediction for Curacao, December 1985 (System ESM-b operating). 74

Figure 38 EMPE Transmission Loss Prediction for Curacao, December 1985 (System ESM-b operating). 75

Figure 39 EREPS (PROPR) Prediction for Curacao, December 1985 (System FCS operating). 76

Figure 40 EMPE Transmission Loss Prediction for Curacao, December 1985 (System FCS operating). 77

Figure 41 Refractivity Profile For Abu Dhabi. 82

Figure 42 Refractivity Profile For Bandar Abbas. . . . 83

Figure 43 Refractivity Profile Of Diego Garcia. . . . 84

Figure 44 Refractivity Profile Of Bangkok. 85

Figure 45 Refractivity Profile Of Curacao. 86

Figure 46 Refractivity Profile Of Puerto Rico. 87

Figure 47 EMPE Signal Strength Prediction For The Persian Gulf (System ESM-a, 600 MHZ At 300 Feet), dB is relative to FS. 89

Figure 48 EMPE Signal Strength Prediction For The Persian Gulf (System ESM-b, 600 MHZ At 50 Feet), dB is relative to FS. 90

Figure 49 EMPE Transmission Loss Prediction For The Persian Gulf (System ESM-a operating). 91

Figure 50 EMPE Transmission Loss Prediction For The Persian Gulf (System ESM-b operating). 92

Figure 51 EMPE Signal Strength Prediction For The Indian Ocean (System ESM-a, 600 MHZ At 300 Feet), dB is relative to FS. 94

Figure 52 EMPE Signal Strength Prediction For The Indian Ocean (System ESM-b, 600 MHZ At 50 Feet), dB is relative to FS. 95

Figure 53 EMPE Transmission Loss Prediction For The Indian Ocean (System ESM-a operating). 96

Figure 54 EMPE Transmission Loss Prediciton For The Indian Ocean (System ESM-b operating). 97

Figure 55 EMPE Signal Strength Prediction For The Caribbean (System ESM-a, 600 MHZ At 300 Feet), dB is relative to FS. 99

Figure 56 EMPE Signal Strength Prediction For The Caribbean (System ESM-b, 600 MHZ At 50 Feet), dB is relative to FS. 100

Figure 57 EMPE Transmission Loss Prediction For The Caribbean (System ESM-a operating). 101

Figure 58 EMPE Transmission Loss Prediction For The Caribbean (System ESM-b operating). 102

Figure 59 Atmospheric Refraction Based on M Scaling Representation (From Hoipkemeier, 1980, p. 23). . 113

ACKNOWLEDGMENT

I would like to extend my grateful appreciation to Professor Kenneth L. Davidson and Mr. Michael Pastore, from the Naval Research Laboratory Tactical Oceanography Department, for their direction and help in the preparation of my thesis. Also, to Dr. Harvey Ko and his superb staff at the Johns Hopkins University Applied Physics Laboratory, I would like to extend a very heartfelt thank you for all their outstanding support and understanding while I was on my experience tour.

In closing, I would like to also thank my family: my mother and father, for all their support through the years, and especially to my husband, Glen, for his patience and support while I was at the Naval Postgraduate School.

I. INTRODUCTION

The purpose of this thesis is to evaluate the potential impact that the earth's atmosphere has on two specific Navy tactical EM systems. An active "generic" radar fire control/guidance system and a tactical ESM/CM system will be evaluated for various worldwide operational ocean areas. This evaluation will consider the atmosphere's influence through the use of two advanced EM propagation assessment models. A recently formulated parabolic equation EM propagation model and a standard engineering EM propagation model will be used to evaluate the impact of several operational environments on these two tactical EM systems.

This thesis will review EM propagation through the atmosphere, discuss environmental factors affecting it, and describe the existing models being used to determine atmospheric effects on these two operational EM systems. A background on atmospheric measuring devices will be provided, as well as details on propagation models that are available. Atmospheric measuring devices are necessary for defining vertical variations (known as profiles) with respect to temperature and humidity at operational locations and times of interest.

The profiles used vary according to the horizontal variation; consisting of homogeneous and inhomogeneous profiles. The areas examined are the Persian Gulf, Indian Ocean, and the Caribbean. For the inhomogeneous profiles, two sites were required for each area. All data were obtained from reports available at the Johns Hopkins University Applied Physics Laboratory (JHU/APL) giving representative radiosonde profiles for different areas of the world.

II. BACKGROUND

Electronic Warfare (EW) plays an important role in the overall scheme of military strategy. A role of EW is to be able to exploit EM emissions from a hostile source, and turn that information into intelligence on an adversary's order of battle, intentions, and capabilities and to render communications and weapons systems useless, while protecting own system through CM. Three major divisions that make up EW are: Electronic Support Measures (ESM), Electronic Countermeasures (ECM), and Electronic CounterCountermeasures (ECCM).

Anomalous propagation caused by ducting over the ocean can extend Radio Frequency (RF) detection ranges well beyond the visible horizon about 30% of the time (Wiseman, 1986, p. 355); however, anomalous propagation exists 95% of the time in some areas of the world (Ko et al, 1987, p. 394). With this high percentage of occurence, it can be noted that anomalous in this case is not synomonous with infrequent or rare. For strong enough gradients of the index of refraction, n, rays can often have the same curvature as the earth, making it very possible for rays that are horizontal initially, to follow the surface for some distance. Understanding this phenomena enables those in EW to take advantage of the environment to its full extent.

Since the U. S. Navy frequently operates in areas where anomalous propagations are known to occur, tactical commanders that can accurately predict and exploit the ducts that cause anomalous RF propagation, possess an effective tool to establish a tactical advantage. On the other hand, battle group management must also pay particularly close attention to regions of reduced coverage called radar holes, high propagation loss areas. These radar holes may develop when a shipboard radar transmitter is near or below the height of the Evaporation Duct (ED), or within a Surface-based Duct (SBD), and when a widebeam transmission is used (Geernaert, 1989, p. 3). This will enable hostile, low-flying missiles or aircraft to go undetected. Height errors are also present during ducting conditions; this will cause a radar system to indicate a threat is located at a different position of height. With the future giving way to the use of remotely sensed information that can calculate the height of the ED, smart systems that will be incorporated into aircraft or missiles can be integrated into operational planning for the battle group. Therefore, defensive targeting actions must be prioritized for certain elevation angles and equipment operating modes making it most likely to detect any threat intrusion.

It is important to note that extended range is not the only effect experienced. Due to the reciprocal path, there is an enhancement of sea clutter and noise in a ducting environment, that when received, can severely degrade overall performance of a surveillance system.

This thesis will present information on a "generic" passive ESM system that acquires signals in the UHF range (300 - 1000 MHZ), and a "generic" fire control system, operating in the KU band (12 - 18 GHZ), along with the effects of these systems when subjected to operating under ducting conditions. Two EM propagation algorithms were used to describe effects on these systems from ducting; the propagation loss subprogram (PROPR) of EREPS (Engineer's Refractive Effects Prediction System) and EMPE (Electromagnetic Parabolic Equation).

The EREPS (PROPR) portion was used to assess the performance of these systems under specified ducting conditions, identifying values of propagation loss versus range for the transmitting systems (used to measure performance of the ESM system) and the fire control system. EMPE was used to illustrate specific values everywhere for propagation loss, to display the peculiar downrange behavior for horizontally inhomogeneous environments, to show how excessive energy can be diverted away from normal coverage areas and lead to coverage holes and/or enhanced clutter, and to analyze situations with antennas in or far away from anomalous refractive layers. Both horizontally homogeneous and inhomogeneous environments were considered.

A. "GENERIC ESM SYSTEM" (Systems ESM a and ESM b)

The ability to search, intercept, locate, and identify sources of EM radiation are the functions of ESM receivers. ESM is used as a means to provide the earliest warning of enemy presence.

ESM receivers designed to exploit communication systems must have wide dynamic ranges and be able to operate in a dense, overlapping signal environment. Since the operating environment is predicted to become even denser, ESM receivers suitable for electronic intelligence gathering (ELINT) will have difficulty handling the processing task. Since communication systems tend to operate on discrete channels, are quite powerful, use widebeam antennas, and employ modulated continuous wave transmissions, direction finding (DF) is a valuable asset for sorting and locating communication emitters. (Schleher, 1986, p. 46)

This thesis considers a passive ESM system that exhibits a 360 degree coverage angle, i.e., an omni antenna; is able to acquire and DF threat signals in the 600 MHZ range with a vertical polarization, a power of 100 W, an antenna vertical beamwidth of 4 degrees and a beam elevation of 1 degree. No vertical gain over sky noise was considered. Receiver sensitivity was chosen as -100 dBm. For graphical purposes, a maximum range of 250 nmi was used, with a height of 1000 feet. The transmitting systems were placed 300 feet above mean sea level (amsl) for system ESM-a, and 50 feet amsl for system ESM-b. It is noted that systems ESM-a and ESM-b are really two different threat transmitters subject to detection by the passive ESM system. The antenna parameters for both transmitting systems are outlined in Tables I and II.

TABLE I ANTENNA SUMMARY FOR SYSTEM ESM-a, 600 MHZ AT 300 FEET.

Frequency in MHz	600.0000
Height of antenna in feet	300.
Power of antenna (in KW)	0.100
Antenna polarization	VERTICAL
Antenna vertical beamwidth	4.00
Beam elevation angle	1.00

TABLE II ANTENNA SUMMARY FOR SYSTEM ESM-b, 600 MHZ AT 50 FEET.

Frequency in MHz	600.0000
Height of antenna in feet	50.
Power of antenna (in KW)	0.100
Antenna polarization	VERTICAL
Antenna vertical beamwidth	4.00
Beam elevation angle	1.00

B. "GENERIC FIRE CONTROL SYSTEM" (System FCS)

Naval gunnery positions are classified according to the intentions for which they were developed, i.e., for long-range low-angle firing against surface targets or low-flying aircraft, for high-flying aircraft, or for close range defense (Bowen, 1954, p. 530); the latter will be the type represented in this thesis.

The close-range weapon system in this thesis is an autonomous system whose purpose is to provide a last-effort self-defense against incoming anti-ship missiles (ASM), cruise missiles, dive bombers, torpedo-carriers, etc., at a range within 10 nmi. The frequency of this system was chosen as 13 GHZ. It employs a single transmitter, but has separate search and tracking radars for target detection. This is referred to as monopulse radar, but only applies to the track mode operation in this case. The search radar actively seeks targets with an elevation between 0 and 5 degrees, through a 360 degree azimuth coverage. Detection of a target requires its range, range rate, height, and bearing. If the target is determined to be a threat, and meets the preset sector and range rate criteria, it is attacked. The search radar ceases operation and the tracking radar is initiated when the target is declared a threat. A weapons control group is provided with target range and range rate information by the radar. Once the target enters the computed engagement zone, commencement of firing is ordered. When the target is destroyed, firing ceases, and the search mode is activated.

The system considered in this thesis has a vertical polarization, an average power of 850 W, an antenna vertical beamwidth of 4 degrees with a 0 degree beam elevation (horizontal beamwidth was not considered). A maximum range of 100 nmi was used to display the system's vulnerability to ESM detection in the various ducting environments. A maximum height of 1000 feet was used in the graphs for consistency. The transmitter was placed at 60 feet amsl (system FCS). The antenna parameters for the system are outlined in Table III.

TABLE III ANTENNA SUMMARY FOR SYSTEM FCS, 13 GHZ AT 60 FEET.

Frequency in MHz	13000.0000
Height of antenna in feet	60.
Power of antenna (in KW)	0.850
Antenna polarization	VERTICAL
Antenna vertical beamwidth	4.00
Beam elevation angle	0.00

III. ATMOSPHERIC PROPAGATION

A. REFRACTIVITY

Refraction occurs due to variations in the speed along the wave front as determined by the index of refraction, n. In the atmosphere $n = \sqrt{\epsilon_r}$, where ϵ_r is the dielectric constant for the medium. A EM wave incident upon two adjacent media having different indices of refraction will be bent or refracted. This should not be confused with the bending of waves around a solid object in its path, referred to as diffraction. EM waves will be bent towards the higher n media, described by Snell's Law:

$$n1 \text{ Sin } \theta_1 = n2 \text{ Sin } \theta_2 \tag{1}$$

where n1 and n2 are different indices of refraction, and θ_1 and θ_2 are different angles of incidence.

The atmosphere is horizontally homogeneous more often than vertically homogeneous with respect to specific range intervals. With these vertical changes, boundaries of gradient refractivity are defined and this is important in meteorological measurements. Temperature, humidity, and pressure are responsible for changes in the dielectric properties of the atmosphere. Since it is defined by density, pressure decreases with height, z. The radar/radio refractive index, n, varies between 1.000250 and 1.000400, in terms of refractivity, or N, it is defined as:

$$N=(n-1)10^6 \qquad \textbf{(2)}$$

Normal surface values of N range from 250 to 400. Radar/radio wave refractivity is expressed as a function of pressure of the atmosphere, temperature of the air, and humidity, given as follows:

$$N=\frac{(77.6P)}{T}+\frac{(3.73\times10^5 e)}{T^2} \qquad \textbf{(3)}$$

where

P = Barometric pressure, mb

e = Water vapor pressure, mb

T = Absolute temperature, K.

Refractivity influences can be better described by the gradient dN/dz; where z is height. Normal refraction decreases with altitude. With this gradient, the ray path is bent downward at a rate less than the curvature of the earth. In a standard atmosphere, the decrease with height is 39 N/km.

Anomalous situations occur when refractivity decreases significantly with height. A modified refractive index, M, is more commonly used to identify this case, and is defined as M = N + 157 z; z is the height above the earth in km and N is the refractivity at that height. M increases with height under standard conditions. For a ray to follow the earth's surface, dN/dz = -157 or dM/dz = 0.

Whenever a decrease in M with height occurs, a trapping layer forms where the EM wave can be refracted back towards the earth's surface to form a duct. Since trapping exists for negative gradients of M, trapping layers are easily identified using M refractivity units.

B. DUCTING CONDITIONS

1. Formation

A trapping layer must exist for a duct to occur, although a ducting region can go beyond a trapping layer. Existence of trapping is determined by a temperature increase and/or a decrease in humidity with height, as described by Equation 3. The following cases can result in the formation of trapping layers/ducts (Sakkas, 1984, pp. 24-25):

- A temperature inversion at the ground, that often is responsible for producing abnormal propagation, results from the nocturnal radiation which occurs on clear summer nights.
- Strong ducts will be formed when warm, dry air moves over a mass of cooler water, causing the air to be cooled near the sea, and moisture to be added simultaneously.
- Ducts will be present in the area of a thunderstorm, because of the existence of a temperature inversion, which occurs when cool air spreads out from the base of a storm in the lowest few thousand feet. The duct will last under this condition for only 30 minutes to one hour.
- Subsidence (a descent in the motion of air in the atmosphere) inversion can lead to development of a duct; particularly when moist air near the ground is present.

The locations and strengths of trapping layers can lead to three types of ducts: elevated, surface-based, and evaporation. Figure 1a represents an elevated duct that is formed when a trapping layer associated with the transition between a lower cool, moist air mass and an upper warm, dry air mass. These ducts occur more than 50% of the time in certain parts of the world (Hitney, 1988, p. 3). Figure 1b illustrates a surface-based duct. Created in the same way as elevated ducts, but with the difference being a vertical dimension that extends to the surface. Occurring 8% of the time throughout the world, they vary from place to place, 1% of the time they are present in the North Atlantic, and exist in the Persian Gulf 46% of the time (Hitney, 1988, p. 3). These ducts are responsible for increasing surface radar ranges at all radar bands when the radar and target are operating in or near the duct. An average thickness of 85m is common for surface-based ducts throughout the world; however, thickness as much as a few hundred meters are not unusual.

An evaporation duct, shown in Figure 1c, is formed by the rapid decrease of moisture right above the sea surface. Evaporation ducts are thinner and weaker as compared to surface-based ducts and will generally affect frequencies above the UHF range. These ducts have an average height of 13m worldwide; hardly ever exceeding 40m (Hitney, 1988, p.4). This type of duct has its greatest effect on frequencies above 3 GHZ.

The evaporation duct is very similar to a surface duct in that it is developed due to an extremely rapid decrease of moisture, water vapor, or humidity immediately near the sea surface.

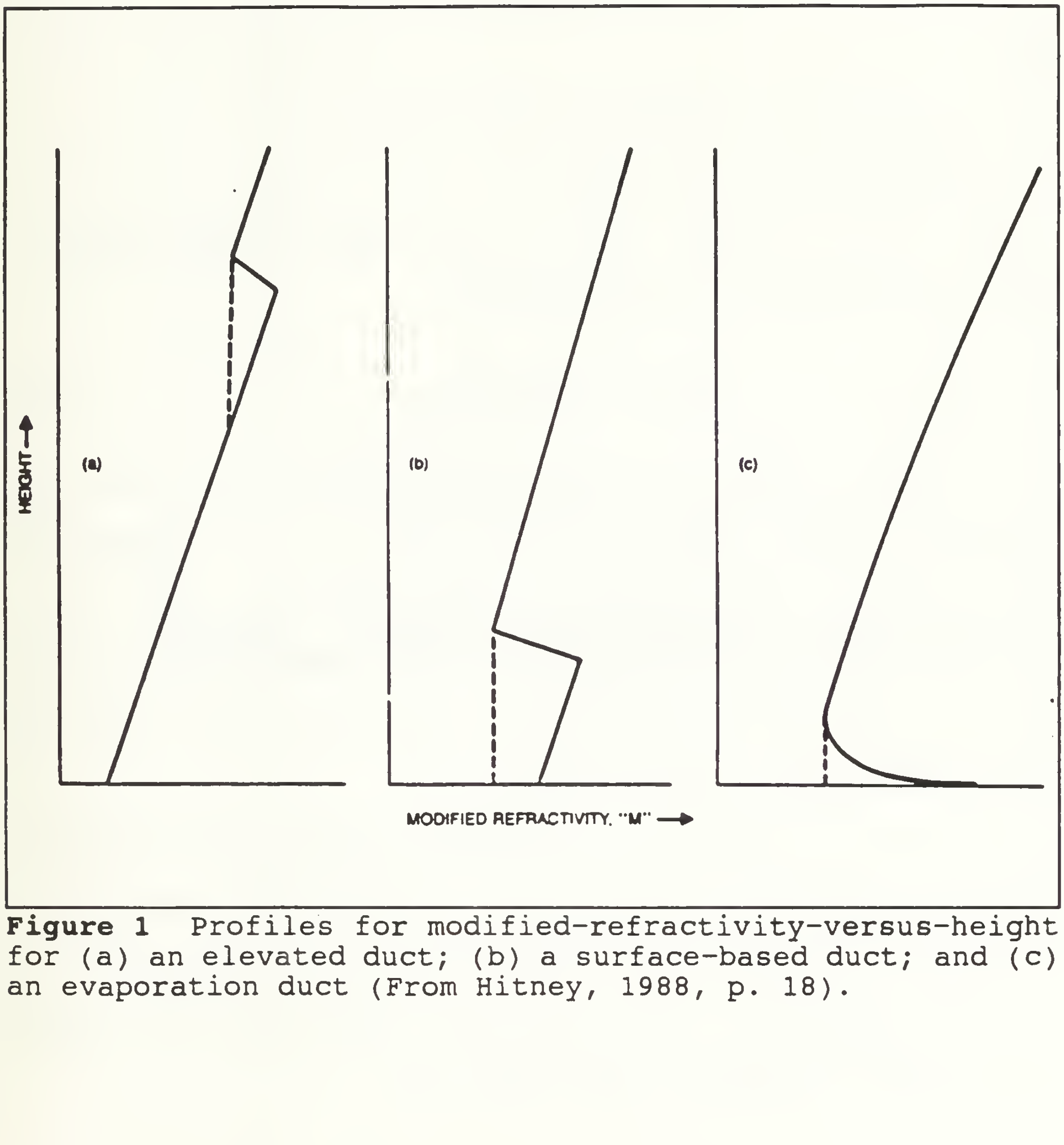

Figure 1 Profiles for modified-refractivity-versus-height for (a) an elevated duct; (b) a surface-based duct; and (c) an evaporation duct (From Hitney, 1988, p. 18).

C. SPECIAL FEATURES OF SURFACE-BASED DUCTS

1. Minimum Frequency

The minimum frequency, f(min), of EM energy that will become trapped in a surface-based duct is approximated as:

$$f(\mathrm{min}) = 3.6033\times10^{11} d^{-3/2} \tag{4}$$

where

f(min) = operating frequency in HZ, and

d = thickness of duct in meters.

A critical duct height required to significantly affect a certain frequency is represented as:

$$h(m) = \left(\frac{3.603\times10^{11}}{f}\right)^{-2/3} \tag{5}$$

The calculation of f(min) does not indicate a cut-off frequency, because this "cut-off effect" in duct propagation occurs over a wide frequency range and not just at a particular frequency. Frequencies that are higher than f(min) will be guided; while frequencies less than this value will still be affected, but not as much.

Due to the duct's thickness impacting the range of frequencies that will get trapped, extended range propagation will normally be expected at higher microwave frequencies than at lower frequencies, since ducting layers are not usually thick (refer to Figure 2 and Table IV).

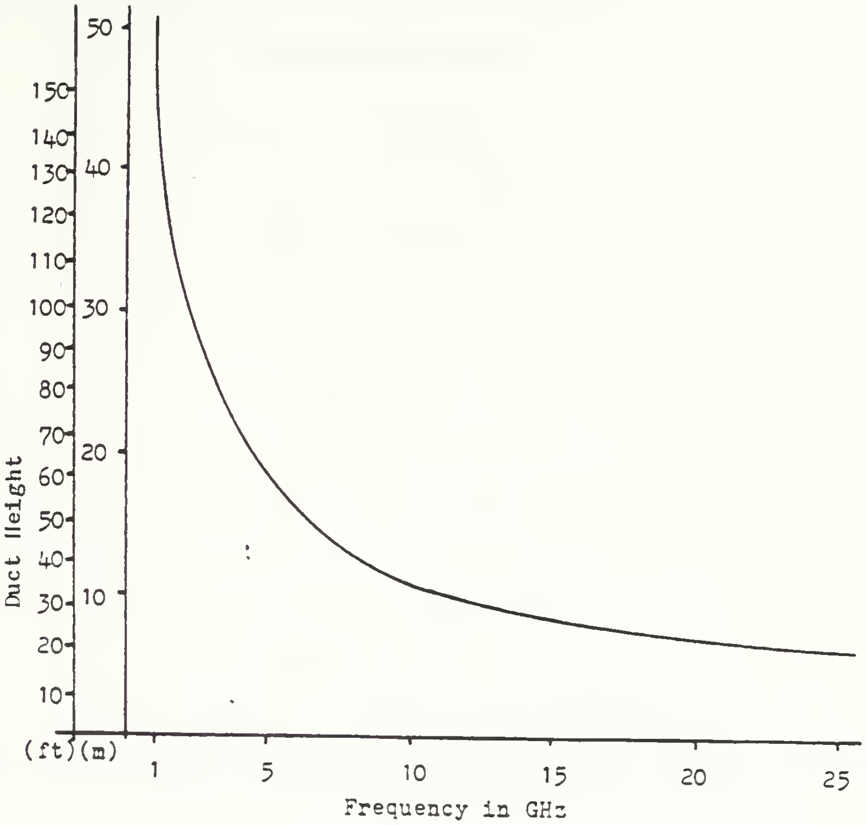

Figure 2 Trapping Requirements of Frequency vs. Duct Height (From Hoipkemeier, 1980, p. 52).

TABLE IV MINIMUM DUCT THICKNESS REQUIRED FOR TRAPPING DETERMINED BY RADAR FREQUENCY BAND (From Cook, 1987, p. 9).

BAND	FREQUENCY RANGE	DUCT THICKNESS (m)
VHF	30 MHZ - 300 MHZ	610 - 122
UHF	300 MHZ - 1 GHZ	122 - 52
L	1 GHZ - 2 GHZ	52 - 32
S	2 GHZ - 4 GHZ	32 - 20
C	4 GHZ - 8 GHZ	20 - 12
X	8 GHZ - 12 GHZ	12 - 9
K	12 GHZ - 40 GHZ	9 - 4

2. Skip Zones and Coverage

A surface-based duct will have no influence on propagating waves when a "skip zone", which is present near the normal horizon, occurs. The occurrence of these "skip zones" is dependent upon the deficit of M, or ΔM. Therefore, energy gets trapped in the duct for long ranges, but tends to skip over shorter ranges; this is why a minimum range exists for a surface-based duct enhancement (Hitney, 1988, p.4).

A ducting condition "forces" a two dimensional, cylindrical wave to propagate, rather than a three dimensional, spherical wave propagation that exists in free space. Power density spreading is the result of the inverse first power of the range (1/R) vice ($1/R^2$). The receiving energy for two way propagation under conditions of ducting will be proportional to ($1/R^2$) instead of ($1/R^4$) as is the case in free space. The extension of the radar range experienced within the duct occurs because of the refraction of energy, causing it to be directed into the ducting layer. A reduction of coverage in other directions is experienced by the propagation of less energy, leading to "holes" or poor areas of detection outside of the duct. For example, a radar range will be extended by the duct for surface targets, but targets just above the duct would be missed, that otherwise might have been detected. In addition, a target may be detected by a ray that has been diverted from its intended path; the target would appear to be along the originally intended direction, as indicated by the radar system, but at a different height. This height difference is known as "Height Error." It can be concluded that evaporation or surface ducts are better for detecting surface or sea skimming targets and are not useful for detecting targets with angles of elevation larger than 1 degree. This supports the statement that rays extending out nearly parallel to the duct will become trapped. (Marom, 1988, p. 66)

IV. EM PROPAGATION MODELS

A. INTRODUCTION

Several methods exist to aid in the detection of refractive profiles, these are described in Appendix C. An important fact to keep in mind is knowing that a duct exists, and what effect it will have on operational EM systems. Of considerable interest are computer models that can display a prediction of expected coverage, by combining antenna parameters and system characteristics with the atmospheric conditions. Such systems are covered below.

1. EMPE (Electromagnetic Parabolic Equation)

EMPE is a EM wave propagation code that uses a physical optics code (PCEMPE User's Manual, 1991). It was first developed from an acoustic program by the Johns Hopkins University Applied Physics Laboratory's (APL) Submarine Technology Department's personnel. The mathematical approach for EMPE has been described by Sari et al (1986, p. 356). The EMPE code calculates EM wave propagation loss through a variety of atmospheric-duct type environments and is considered to be the best propagation model for predicting the performance of EM systems (Hitney, 1988, p.6).

EMPE has provided a means to accurately predict the EM energy distribution in the lower atmosphere in any type of refractive environment where other propagation models usually have problems.

EMPE has the ability to calculate the effects of propagation from near-zero ranges through the optical interference region, and can transition into the region extending beyond the horizon, where the effects of ducting are more defined. As with EREPS, balloon-borne radiosondes, or the Airborne Microwave Refractometer (AMR, see Appendix C) measurements of the atmosphere are inputs for the EMPE program. EMPE outputs take into account refractivity estimates and predict for a given antenna configuration, expected propagation loss as a function of height and range.

In 1946, Fock and Leontovich used the "parabolic approximation" to describe tropospheric propagation in a vertically inhomogeneous, horizontally homogeneous atmosphere over a spherical earth (Ko et al, 1988, p. 90). The vector wave equation used in describing propagation over a spherical earth can be reduced to a scalar parabolic equation through many approximations that have backscattered field neglect and limit the refractive gradients' size that can be modeled (Dockery, 1987, p. 405).

Antenna coverage pattern capability is predicted with the use of APL's EMPE code. A physical optics solution for the atmosphere propagation loss characterized by changes in the inhomogeneous refractive index, including diffraction and atmospheric absorption effects, is provided by EMPE.

Refractive gradients that are range-dependent are computed from the temperature, pressure, and humidity, and used with EMPE to predict the expected loss in propagation, or radiation patterns to also include coverage voids and clutter areas, as a function of height, range, time of day, and for a given antenna configuration. This can be helpful in attempting to predict how often and under what type of conditions anomalous propagation can be experienced at a certain antenna site. (Schemm et al, 1987, p. 394)

EMPE can provide solutions for horizontally inhomogeneous and vertically complex atmospheres. The advantages EMPE has over other models are its efficiency and ability to handle complex, changing atmospheric-refractive environments, plus its physical optics solution that can take arbitrary horizontal and vertical variations in refractivity, and can compute rather rapidly for all modes. A 386-33 MHZ personal computer (PC) system was used for the calculations involved. Average computing times for systems ESM-a and ESM-b were approximately one half hour; for system FCS the computing times were approximately one hour.

Limitations of EMPE are, (PCEMPE User's Manual, 1991):

- It assumes a smooth earth.
- Only one-way calculations are performed (from the transmitting source to the target).
- A sinx/x beam is generated with the main lobe having an azimuth angle equal to the elevation angle.

- A four profile limitation is mandated in a horizontally inhomogeneous atmosphere.

Currently, EMPE is able to provide great insights for the behavior of EM systems under anomalous propagation conditions. Results from the outputs can be used to illustrate numerous problems which impact technical design, tactical planning, and operational procedures.

2. EREPS (Engineer's Refractive Effects Prediction System)

EREPS was used in this thesis to represent, on a single display, signal loss relative to Free Space, to a standard environment. This system is a path-loss-versus-range model developed by the Naval Ocean Systems Center (NOSC).

It is designed to assist various engineering efforts, and takes into account the interference region, diffraction, tropospheric scatter, surface-based ducts, evaporation ducts, and water vapor aborption over a 100 MHZ to 20 GHZ frequency range. Hitney 1988 describes EREPS limitations, i.e., EREPS does not take into account the ducting effects in the optical interference region. A surface-based duct model that reveals the skip zone phenomenon well and also provides approximate path-loss values for ranges well beyond the horizon, is contained in EREPS (Hitney, 1988, p. 8). Even with some limitations, an assessment of the lower atmosphere on radar, EW, or communication systems can be done with EREPS.

EREPS uses atmospheric parameters obtained by radiosondes and the AMR to calculate propagation conditions. It consists of three parts: 1) PROPR, used to generate a plot of path loss, propagation factor, or a radar Signal to Noise ratio (SNR); 2) Surface Duct Summary (SDS), a duct occurrence statistics, in which displayed is an annual historical summary of evaporation ducts, surface-based ducts, and other meteorological parameters for 10 by 10 degree squares of the earth's surface; and 3) RAYS, a ray trace program that displays altitude versus range trajectories for a series of rays for any refractive index profile.

Limitations of EREPS are, (EREPS User's Manual, 1988):

- It assumes a smooth earth for height gain profiles.
- It is limited to frequencies between 100 MHZ and 20 GHZ.
- It assumes horizontal homogeneity.
- It uses small angle assumptions.
- Limitations exist with certain duct height and frequency combinations; the ducting model of EREPS works well if only one mode dominates.
- While operating the subprogram PROPR, the placement of the transmitting antenna was limited to a height of 300 feet.

V. ASSESSMENT OF HORIZONTALLY HOMOGENEOUS PROFILES

A. INTRODUCTION

1. Overview

Results of the propagation prediction models for a horizontally homogeneous atmosphere are presented in this chapter. These will be for two different EM systems. As described previously 1) a short range fire control radar (system FCS), and 2) an emitter placed at two different heights (systems ESM-a and ESM-b) to determine the performance of the passive ESM system.

The use of EREPS (PROPR) provided the propagation loss in dB versus range and gives a comparison of a Free Space environment and a standard environment (no ducting) with that of a specified ducting environment. It can be used for determining the maximum detection, communication, or intercept ranges by using thresholds.

The EREPS (PROPR) graphs illustrate how a ducting environment allows for enhanced system performance over a standard environmental condition. In many cases, the ducting environment had better affects on system performance than the free space environment. Values for the environmental parameters entered into the EREPS (PROPR) subprogram were obtained from EREPS (SDS); for the Persian Gulf, a ducting profile from two sites averaged together into one profile was used to represent the area; the site of Diego Garcia was used to represent the Indian Ocean; and the site of Curacao was used for the Caribbean.

For the ESM system, (systems ESM-a and ESM-b) threshold losses (T) is referred; therefore, path losses less than this threshold represent an intercept capability, as displayed in Figure 3a. The equation used to calculate the threshold value is given as follows:

$$T=10Log_{10}(P)+60+G-S-L \tag{6}$$

where

P = transmitter power in Watts,

G = antenna gain in dB,

S = receiver sensitivity in dBm, and

L = system losses in dB.

For the cases represented in this thesis, P = .1 KW, G = 32 dB, S = -100 dBm, and L = 0 dB, giving a threshold value of 182 dB.

The free space (FS) path loss for the radar (system FCS) is given as $L_{fs} = (4\pi r)^2/\lambda^2$; where r (FS range) and λ are both in meters. For the graphs displayed in this thesis, λ = .023 m and r = 1.2×10^4 m, resulting in a L_{fs} value of 136 dB (refer to Figure 3b).

EMPE will display any effects of leakage, interference, and diffraction of active systems. An EMPE plot for a standard atmospheric condition was done for both systems for a comparison against the ducting environments.

EMPE's Transmission Loss plots, i.e., like the one in Figure 3c, illustrate how the transmission loss varies with range by slicing across a field strength plot for a constant height. For systems ESM-a and ESM-b, a constant height of 165 feet (EMPE defaulted to a value of 166.3 feet) was chosen to represent the ESM receiver. For system FCS, a constant height of 50 feet was chosen.

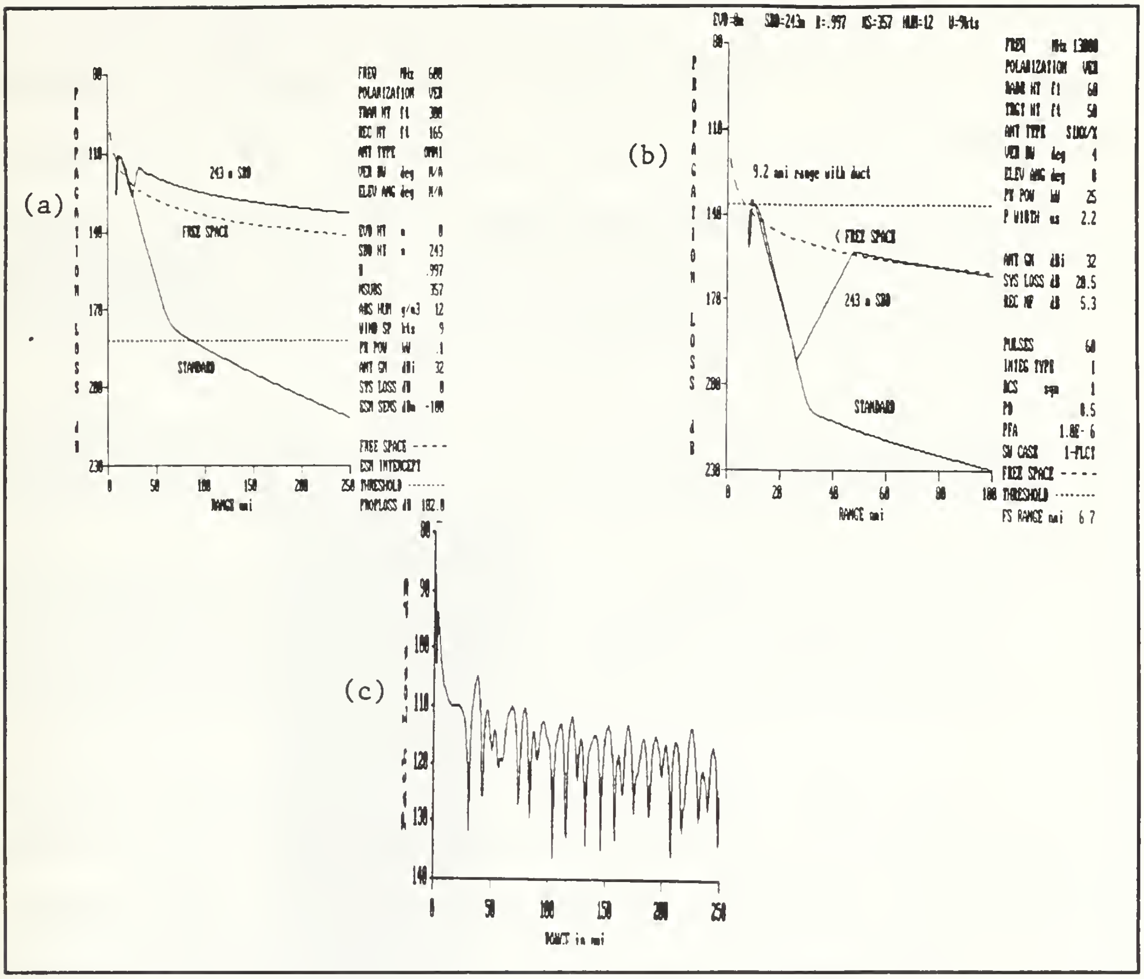

Figure 3 Illustrations of (a) a EREPS (PROPR) Graph (System ESM-a); (b) a EREPS (PROPR) Graph (System FCS); and (c) a EMPE Transmission Loss Graph (System ESM-b).

2. Outputs

Three propagation regions that are shown in all PROPR displays are:

- Optical interference region (< 10 nmi), which is characterized by path loss values that oscillate around the free space level (the number of nulls used was 1); the behavior corresponding to coherent interference of the direct and sea reflected waves.
- Diffraction region (10 - 30 nmi), where the path loss increases much faster than the free space reference due to diffraction (the process in which waves propagate around the earth's curved surface).
- Troposcatter region (> 30 nmi), where ranges greater than 30 nmi causes the path loss to fall at a lesser rate due to tropospheric scatter, where the process results from multiple patches of refractive inhomogeneities scattering.

Although troposcatter is not usually an important consideration for radar applications, it can be the dominant propagation mechanism for communications or ESM systems.

The EMPE signal strength prediction is displayed on the computer screen in color; according to dB loss relative to Free Space (dB rel to FS). However, the hardcopy for EMPE is provided as different greyscale shades, with some of the dB blocks being cross-hatched. The lowest dB loss (-10 dB) is located near the transmitter location and is in the main beam area; some higher losses are shown to be at farther distances, and outside the duct. A comparison of loss in dB of what a system would encounter in free space to that of a ducting environment appears in the dB blocks at the bottom of the EMPE greyscale displays. Losses ranging from -10 to 30 dB, in increments of 10, are used in this comparison. Figure 4 is such an illustration for a standard atmospheric condition for system ESM-a.

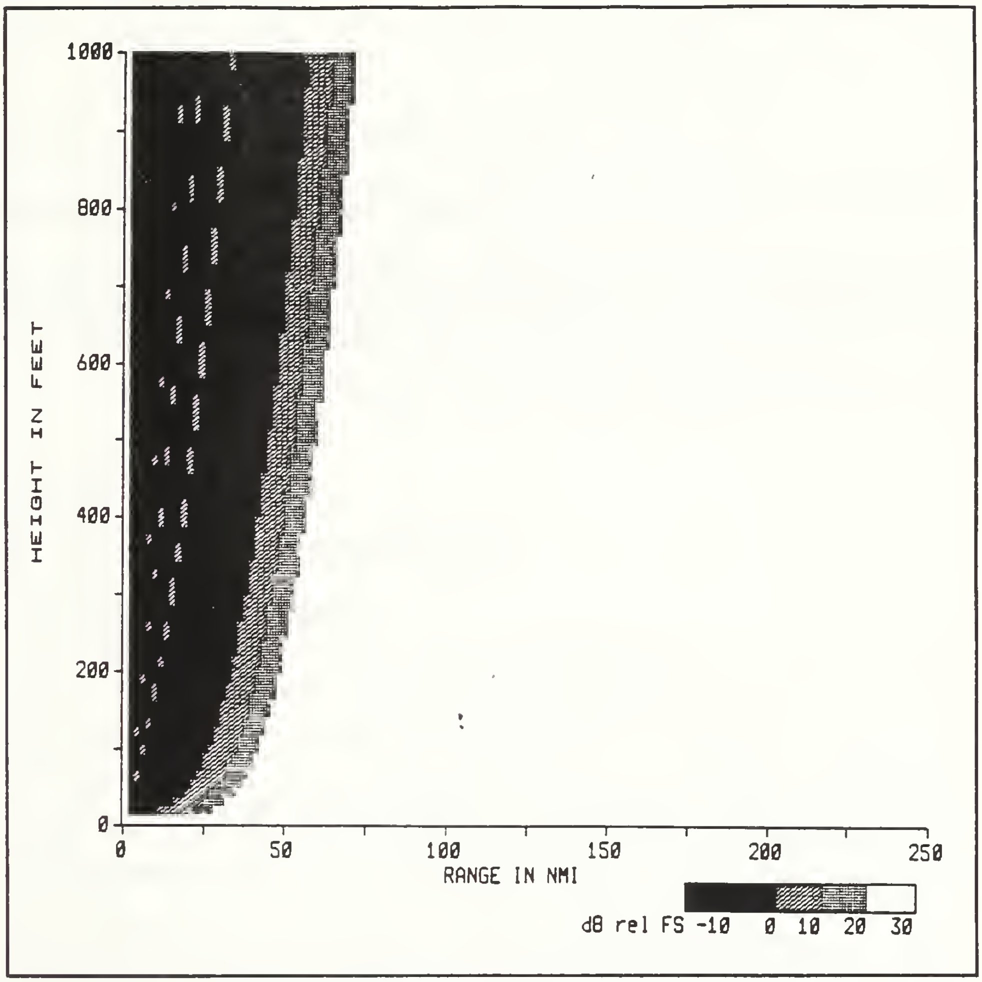

Figure 4 EMPE Signal Strength Prediction for a Standard Atmosphere for System ESM-a, 600 MHZ at 300 Feet (dB is relative to FS).

3. System Parameters

For the radar fire control system (system FCS), a frequency of 13 GHZ was used with a sinx/x antenna type. The antenna was at a height of 60 feet amsl. For the passive ESM system, a frequency of 600 MHZ was used with an omni directional antenna; with transmitting sources placed at heights of 300 feet amsl (system ESM-a) and 50 feet amsl (system ESM-b).

4. Environments

The case summary table, Table V, is provided for all the environments evaluated. The areas were selected in order to display both horizontally homogeneous and inhomogeneous environmental profiles. Refractivity profiles for each of the sites are presented in the next chapter.

TABLE V SUMMARY OF HOMOGENEOUS CASES.

CASE	PROFILE	SYSTEM	TRANSMITTER HEIGHT	TRANSMITTER POWER	FREQUENCY	FIGURE
0-0	STANDARD	ESM-a	300 ft	0.1 KW	600 MHZ	4
0-1	STANDARD	ESM-b	50 ft	0.1 KW	600 MHZ	5
0-2	STANDARD	FCS	60 ft	25 KW	13000 MHZ	6 & 7
1A	A/9/25/87	ESM-a	300 ft	0.1 KW	600 MHZ	9
1B	A/9/25/87	ESM-b	50 ft	0.1 KW	600 MHZ	10
1C	A/9/25/87	FCS	60 ft	25 KW	13000 MHZ	11 & 12
2A	D/SPR/82	ESM-a	300 ft	0.1 KW	600 MHZ	20
2B	D/SPR/82	ESM-b	50 ft	0.1 KW	600 MHZ	21
2C	D/SPR/82	FCS	60 ft	25 KW	13000 MHZ	22 & 23
3A	C/DEC/85	ESM-a	300 ft	0.1 KW	600 MHZ	31
3B	C/DEC/85	ESM-b	50 ft	0.1 KW	600 MHZ	32
3C	C/DEC/85	FCS	60 ft	25 KW	13000 MHZ	33 & 34

All cases vertically polarized w/ a 4 degree beamwidth/ESM a & b w/ a 1 degree elev, FCS 0 elev.

B. CASE STUDIES

1. Case 0 - Standard Atmosphere

a. Standard Profile

A representive standard atmosphere in the EREPS (PROPR) code had the following parameters: Evaporation Duct Height (EVD HT) = 0; Surface-based Duct Height (SBD HT) = 0; effective earth radius factor (K) = 1.33; surface refractivity (NSUBS) = 334; Absolute Humidity (ABS HUM) = 7.5; and Surface Wind Speed (WIND SP) = 12.3 kts (Hitney et al, 1988, p. 22).

The value K is based on the refractivity gradient (dN/dz) as follows:

$$K=1+6.4\times10^{-3}\frac{dN}{dz} \qquad (7)$$

This value affects the location of nulls in the interference region (< 10 nmi), NSUBS affects the troposcatter loss, ABS HUM determines the absorption by water vapor molecules, and the WIND SP affects the depths of the nulls in the interference region.

EMPE predicted signal strength for standard atmospheres are shown by Greyscale displays in Figures 4, 5, 6 and 7. The cases considered are as follows:

- Case 0-0 (Figure 4): A standard atmosphere with system ESM-a operating.
- Case 0-1 (Figure 5): A standard atmosphere with system ESM-b operating.
- Case 0-2 (Figures 6 and 7; at 100 nmi and 10 nmi, respectively): A standard atmosphere with system FCS operating.

b. Case 0 Results

(1) Signal Strength Results. For case 02 (System FCS) a range of 100 nmi was chosen to represent the radar's vulnerability to ESM detection; whereas, 10 nmi was used to properly represent the performance capability.

Since all of these were for a standard atmosphere, all signal strength results reveal no ducting/channeling type effect; therefore, no extension of range, radar holes, or height errors exist. The radio/radar horizon for systems ESM-a, ESM-b, and FCS was approximately 26 nmi, 15 nmi, and 18 nmi (Figures 4, 5, and 6) respectively.

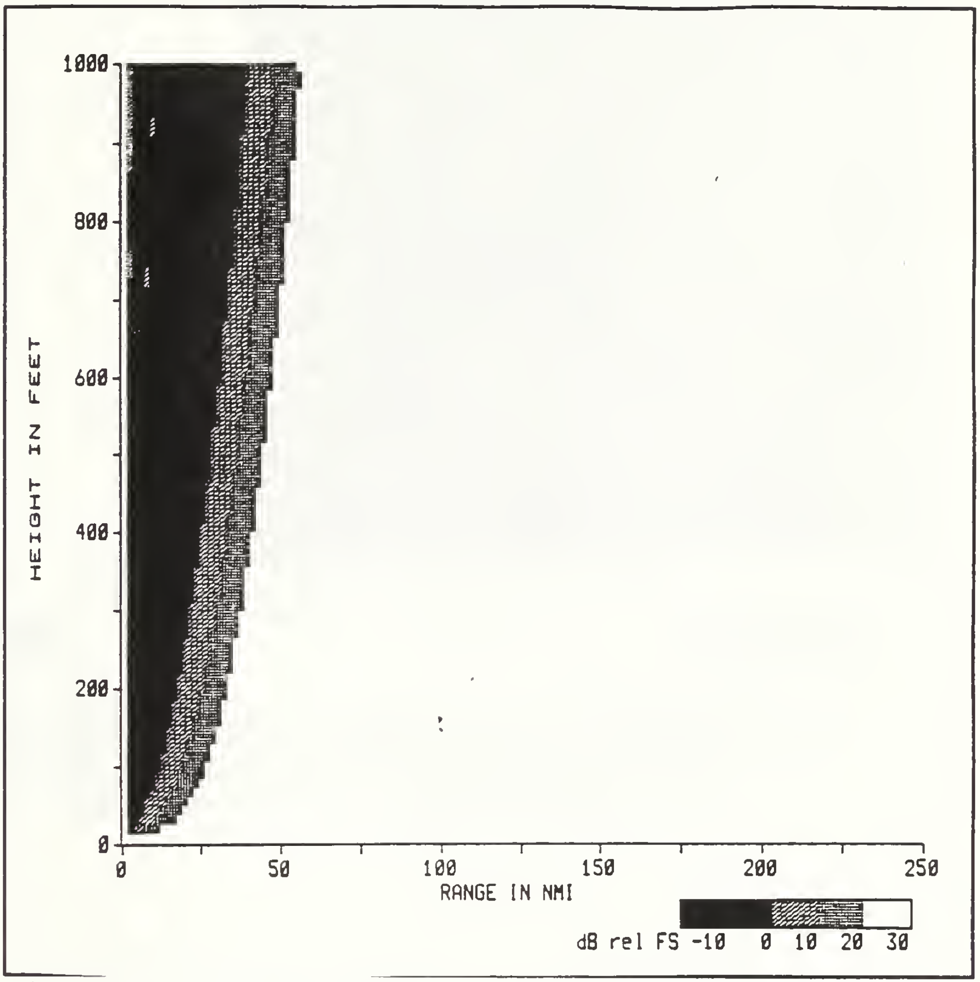

Figure 5 EMPE Signal Strength Prediction for a Standard Atmosphere for System ESM-b, 600 MHZ At 50 Feet (dB is relative to FS).

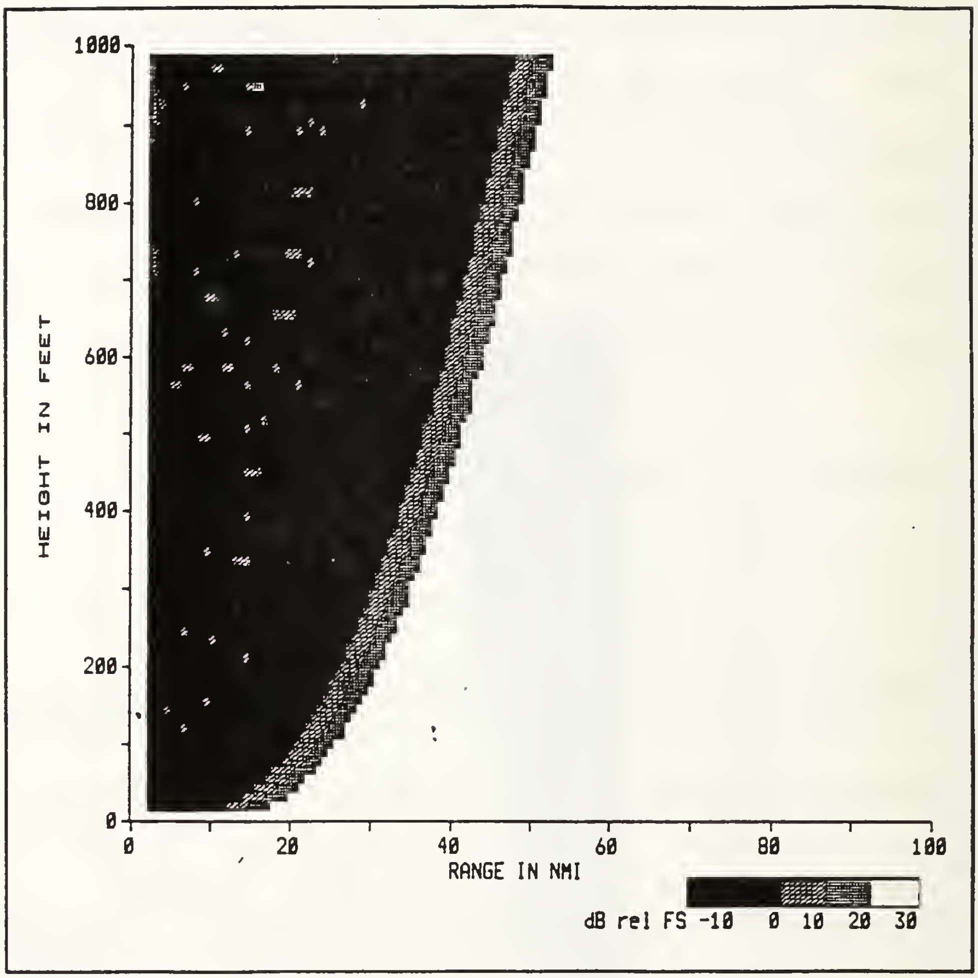

Figure 6 EMPE Signal Strength Prediction for a Standard Atmosphere for System FCS, 13 GHZ At 60 Feet (100 nmi; dB is relative to FS).

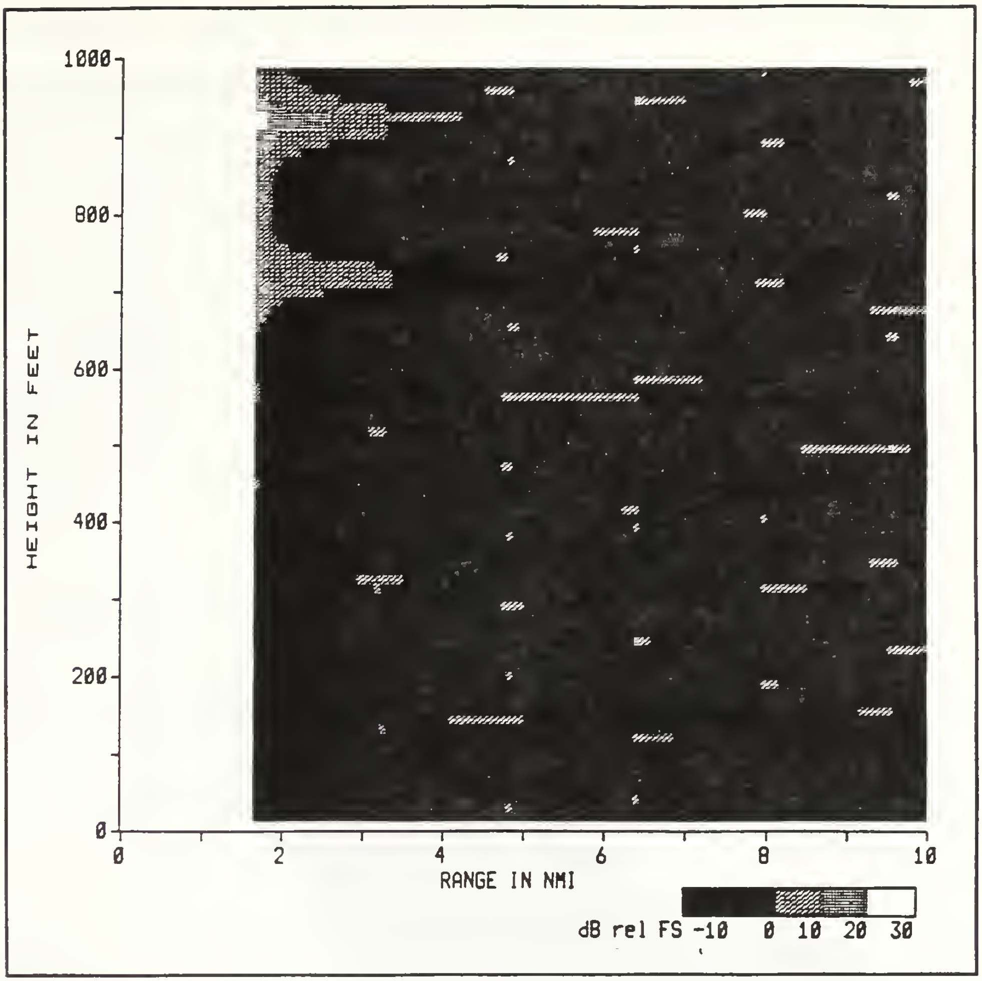

Figure 7 EMPE Signal Strength Prediction for a Standard Atmosphere for System FCS, 13 GHZ At 60 Feet (10 nmi; dB is relative to FS).

2. Case 1 - Persian Gulf

a. Abu Dhabi Profile

The Persian Gulf area is a unique region because it is encircled by arid land. The Persian Gulf region is conducive to ducting, due to the dry upper air from the surrounding land over the moist layer of gulf air. The location considered for this region was Abu Dhabi, (A). Figure 8 is a map of the Persian Gulf labeling the sites used. Abu Dhabi and Bandar Abbas will be used for the horizontally inhomogeneous case. The data are from 25 September 1987, (night), when a surface-based duct was present. The top of the trapping layer and duct thickness was approximately 350 feet. A refractivity profile for this site is provided in the next chapter (Figure 41).

The cases considered are as follows:

- Case 1A (Figure 9): Abu Dhabi atmospheric profile with system ESM-a operating.
- Case 1B (Figure 10): Abu Dhabi atmospheric profile with system ESM-b operating.
- Case 1C (Figures 11 and 12): Abu Dhabi atmospheric profile with system FCS operating.

b. Case 1 Results

(1) Signal Strength Results. EMPE revealed evidence of extended communication ranges for Case 1A (Figure 9). All results in this discussion should be compared with standard atmospheric results in the previous section. Minimal energy loss was depicted on the graph, and the duct affected the signal by extending it out to at least 250 nmi, the maximum range on the graph. This can be compared to the standard atmosphere shown in Figure 4, in which no extended

range exists. Some greater signal loss is experienced within the duct (lighter areas); but the majority of the display reveals this area to be ideal for extended communications capability.

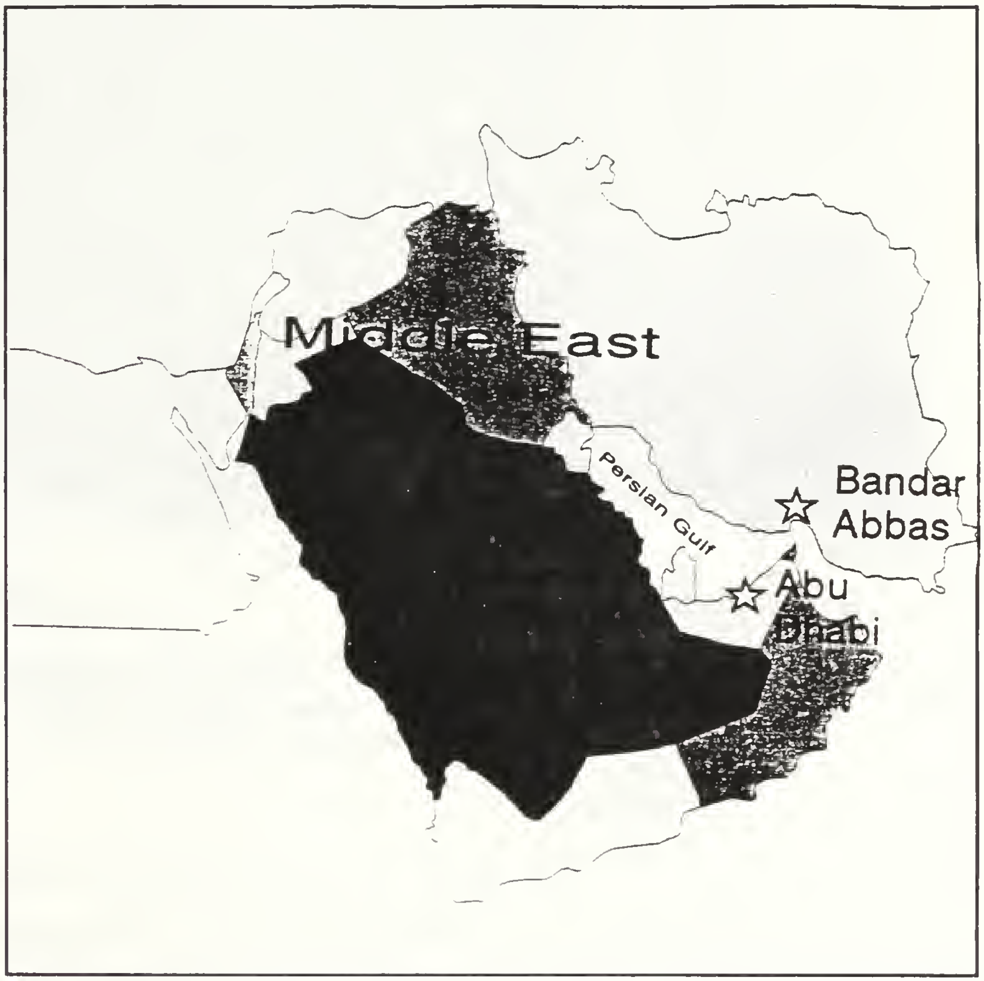

Figure 8 Geographical Locations Of The Persian Gulf Sites.

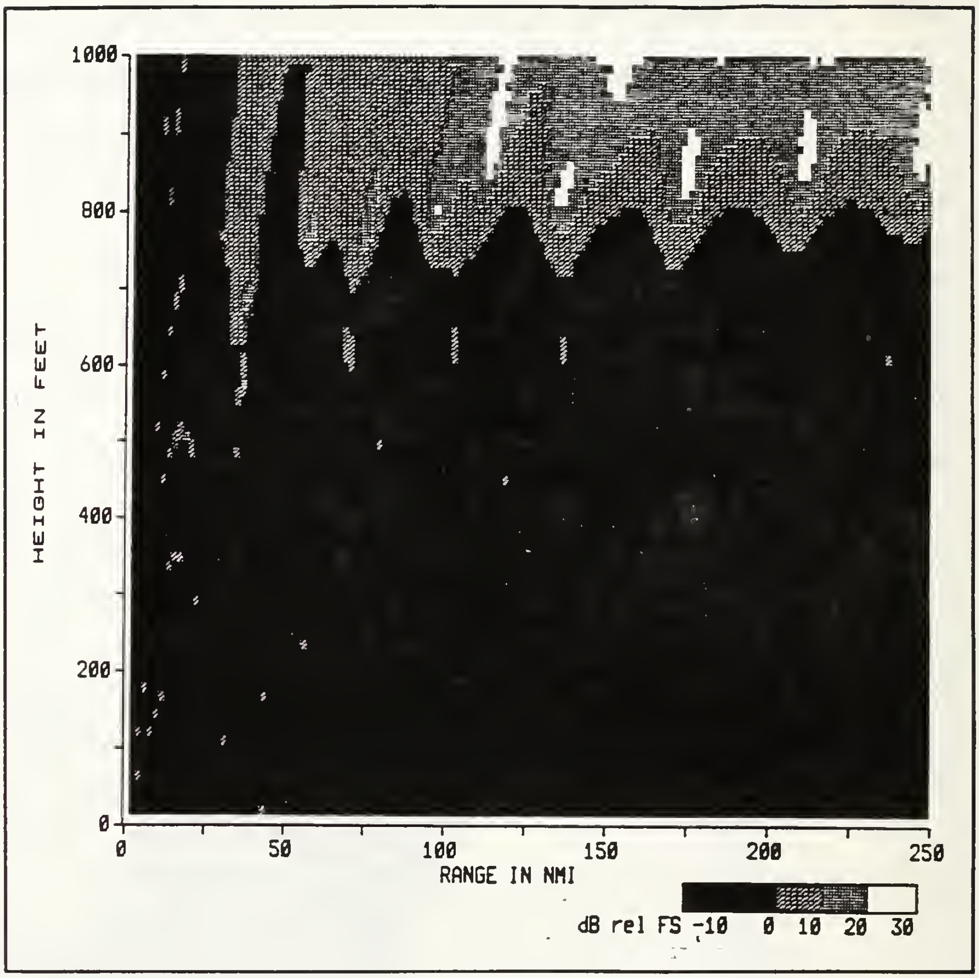

Figure 9 EMPE Signal Strength Prediction for Abu Dhabi, 25 September 1987 (System ESM-a, 600 MHZ At 300 Feet; dB is relative to FS).

A condition for extension (relative to a standard atmosphere) of communications is displayed for Case 1B, Figure 10. The majority of the graph reveals signal strength extended out to at least 250 nmi (the maximum range of the display). Some signal loss is experienced around 50 nmi at heights above 400 feet. Also, signal loss is present from 0 out to approximately 26 nmi.

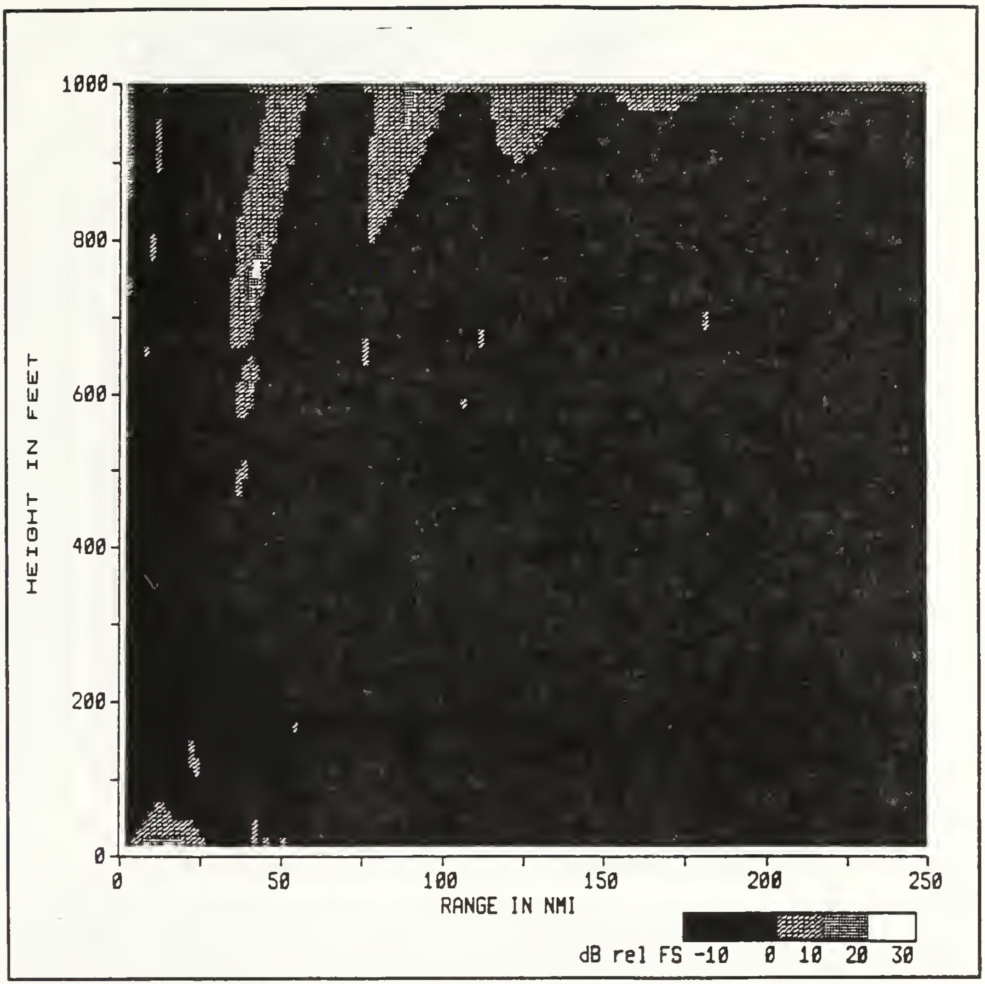

Figure 10 EMPE Signal Strength Prediction for Abu Dhabi, 25 September 1987 (System ESM-b, 600 MHZ At 50 Feet; dB is relative to FS).

Case 1C, Figure 11, examines radar vulnerability. Figure 11 illustrates a condition leading to detection of the radar out to a range of at least 100 nmi. From 10 nmi to approximately 20 nmi, there is a region of greater than 10 dB loss. In addition, since the signal is carried well beyond the expected range of 10 nmi, any target detected would appear to be an immediate concern, putting the tactical commander in a precarious situation which can lead to false conclusions with possible drastic results. The radar would therefore detect a target beyond its capable range, and thought it had a target at its performance range of 10 nmi. With the duct height errors also occur.

A radar hole is present around 50 nmi and above 600 feet.

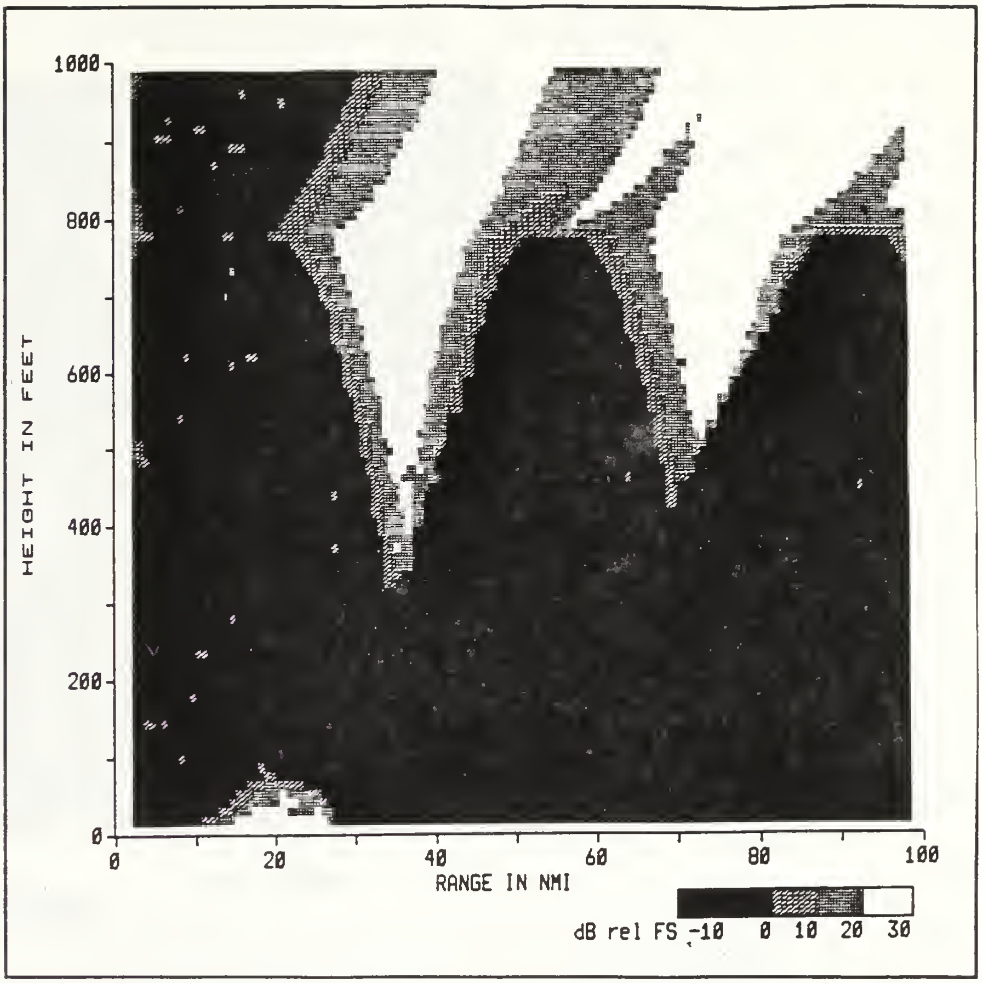

Figure 11 EMPE Signal Strength Prediction for Abu Dhabi, 25 September 1987 (System FCS, 13 GHZ At 60 Feet; 100 nmi). dB is relative to FS.

Figure 12, a different display of Case 1C, indicates how the system's performance could be affected in this type of environment at its performance range, 10 nmi. Some moderately higher signal loss areas are revealed, but the signal strength is large (dark areas) for the majority of the scene. EMPE signal strength predictions on the 10 nmi displays will be essentially the same for all cases.

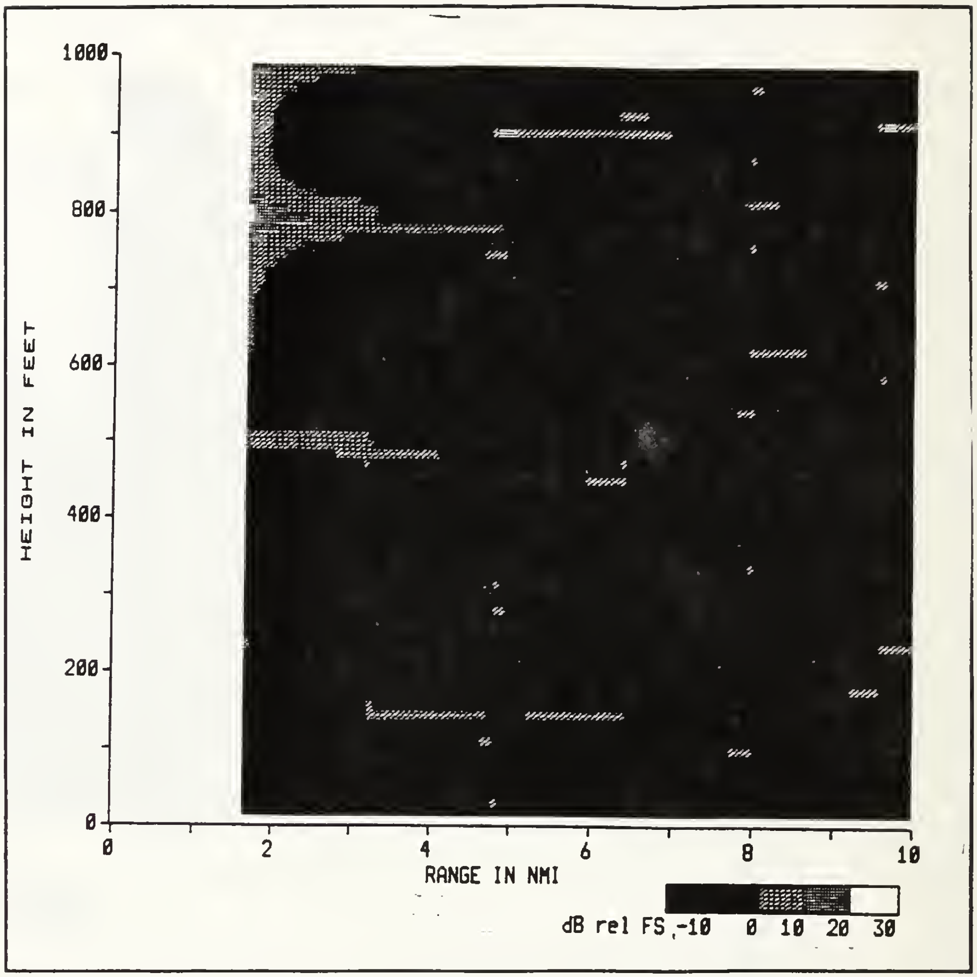

Figure 12 EMPE Signal Strength Prediction for Abu Dhabi, 25 September 1987 (System FCS, 13 GHZ At 60 Feet; 10 nmi). dB is relative to FS.

The EMPE graphs for Cases 1A, 1B and 1C illustrate how ranges are extended within the duct out to at least the maximum range on the graphs. Energy losses were experienced outside the ducting region (refer to Figures 9, 10 and 11). These cases also reveal some small energy losses within the duct.

(2) EREPS and EMPE Loss Predictions. Figures 3a and 3b illustrated how EREPS (PROPR) graphs display signal behavior relative to Free Space, and a standard environment.

Displays for the ESM system (Figures 13 and 14) indicate that if a transmitter and receiver are located more than 90 nmi and 70 nmi apart, respectively, in a standard environment, communications will not be maintained. Beyond these ranges, communications can no longer be maintained because the signal strength falls below the indicated threshold level of 182 dB (losses less than this threshold level indicate intercept capability). Introducing surface-based ducts, causes the maximum range to go out to at least 250 nmi, and signal loss to be even less than that of Free Space.

For the radar system, a threshold level is indicated at approximately 138 dB (Figure 15). The Free Space range for detecting targets is indicated to be 6.7 nmi. With a surface-based duct present, that range of detectability is increased out to 9.2 nmi. The surface-based duct curve is similar to the Free Space curve, with the exception of the skip zone from approximately 18 nmi to 45 nmi.

One lobe was used to characterize the oscillation that occurs around the Free Space level. This oscillation occurs as a result of coherent interference caused by direct and sea-reflected waves.

Figure 13 (EREPS) and Figure 16 (EMPE) indicate a small path loss; however, the EMPE transmission loss plot (Figure 16) reveals many areas in which high drop outs (fluctuations) exist, producing much greater signal loss in some areas than otherwise expected, especially at 200 nmi, where a path loss of approximately 168 dB was experienced.

Figure 14 (EREPS) reveals a small skip zone from approximately 10 nmi to 49 nmi. Figure 17 (EMPE) indicates an interference region, with cyclic signal loss. Where EREPS (PROPR) reveals a steady drop off rate of signal strength, EMPE indicates severe changes in signal degradation.

In Figure 15, a skip zone is present from approximately 15 nmi to 45 nmi, allowing an operator to believe this would be a relatively safe tactical area to operate to avoid detection at long ranges; however, EMPE (Figure 18) reveals this area (around 8 nmi to 80 nmi) was not a skip zone.

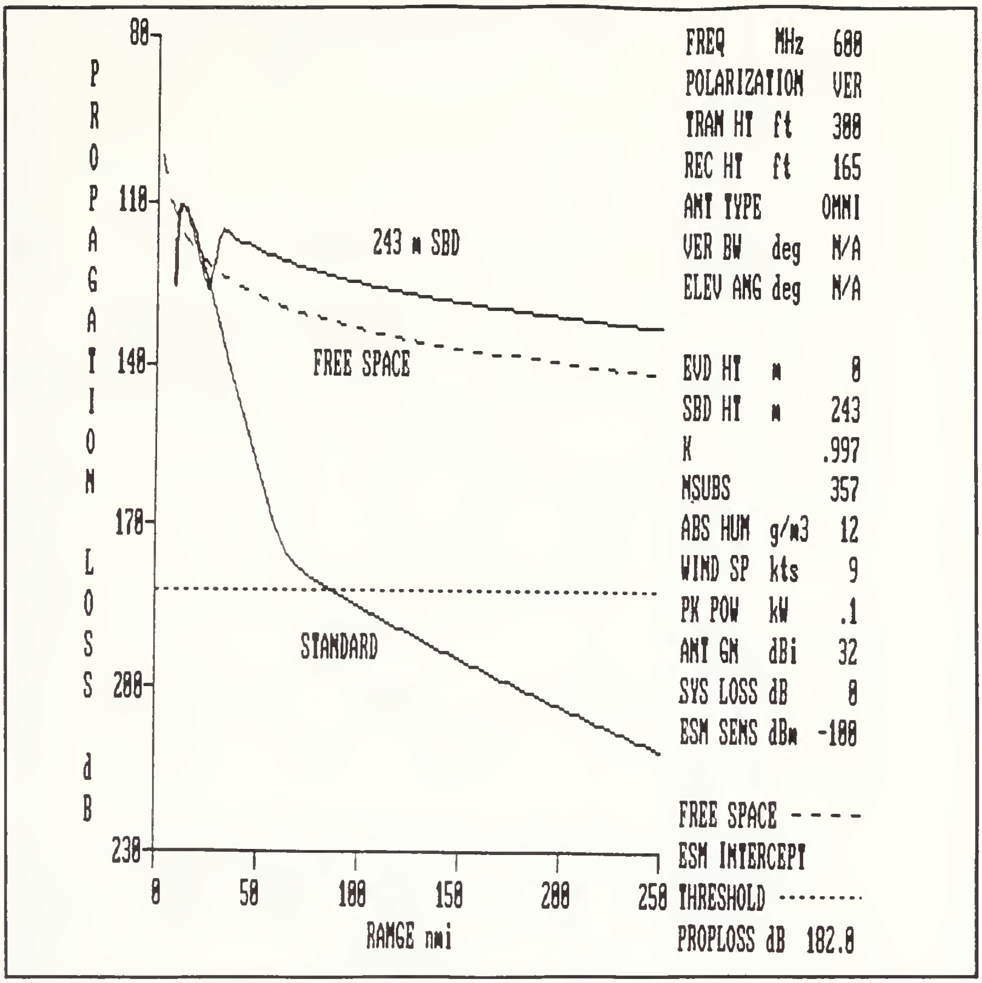

Figure 13 EREPS (PROPR) Prediction for Abu Dhabi, 25 September 1987 (System ESM-a operating).

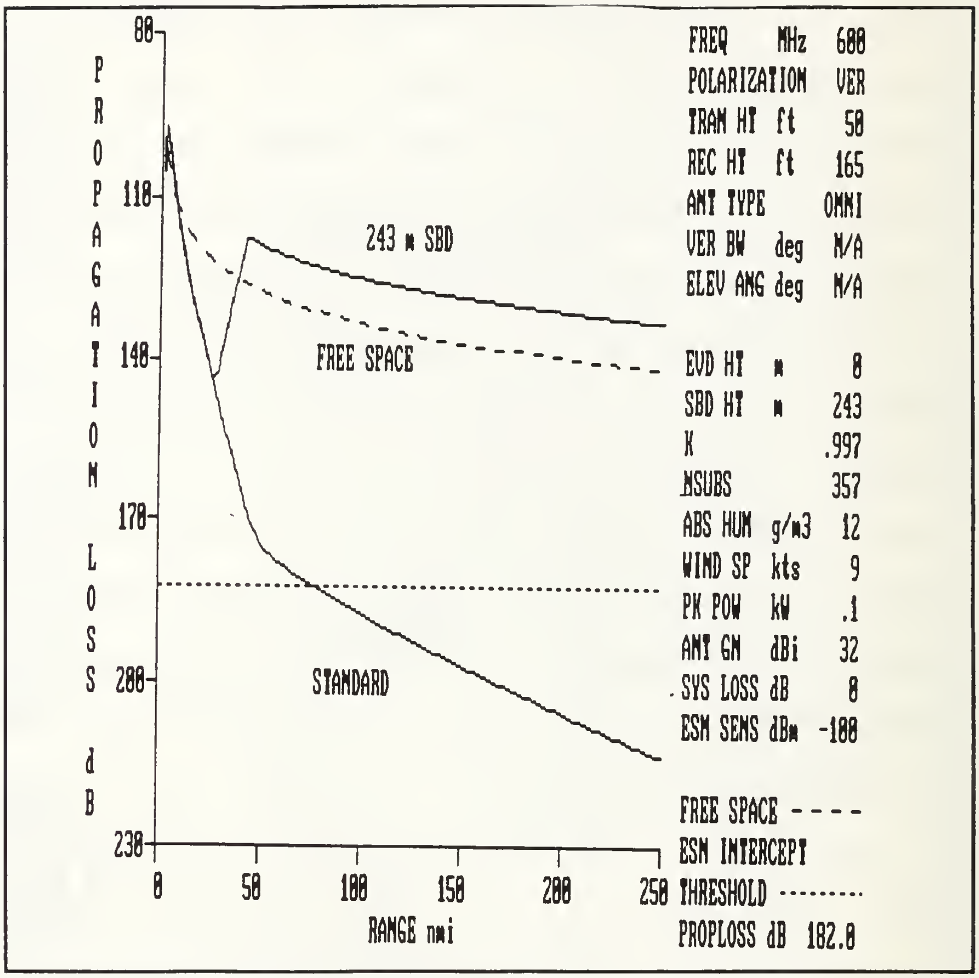

Figure 14 EREPS (PROPR) Prediction for Abu Dhabi, 25 September 1987 (System ESM-b operating).

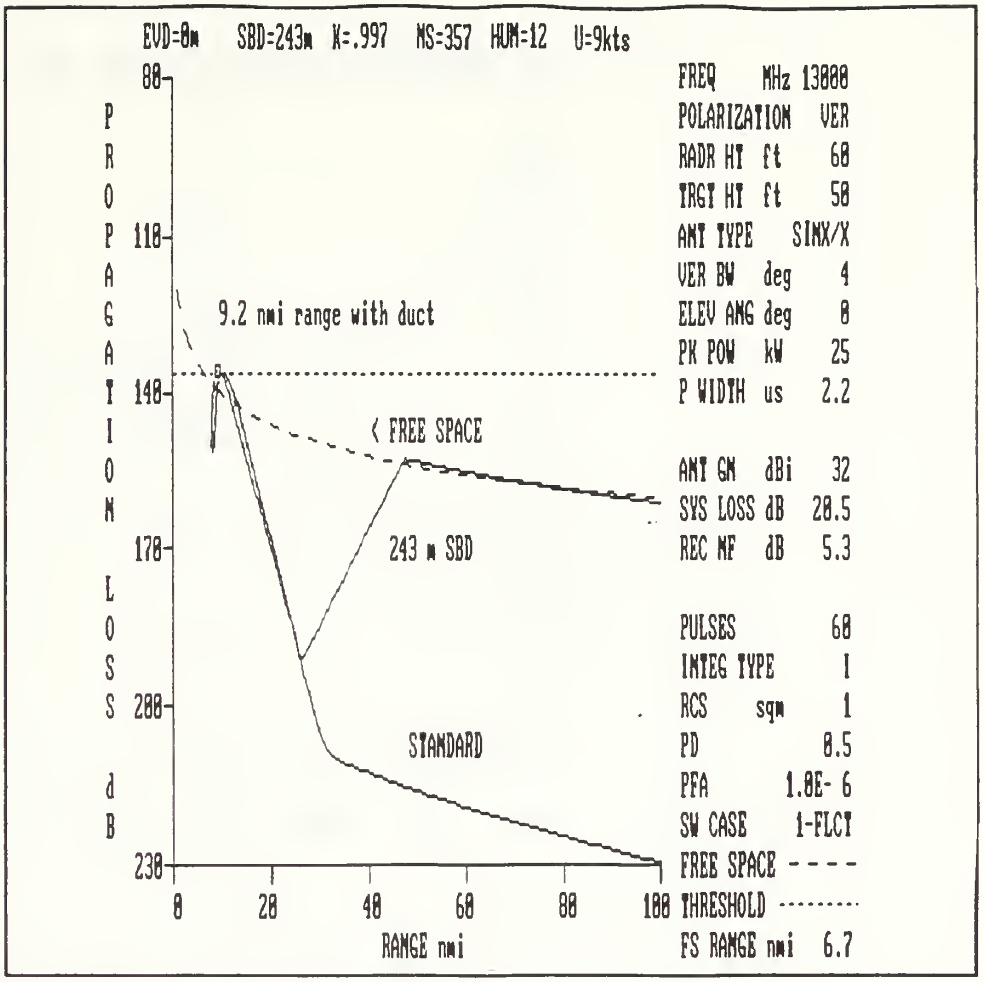

Figure 15 EREPS (PROPR) Prediction for Abu Dhabi, 25 September 1987 (System FCS operating).

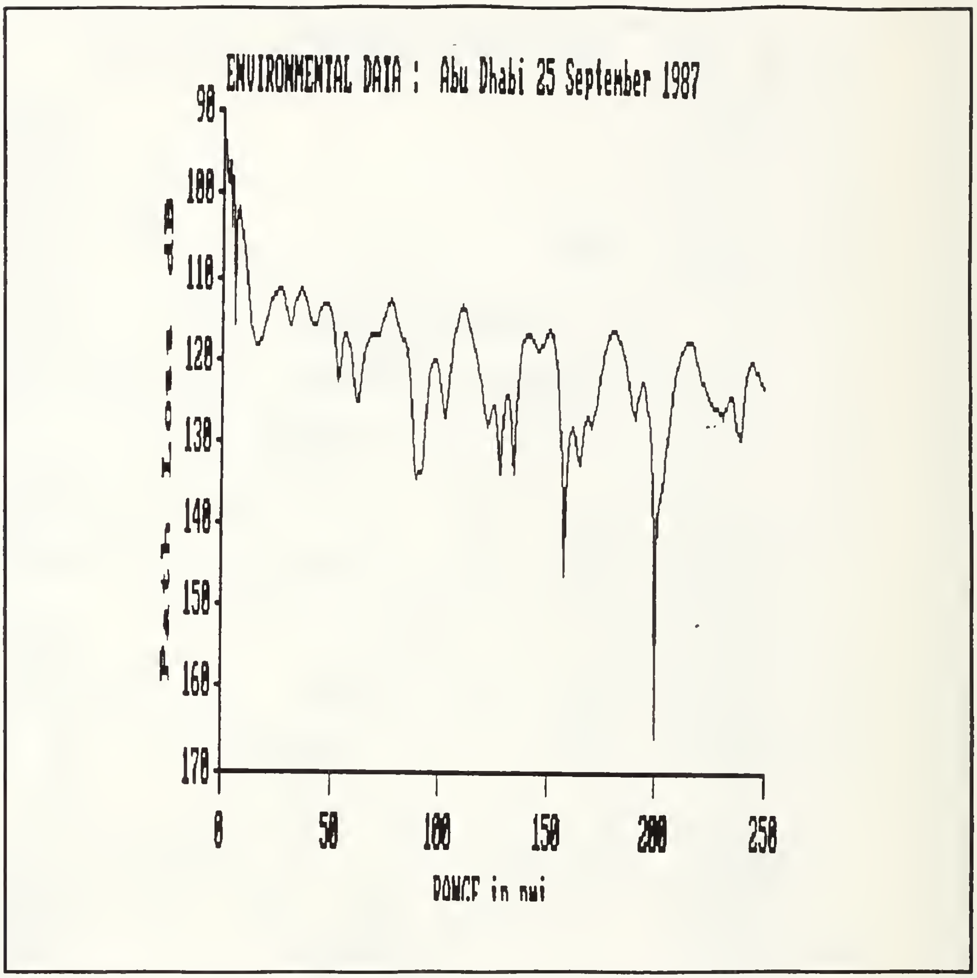

Figure 16 EMPE Transmission Loss Prediction for Abu Dhabi, 25 September 1987 (System ESM-a operating).

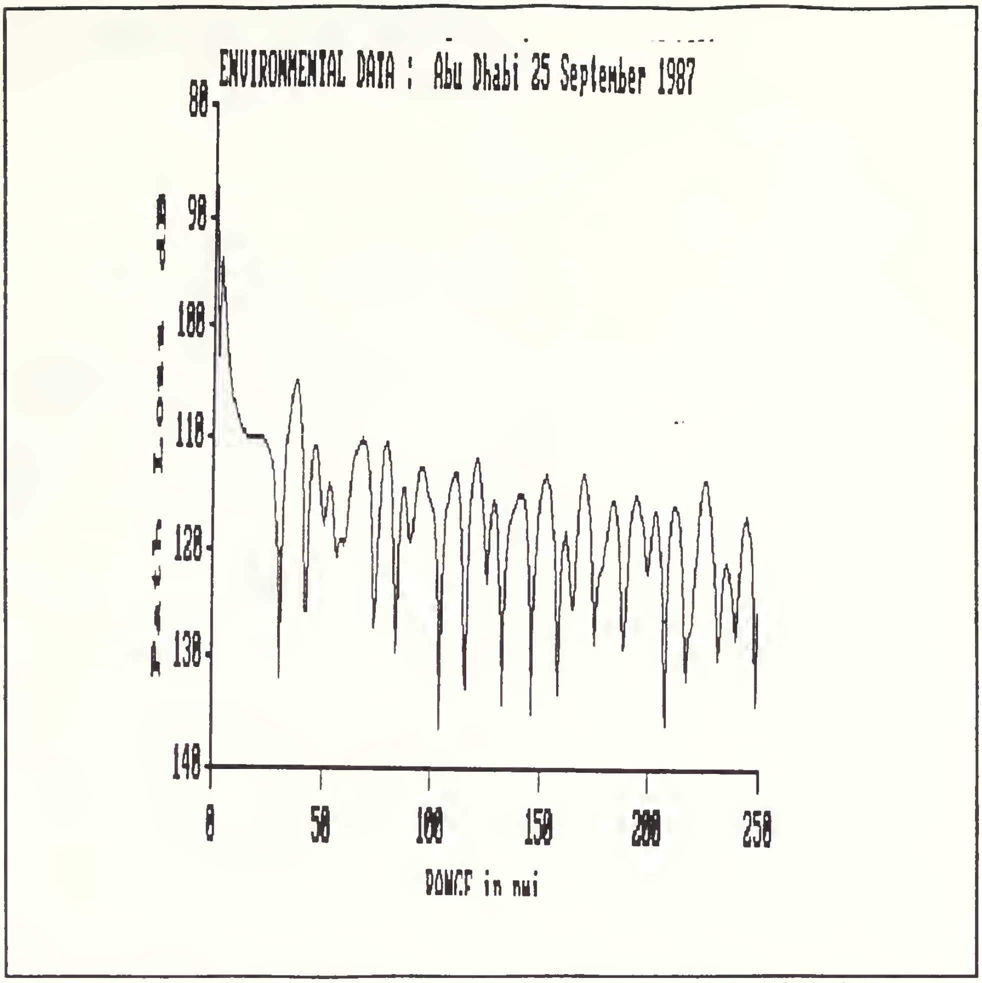

Figure 17 EMPE Transmission Loss Prediction for Abu Dhabi, 25 September 1987 (System ESM-b operating).

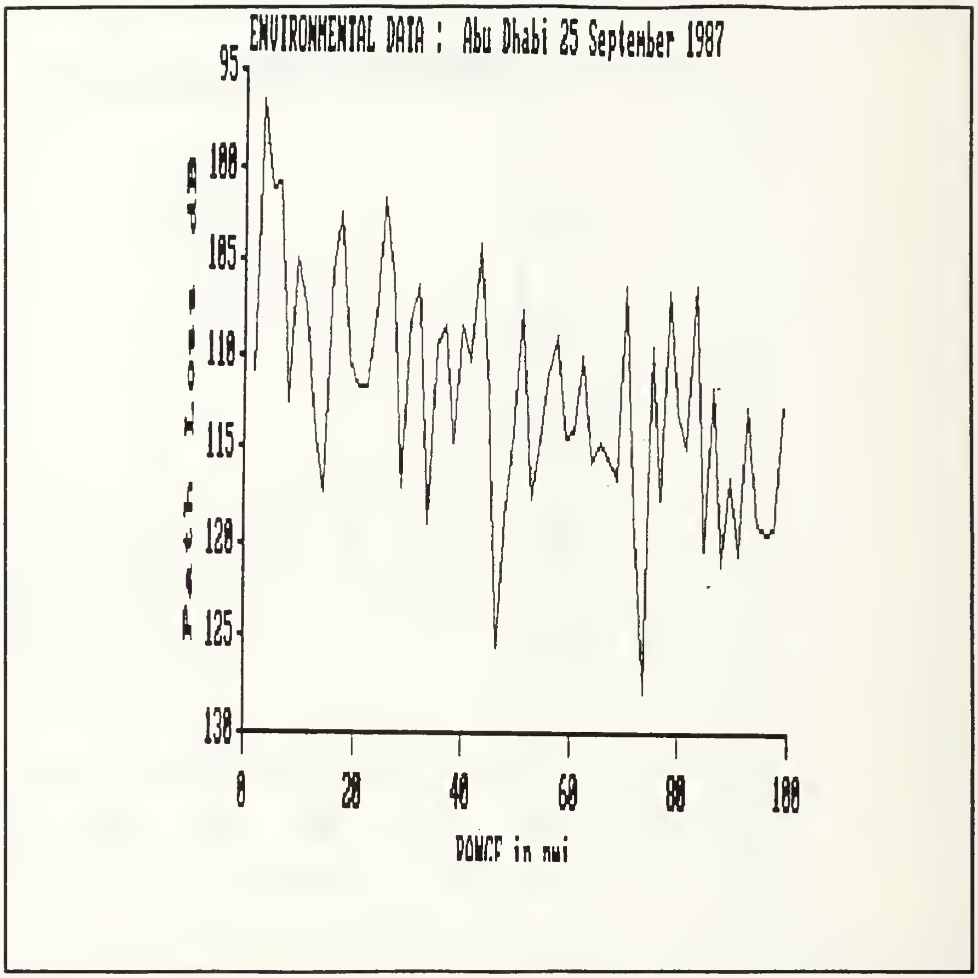

Figure 18 EMPE Transmission Loss Prediction for Abu Dhabi, 25 September 1987 (System FCS operating).

3. Case 2 - Indian Ocean

a. Diego Garcia Profile

Diego Garcia, (D), was the site considered for this region. Figure 19 shows the location of the sites used for this area. Diego Garcia and Bangkok will be used for the horizontally inhomogeneous case. The data are from Spring 1982, (night). The top of the trapping layer and duct thickness was approximately 350 feet. A refractivity profile for this site is contained in the next chapter (Figure 43).

The cases considered are as follows:

- Case 2A (Figure 20): Diego Garcia atmospheric profile with system ESM-a operating.
- Case 2B (Figure 21): Diego Garcia atmospheric profile with system ESM-b operating.
- Case 2C (Figures 22 and 23): Diego Garcia atmospheric profile with system FCS operating.

b. Case 2 Results

(1) Signal Strength Results. Figure 21 shows EMPE signal strength prediction for Case 2B. In this graph, an extended range is experienced out to 250 nmi (this is compared to Figure 5 for the standard atmosphere), with stronger signal strength around 50 nmi to 100 nmi. With this condition present, a ESM system anywhere in this particular area would most likely be able to detect the emitter.

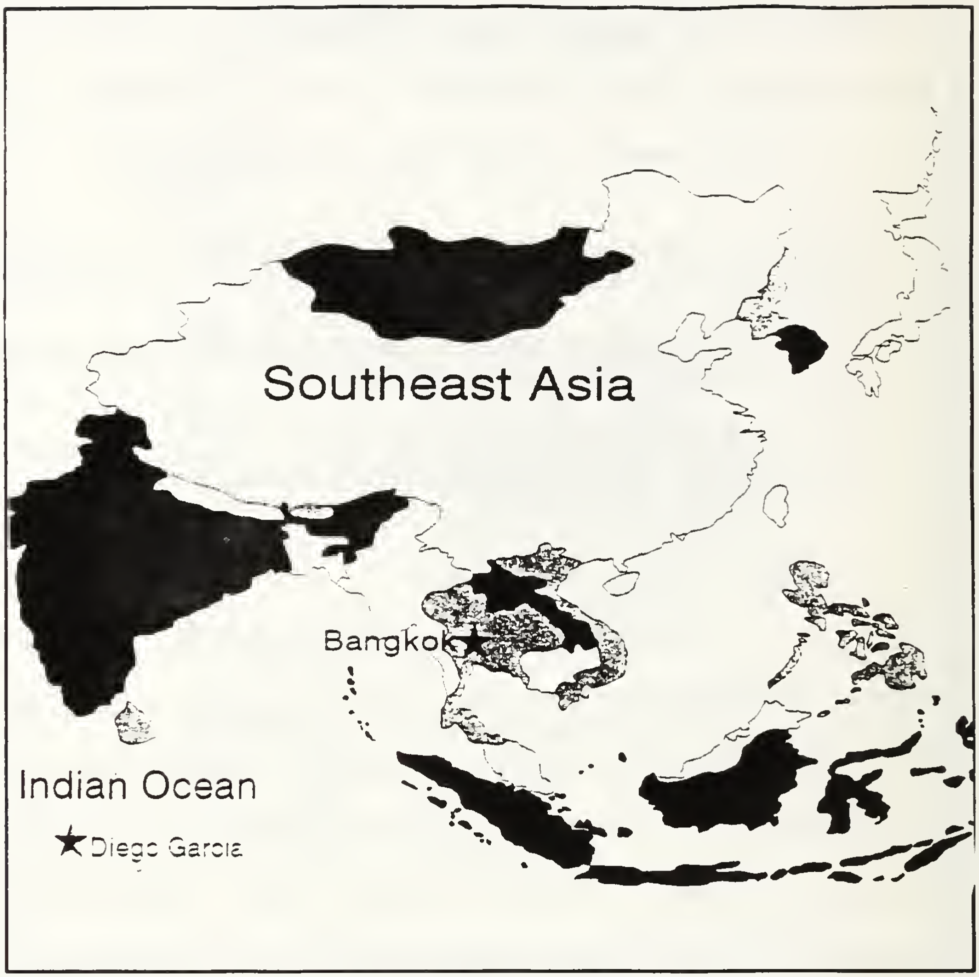

Figure 19 Geographical Locations Of The Indian Ocean Sites.

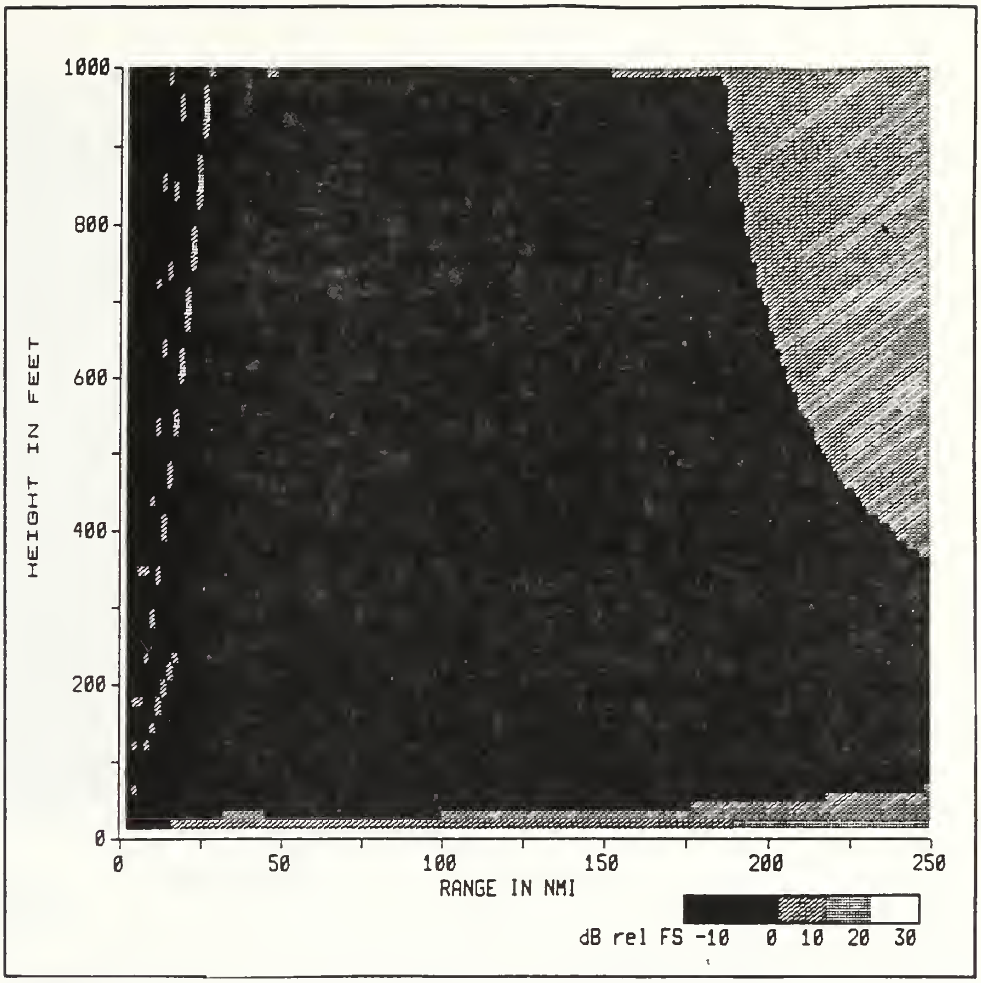

Figure 20 EMPE Signal Strength Prediction for Diego Garcia, Spring 1982 (System ESM-a, 600 MHZ At 300 Feet). dB is relative to FS.

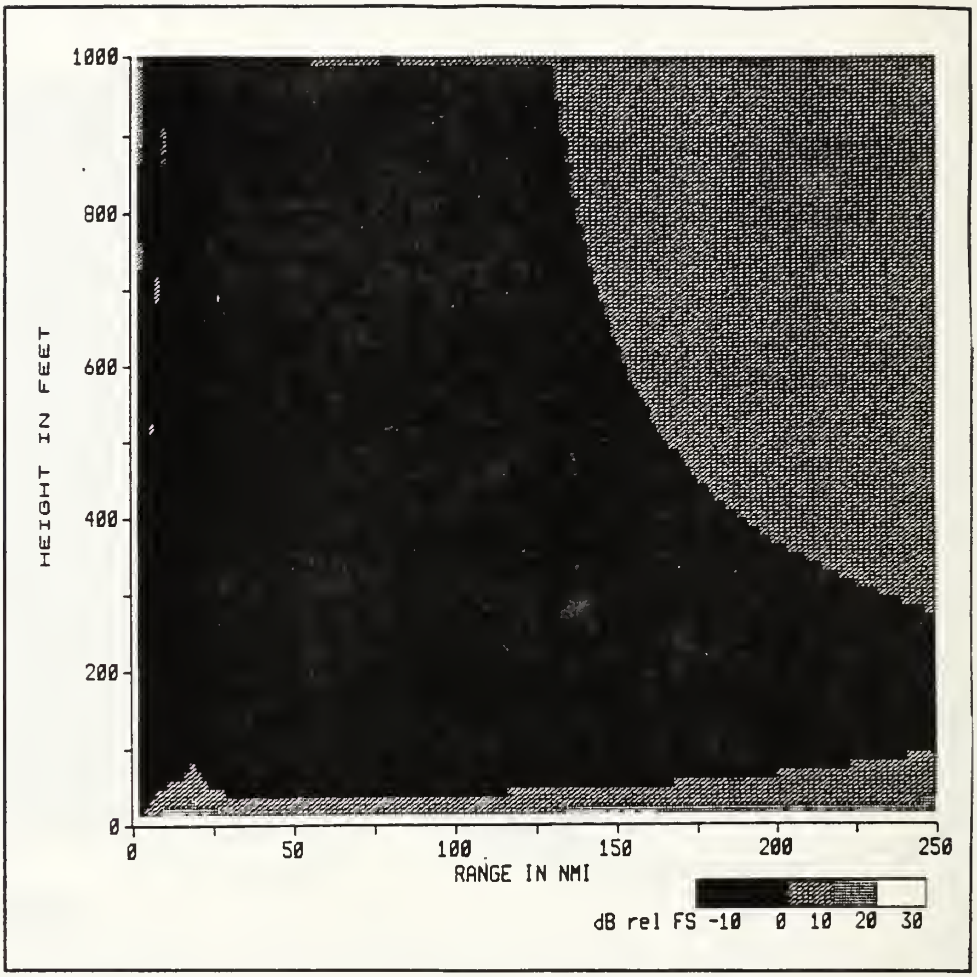

Figure 21 EMPE Signal Strength Prediction for Diego Garcia, Spring 1982 (System ESM-b, 600 MHZ At 50 Feet). dB is relative to FS.

Case 2C, Figure 22 illustrates the vulnerability of the radar to be detected well beyond its expected operating range (at least 100 nmi as shown on the display). The range experienced can be compared to the standard atmosphere in Figure 6. Radar holes are present around 60 nmi to 80 nmi above 300 feet.

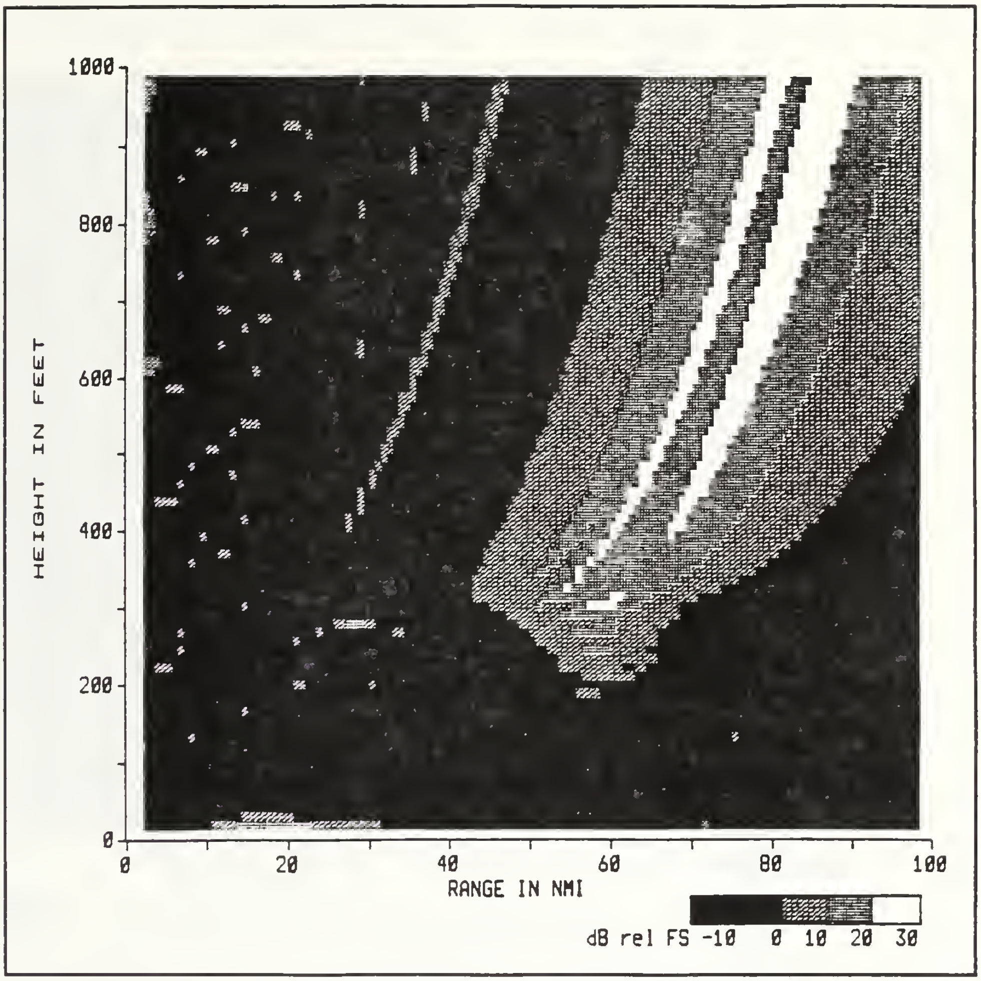

Figure 22 EMPE Signal Strength Prediction for Diego Garcia, Spring 1982 (System FCS, 13 GHZ At 60 Feet; 100 nmi). dB is relative to FS.

Figure 23, a different display of Case 2C, illustrates the system is able to operate with minimal signal loss out to its maximum range of 10 nmi.

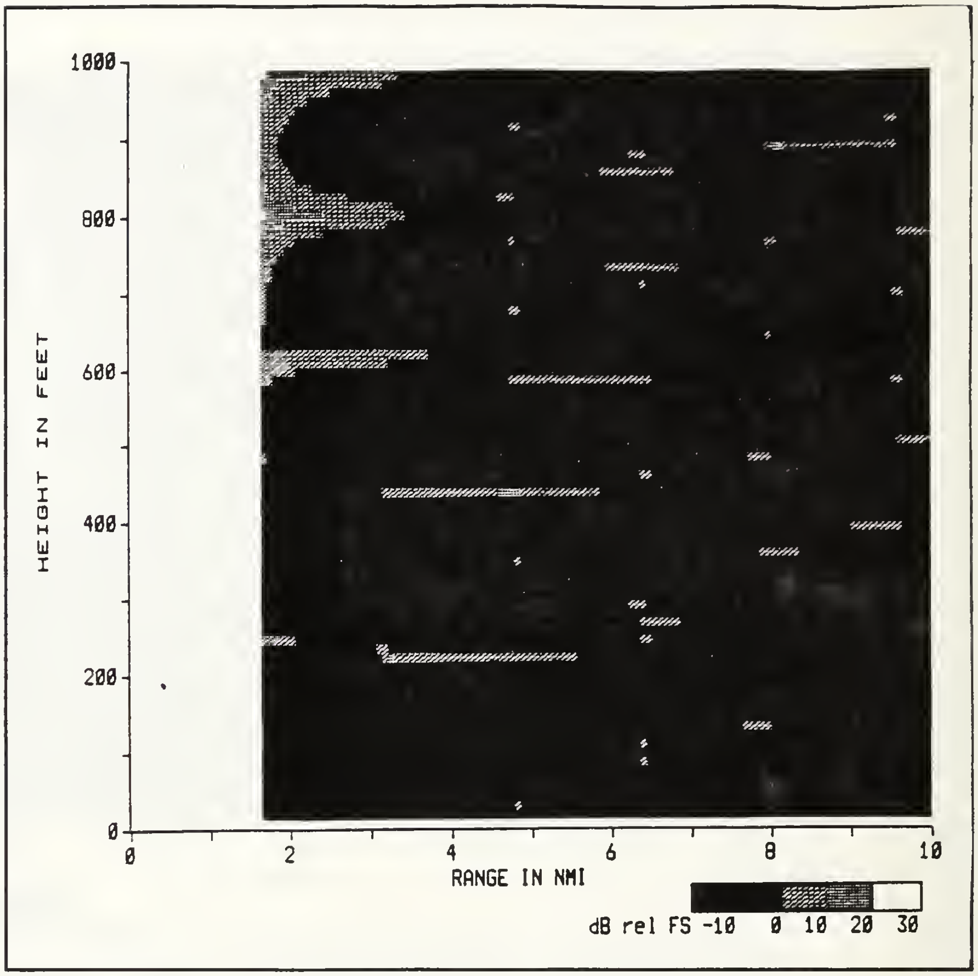

Figure 23 EMPE Signal Strength Prediction for Diego Garcia, Spring 1982 (System FCS, 13 GHZ At 60 Feet; 10 nmi). dB is relative to FS.

(2) EREPS and EMPE Loss Predictions. Figures 24 (EREPS) and 25 (EMPE) indicate some signal loss from 0 to 10 nmi. Figure 24 reveals the presence of a small skip zone from approximately 20 nmi out to around 40 nmi. Figure 25 has no skip zone region depicted, but does display a drastic loss in

signal between 20 nmi and 50 nmi. Both showed signal loss steadily increasing, but EMPE indicates slightly greater losses, i.e., around 250 nmi the loss is approximately 145 dB; EREPS illustrates a loss of approximately 135 dB at 250 nmi.

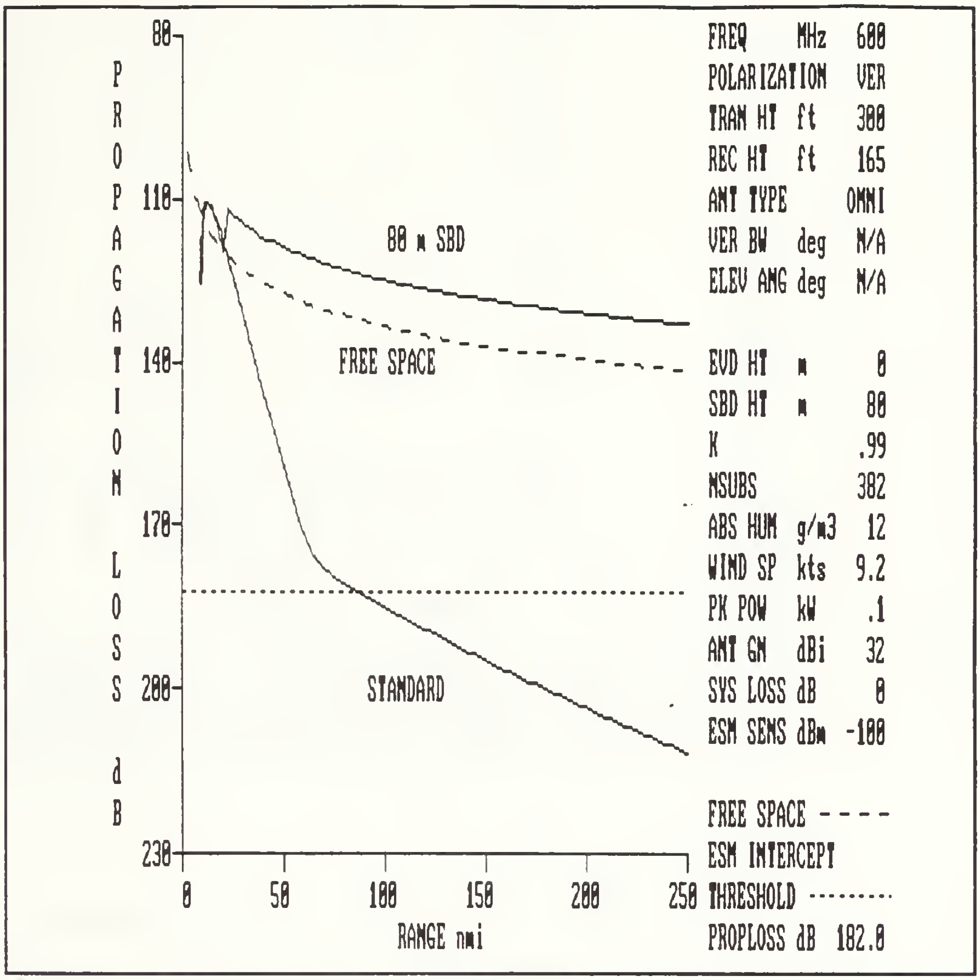

Figure 24 EREPS (PROPR) Prediction For Diego Garcia, Spring 1982 (System ESM-a operating).

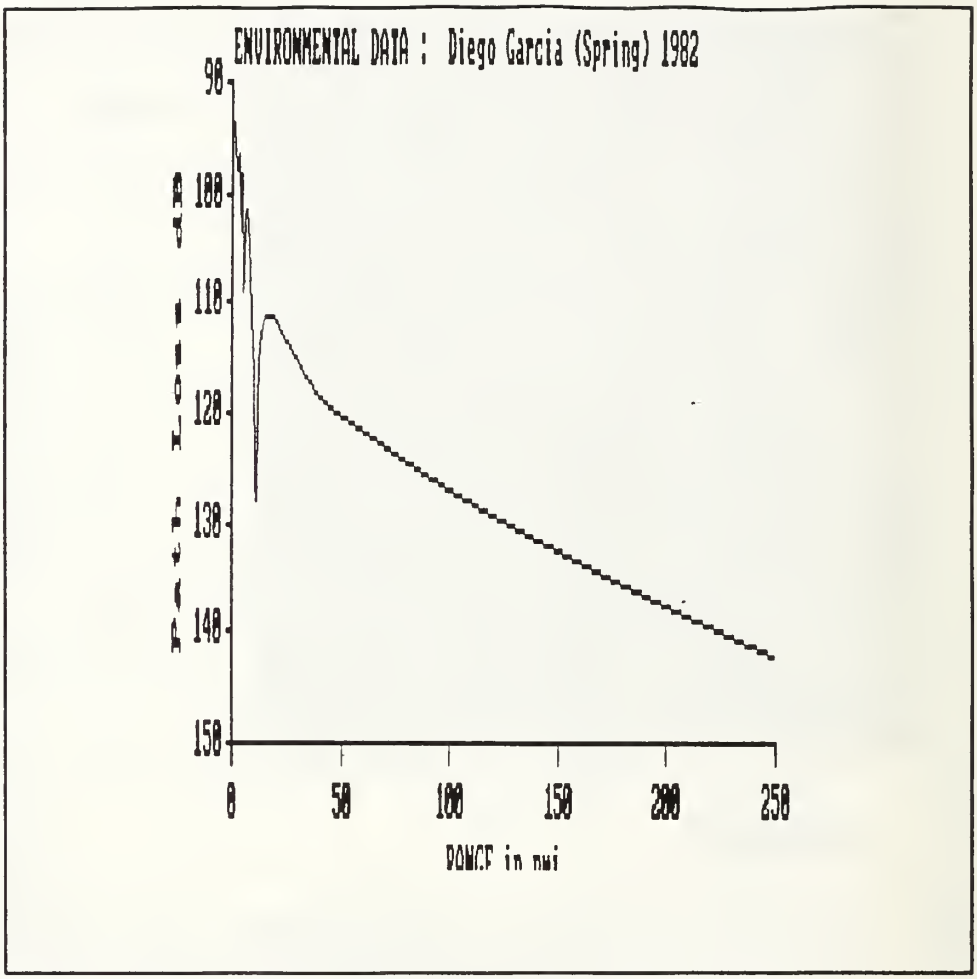

Figure 25 EMPE Transmission Loss Prediction for Diego Garcia, Spring 1982 (System ESM-a operating).

Figure 26 (EREPS) indicates a skip zone region from approximately 10 nmi to 40 nmi. Figure 27 (EMPE) displays a slight signal loss from 0 to approximately 10 nmi.

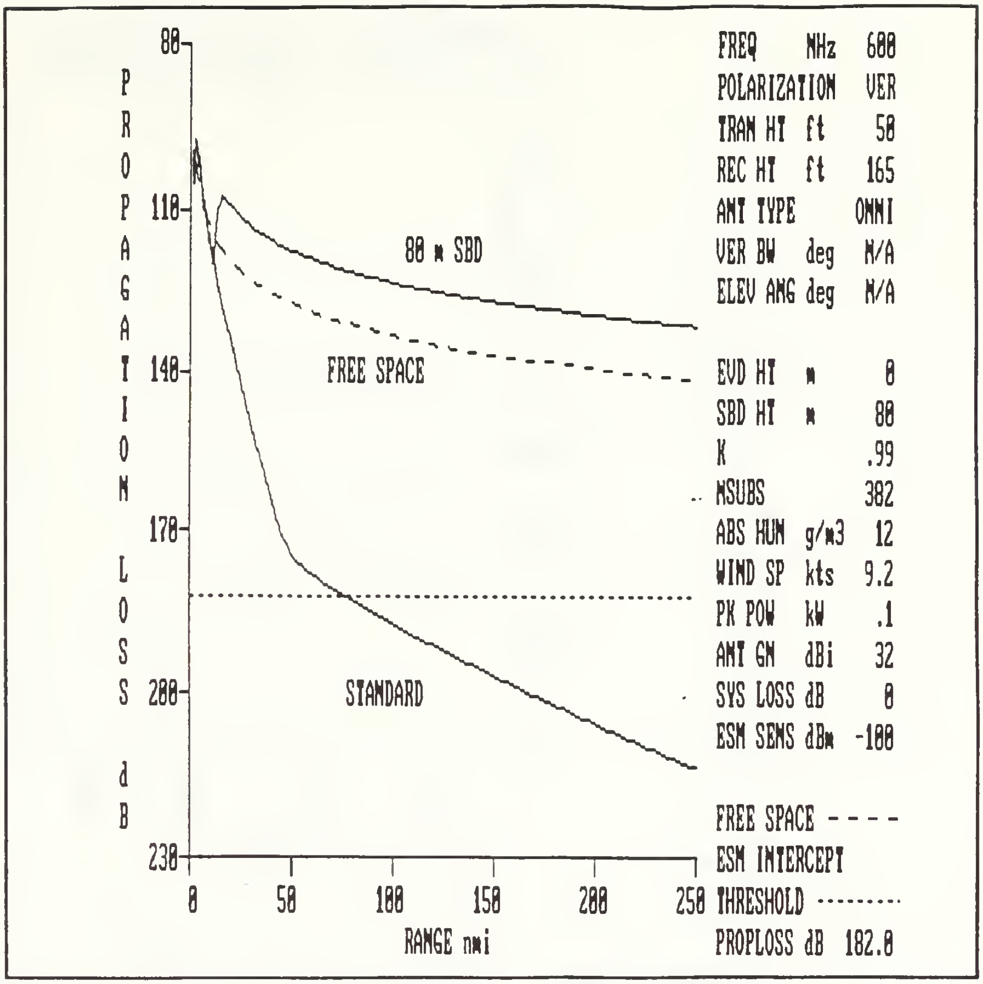

Figure 26 EREPS (PROPR) Prediction for Diego Garcia, Spring 1982 (System ESM-b operating).

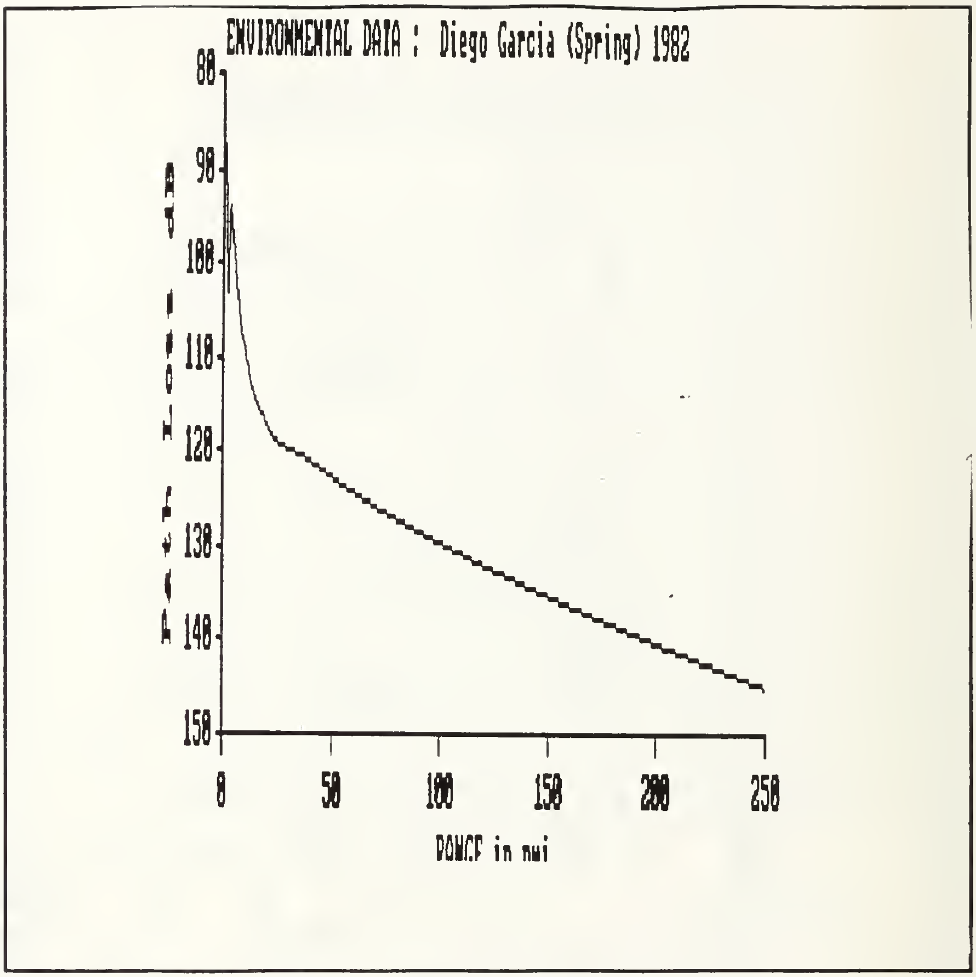

Figure 27 EMPE Transmission Loss Prediction for Diego Garcia, Spring 1982 (System ESM-b operating).

Figure 28 (EREPS) reveals a skip zone region from approximately 15 nmi to 25 nmi, with a steady increase of loss being experienced. In Figure 29 (EMPE) there was no clear indication of a skip zone, but some slight signal loss was shown in that area. What appears to be a tactical advantage point from not being detected in Figure 28, is not the same when looking at Figure 29, because this indicates the possibility of being detected, with the chance of the target going undetected.

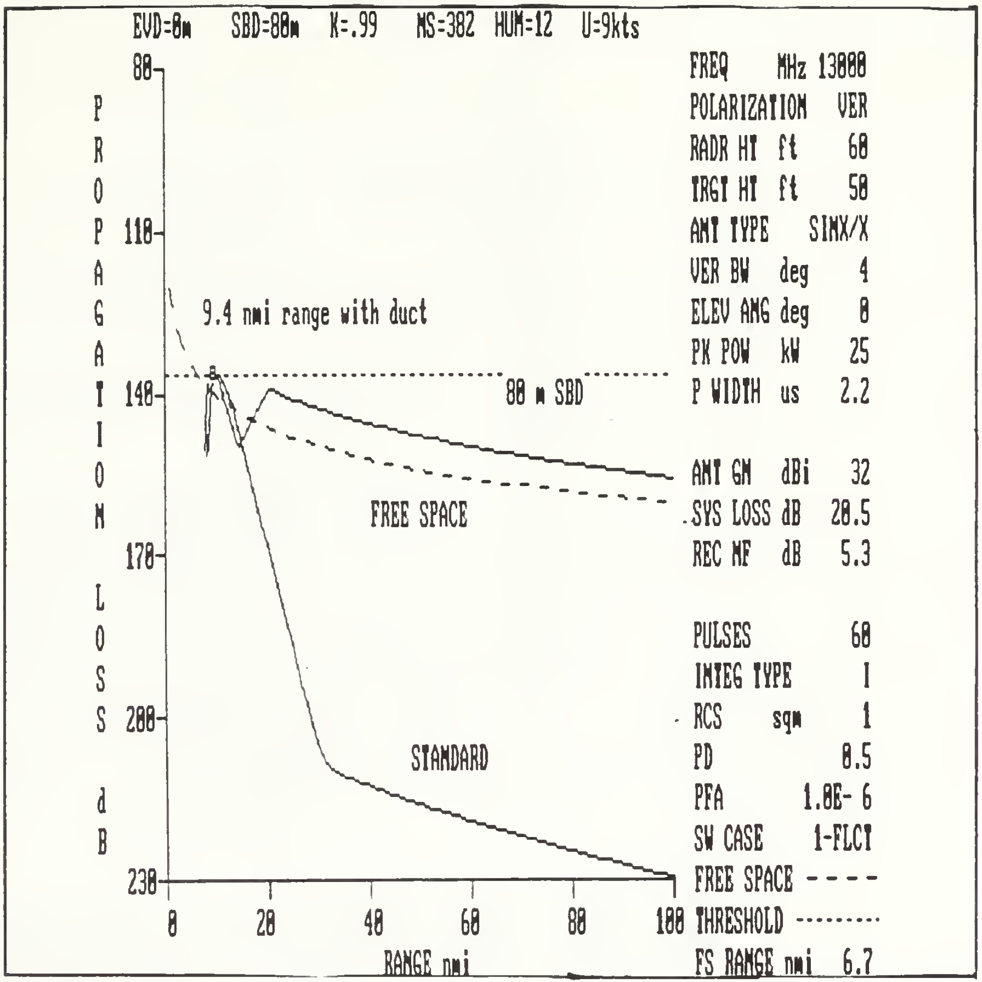

Figure 28 EREPS (PROPR) Prediction for Diego Garcia, Spring 1982 (System FCS operating).

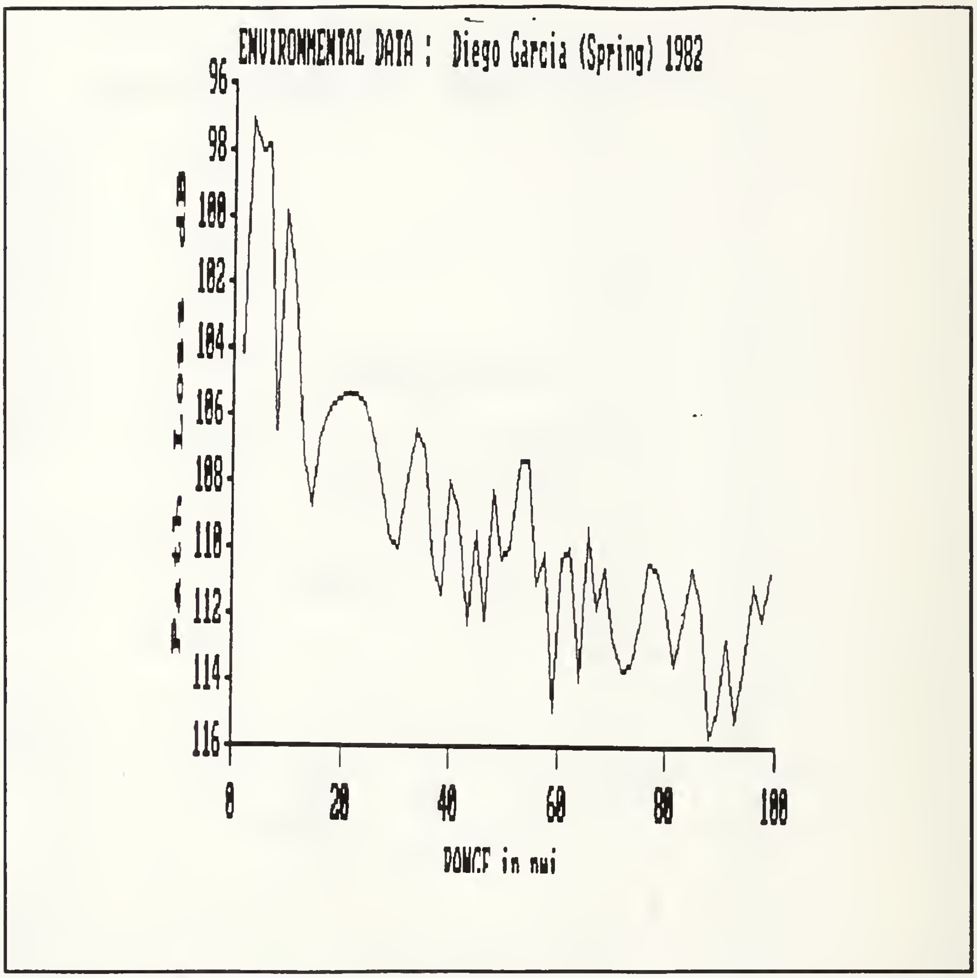

Figure 29 EMPE Transmission Loss Prediction for Diego Garcia, Spring 1982 (System FCS operating).

4. Case 3 - Caribbean

a. Curacao Profile

The location considered for this region was Curacao, (C). Figure 30 shows the locations for this area. Curacao and Puerto Rico will be used for the horizontally inhomogeneous case. The data are from December 1985, (day). The top of the trapping layer and duct thickness was approximately 480 feet. A refractivity profile for this site is displayed in the next chapter (Figure 45). The cases considered are as follows:

- Case 3A (Figure 31): Curacao atmospheric profile with system ESM-a operating.
- Case 3B (Figure 32): Curacao atmospheric profile with system ESM-b operating.
- Case 3C (Figures 33 and 34): Curacao atmospheric profile with system FCS operating.

b. Case 3 Results

(1) Signal Strength Results. Figure 31 reveals the extended range of the transmitted signal and the ability of a ESM system to detect it out to at least 250 nmi, the maximum range on the graph. This is compared to Figure 4 for the standard atmosphere.

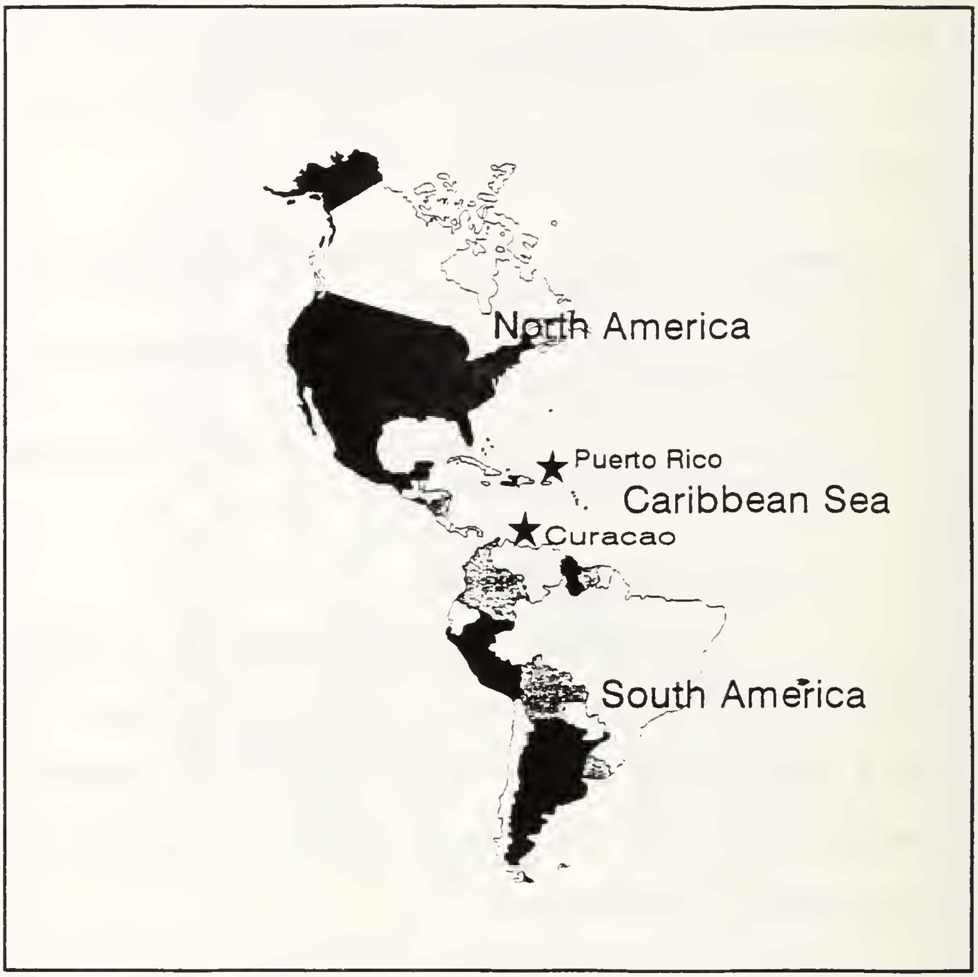

Figure 30 Geographical Locations Of The Caribbean Sites.

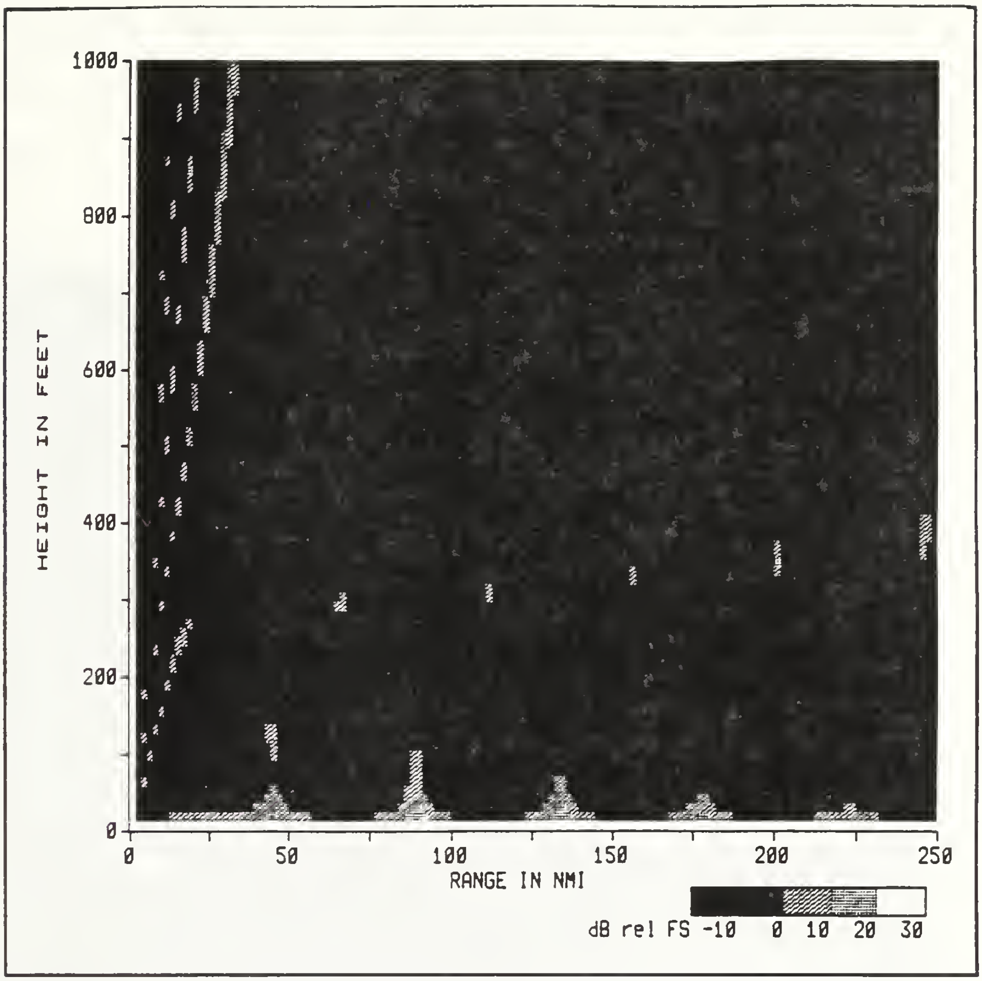

Figure 31 EMPE Signal Strength Prediction for Curacao, December 1985 (System ESM-a, 600 MHZ At 300 Feet). dB is relative to FS.

Figure 32 depicts strong main beam energy out to a least 250 nmi, the graph's maximum range, with some fluctuation present; compare to Figure 5 for the standard atmosphere.

A discontinuity of the signal is present around 25 nmi at 300 feet. A skip zone region is shown from approximately 10 nmi to 25 nmi.

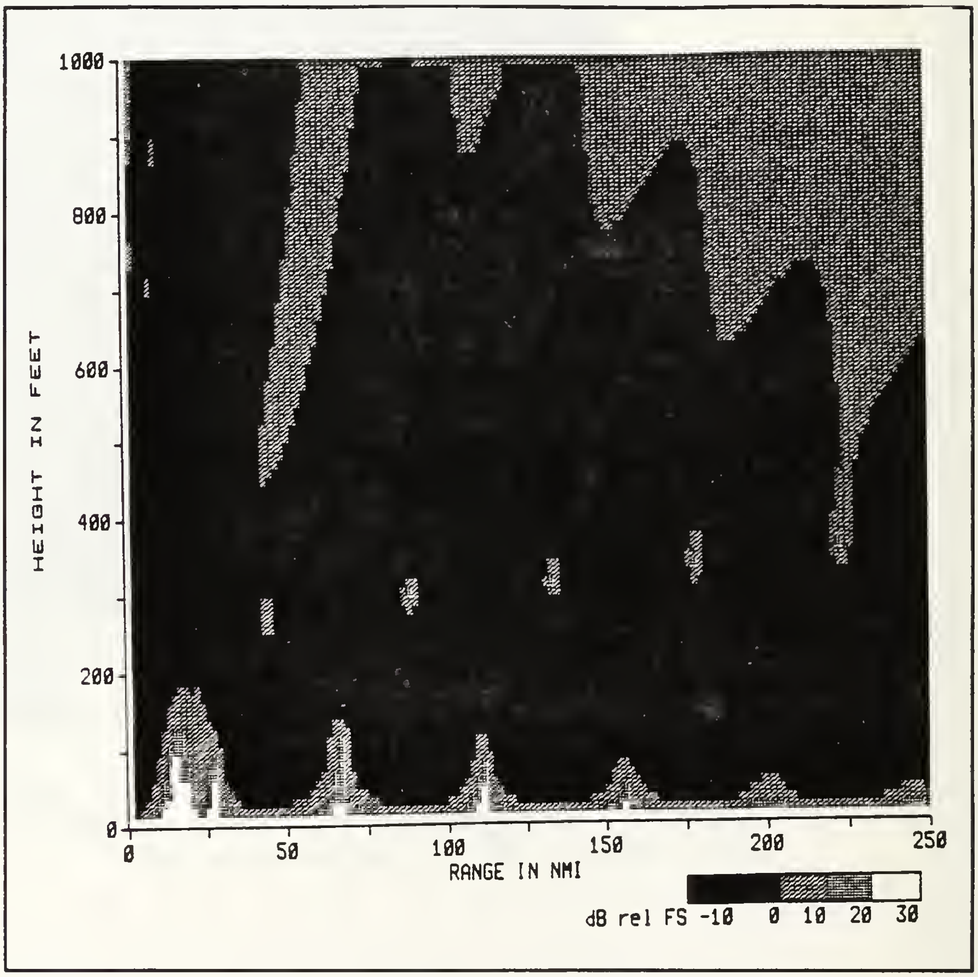

Figure 32 EMPE Signal Strength Prediction for Curacao, December 1985 (System ESM-b, 600 MHZ At 50 Feet). dB is relative to FS.

Figure 33 indicates a strong skip zone area from approximately 15 nmi to 40 nmi and a radar hole from approximately 50 nmi to 80 nmi, at a height above 400 feet.

A strong indication of ducting/channeling effect is present on the graph, extending out to the maximum range of the graph, 100 nmi, with some slightly greater signal loss directly above and below the duct. The probability of detection of the radar is very high in this dark region.

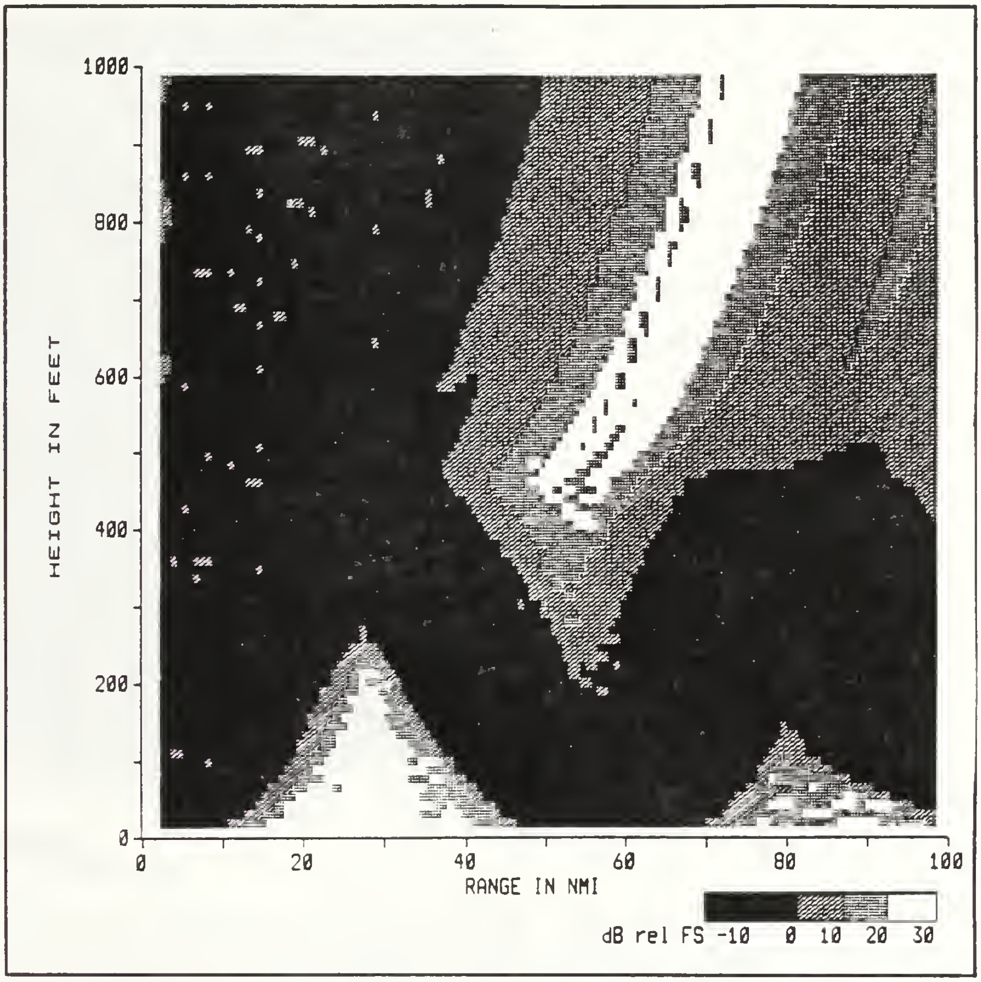

Figure 33 EMPE Signal Strength Prediction for Curacao, December 1985 (System FCS, 13 GHZ At 60 Feet; 100 nmi). dB is relative to FS.

Figure 34 reveals a strong signal out to 10 nmi with slightly higher losses throughout the graph; however, the system is very capable of detecting targets in this region.

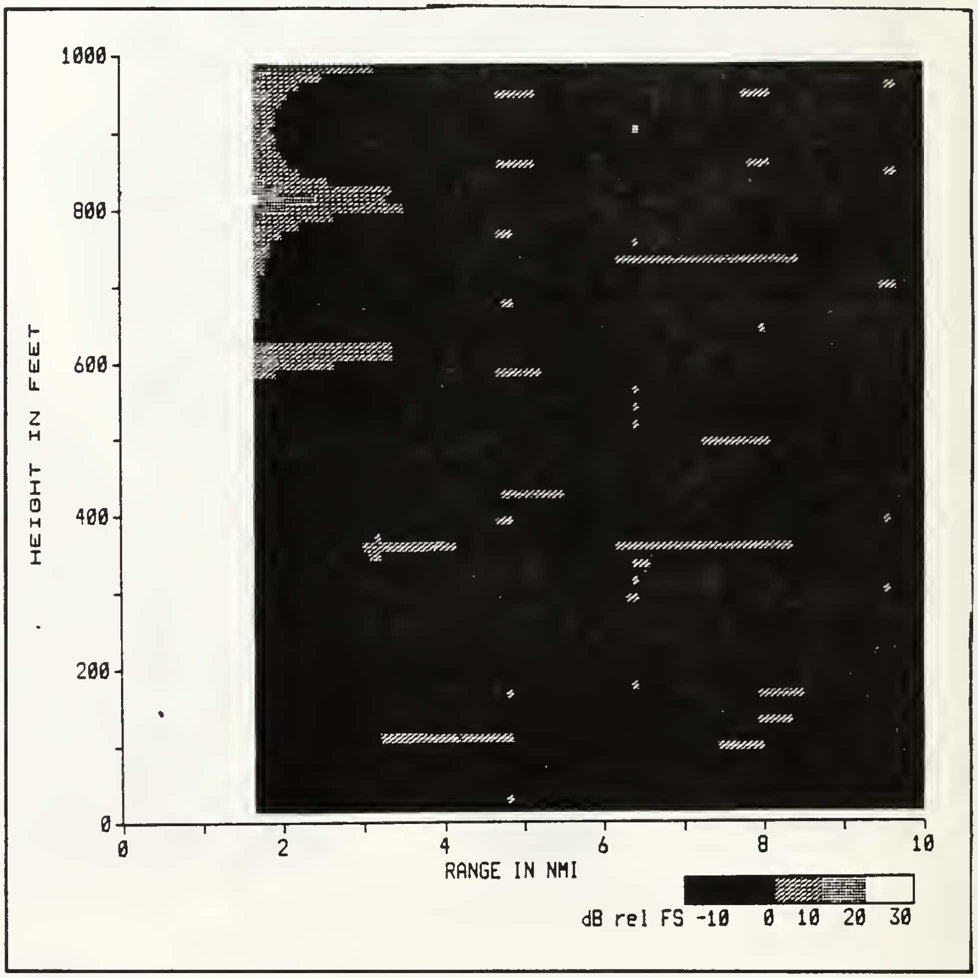

Figure 34 EMPE Signal Strength Prediction for Curacao, December 1985 (System FCS, 13 GHZ At 60 Feet; 10 nmi). dB is relative to FS.

(2) EREPS and EMPE Loss Predictions. EREPS (PROPR) illustrates how a ducting environment enabled systems to perform better as compared to a free space envrionment. EMPE Transmission Loss plots gave a more detailed look at the signal loss experienced at a set height.

Figure 35 (EREPS) reveals a skip zone from about 15 nmi to 40 nmi, with the signal loss steadily increasing out to 250 nmi. Figure 36 (EMPE) illustrates some decrease in signal loss from 10 nmi to 20 nmi, then a drastic increase of signal loss was revealed from about 20 nmi to 49 nmi, with a slight skip zone region present from 20 nmi to 52 nmi. Various dropouts occurred in this region. For a ESM communications system, this variation in signal strength can lead to detection loss of the emitter.

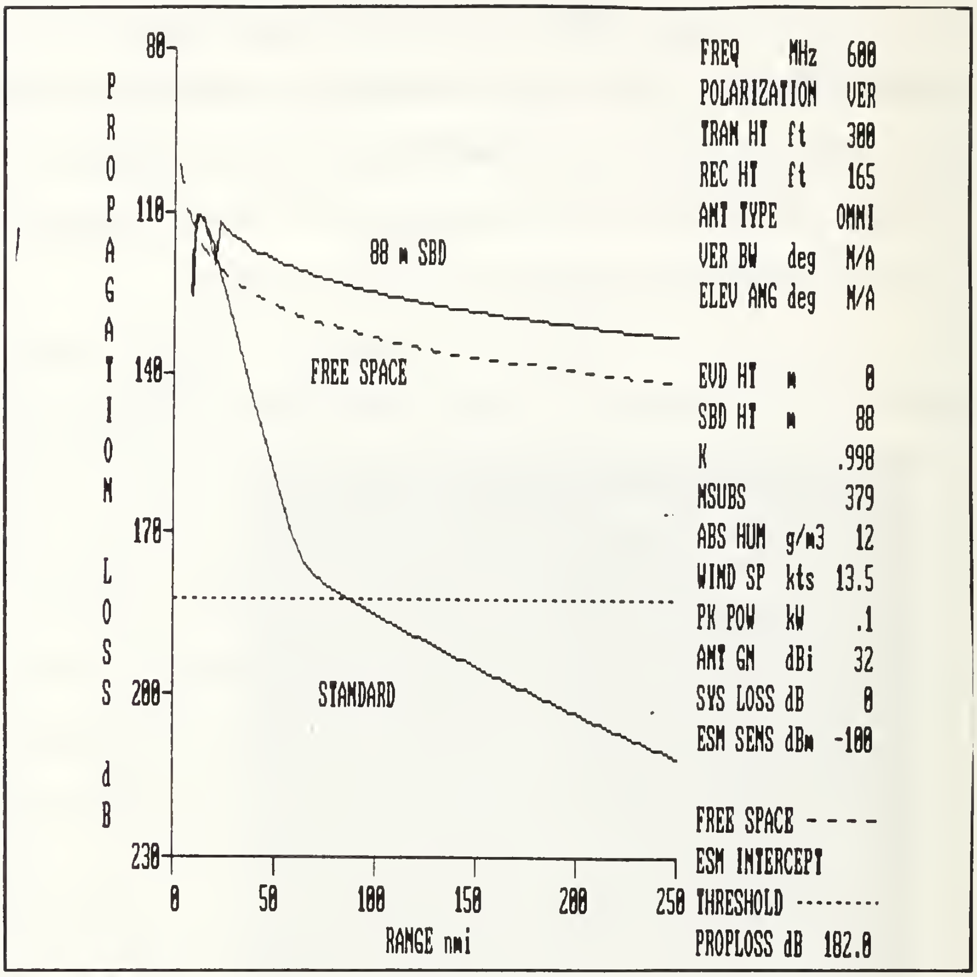

Figure 35 EREPS (PROPR) Prediction for Curacao, December 1985 (System ESM-a operating).

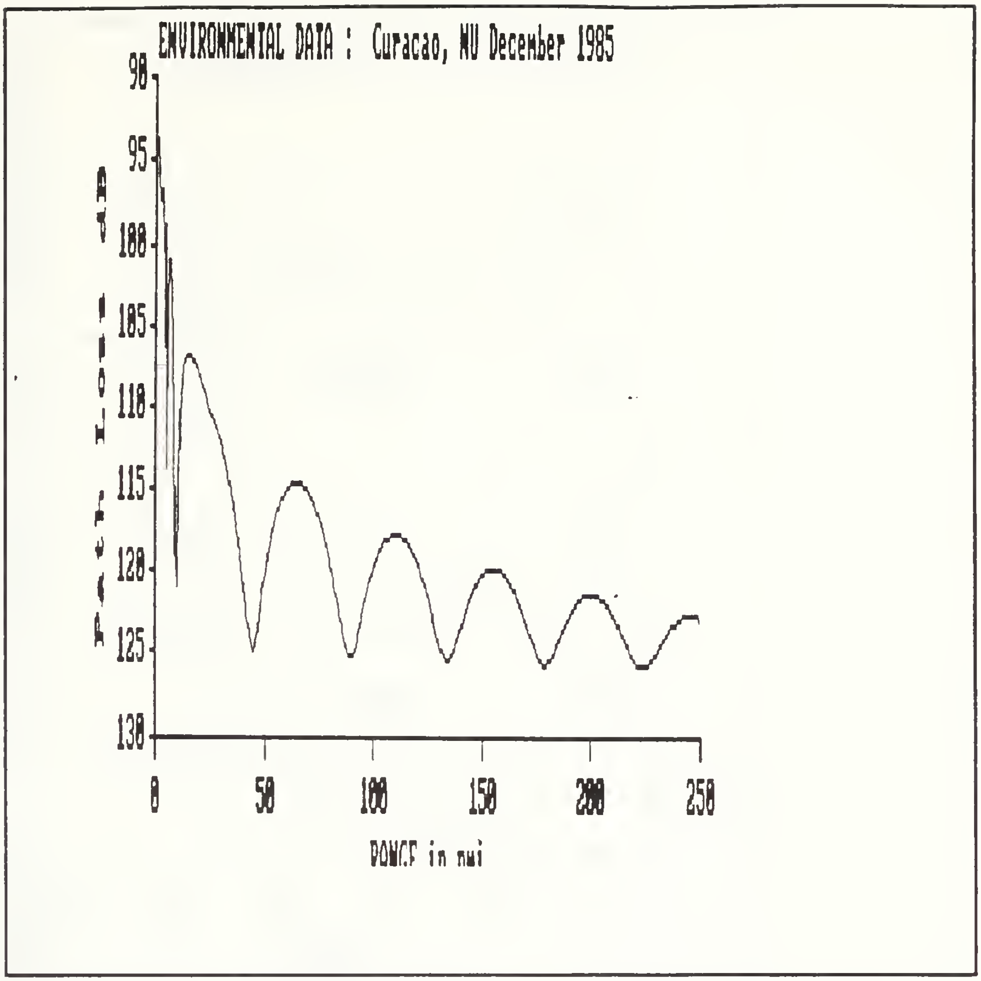

Figure 36 EMPE Transmission Loss Prediction for Curacao, December 1985 (System ESM-a operating).

Figures 37 (EREPS) and 38 (EMPE) reveal a drastic increase of signal loss from 0 to approximately 20 nmi, with some slight fluctuation present in Figure 38 around 25 nmi. Figure 37 indicates a skip zone area from 20 nmi to 30 nmi, then signal loss increasing steadily; whereas, Figure 38 reveals much greater dropouts (fluctuations) in the signal loss.

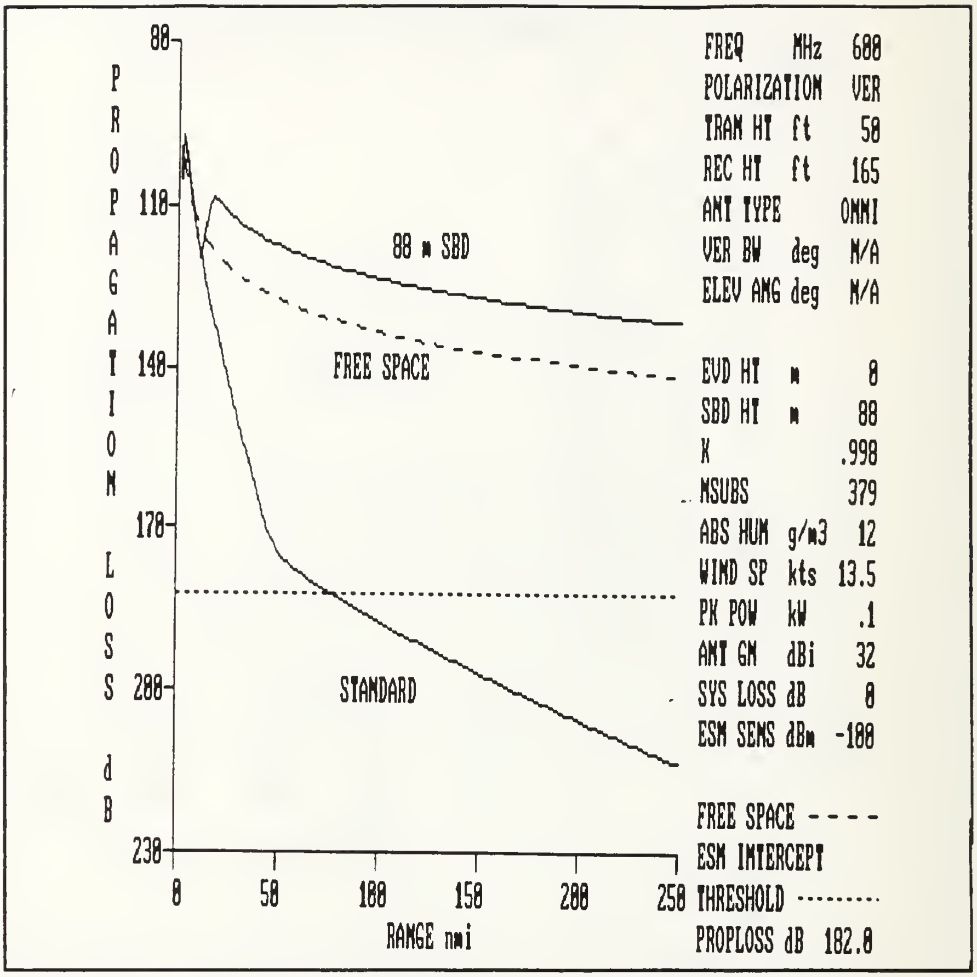

Figure 37 EREPS (PROPR) Prediction for Curacao, December 1985 (System ESM-b operating).

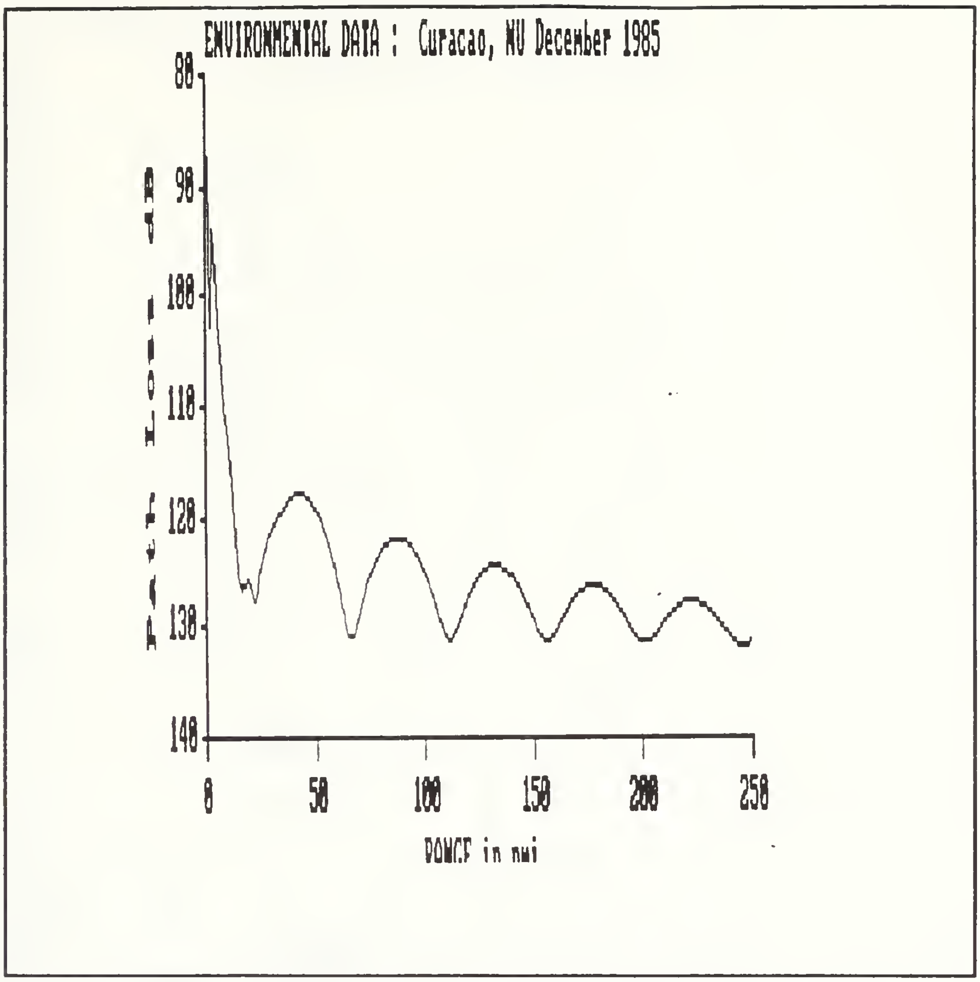

Figure 38 EMPE Transmission Loss Prediction for Curacao, December 1985 (System ESM-b operating).

Figure 39 reveals only a steady decline of signal strength with distance; whereas, Figure 40 indicates severe signal fluctuation across that area.

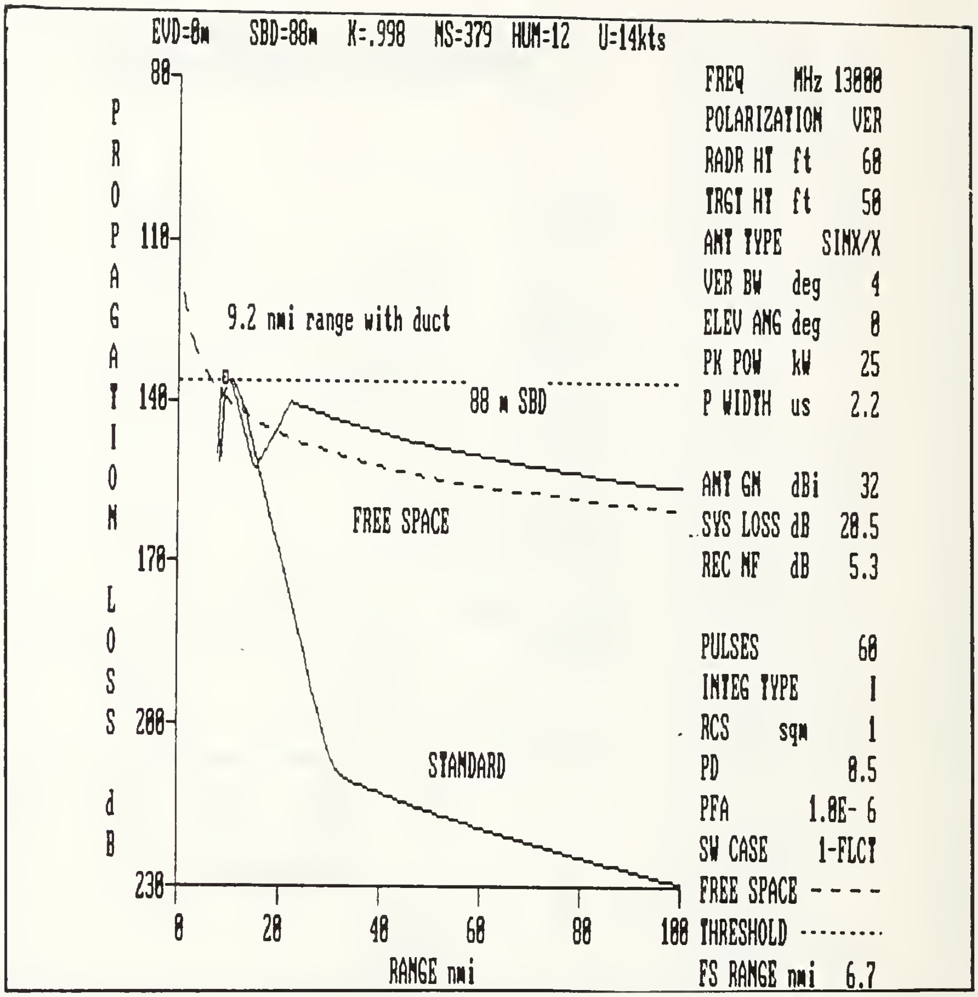

Figure 39 EREPS (PROPR) Prediction for Curacao, December 1985 (System FCS operating).

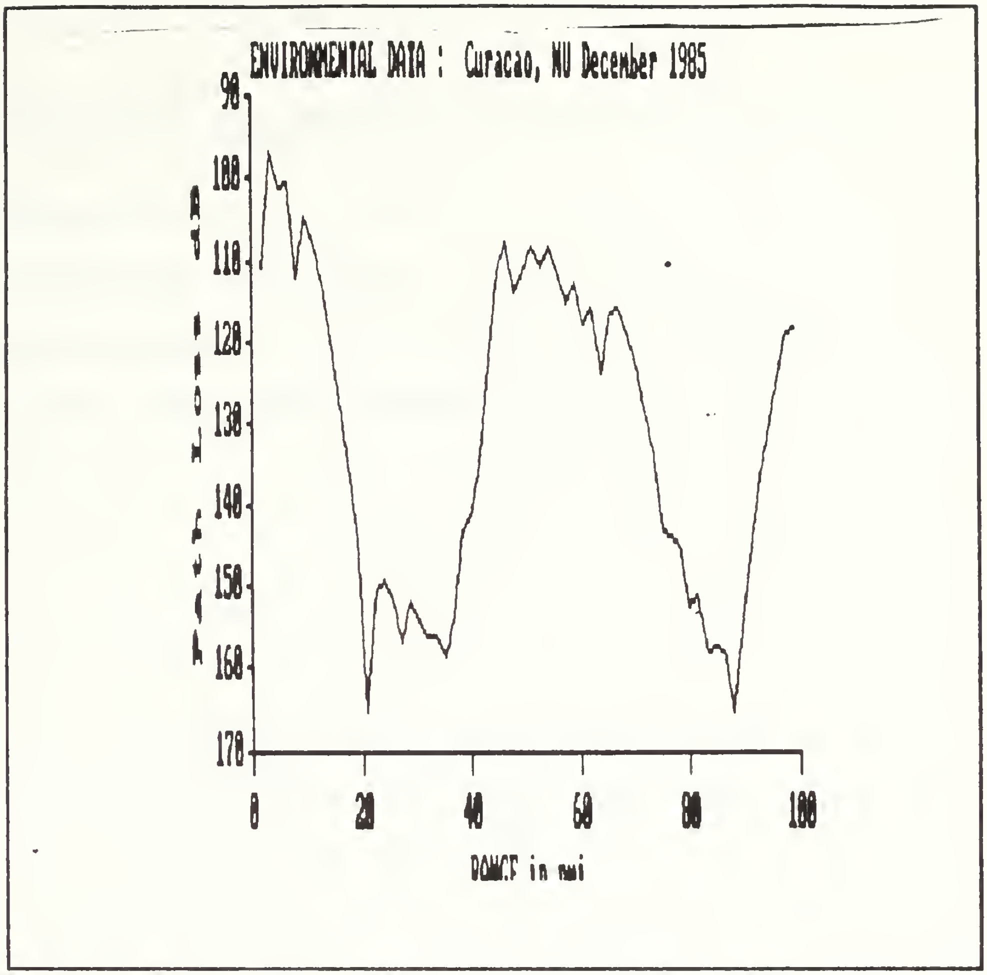

Figure 40 EMPE Transmission Loss Prediction for Curacao, December 1985 (System FCS operating).

C. SUMMARY

The purpose of this chapter was to show the different effects of various atmospheres on a fire control radar system and a passive ESM system. A comparison between a homogeneous ducting environment to that of no ducting, or a standard atmosphere, was conducted to reveal how a ducting environment can lead to extended RF ranges, radar/radio holes and height errors that affect operational systems. Results were variable between systems, as well as between the different environments. This variation, therefore, supports the need to rely on EM propagation systems to help determine individual system performances in a particular operating environment. EMPE and EREPS were chosen for the purpose of displaying how variations in signal strength existed for different systems.

VI. ASSESSMENT OF HORIZONTALLY INHOMOGENEOUS PROFILES

A. INTRODUCTION

This chapter will present results with horizontal inhomogeneous profiles. Because environmental refractivity changes occurred over long ranges, these results will be analyzed with regard to effects on systems ESM-a and ESM-b only. The purpose of selecting horizontally inhomogeneous profiles was to demonstrate how EMPE can be useful to model this condition and also show that even though similarities exist between homogeneous and inhomogeneous profiles, differences are present and errors can result when horizontal homogeneity is incorrectly assumed.

The same operating systems and times of year used for the horizontal homogeneous cases were also used in this portion.

B. CASE STUDIES

Three different geographical parts of the world are viewed as follows:

- For the Persian Gulf area, an inhomogeneous profile was done from Abu Dhabi to Bandar Abbas (185 nmi apart). Figures 41 and 42 indicate the duct thickness for each of the individual sites.
- For the Indian Ocean area, an inhomogeneous profile was done from Diego Garcia to Bangkok (2069 nmi apart). Figures 43 and 44 represent the refractivity profile for each individual site.

- For the Caribbean area, an inhomogeneous profile was done from Curacao to Puerto Rico (411 nmi apart). Figures 45 and 46 indicate the duct thickness for each individual site.

These profiles are presented to show the effects of various atmospheric conditions across a coastal transition (Persian Gulf), across a large land mass/ocean boundary (Indian Ocean), and between small land masses (Caribbean). When operating in the open ocean, a horizontally homogeneous environment will generally be experienced; however, when operating around such areas as the Persian Gulf, a horizontally inhomogeneous profile will be more prevalent. Six soundings were obtained from historical sources; one for each site above.

Table VI is a summary of the cases related to this chapter.

TABLE VI SUMMARY OF RANGE DEPENDENT CASES.

CASES	PROFILE	SYSTEM	TRANSMITTER HEIGHT	TRANSMITTER POWER	FREQUENCY	FIGURE
4A (1A)	Persian Gulf	ESM-a	300 ft	0.1 KW	600 MHZ	47
4B (1B)	Persian Gulf	ESM-b	50 ft	0.1 KW	600 MHZ	48
5A (2A)	Indian Ocean	ESM-a	300 ft	0.1 KW	600 MHZ	51
5B (2B)	Indian Ocean	ESM-b	50 ft	0.1 KW	600 MHZ	52
6A (3A)	Caribbean	ESM-a	300 ft	0.1 KW	600 MHZ	55
6B (3B)	Caribbean	ESM-b	50 ft	0.1 KW	600 MHZ	56

All cases vertically polarized with a 4 degree beamwidth and a 1 degree beam elevation.

The objective of this chapter will be to evaluate the profiles going one way instead of both ways. Moving the emitter to the receiver site, and vice versa, would not add any new information to the study, as the existing medium would produce a reciprocal path with the same results.

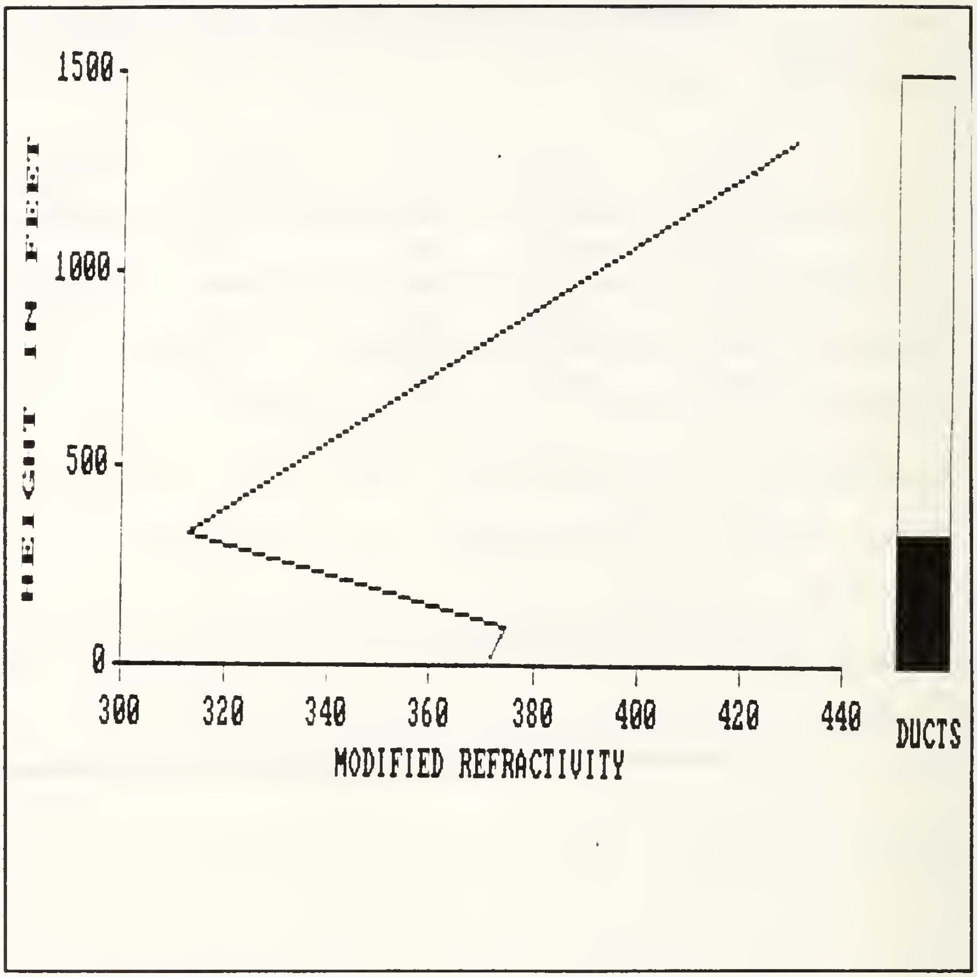

Figure 41 Refractivity Profile For Abu Dhabi.

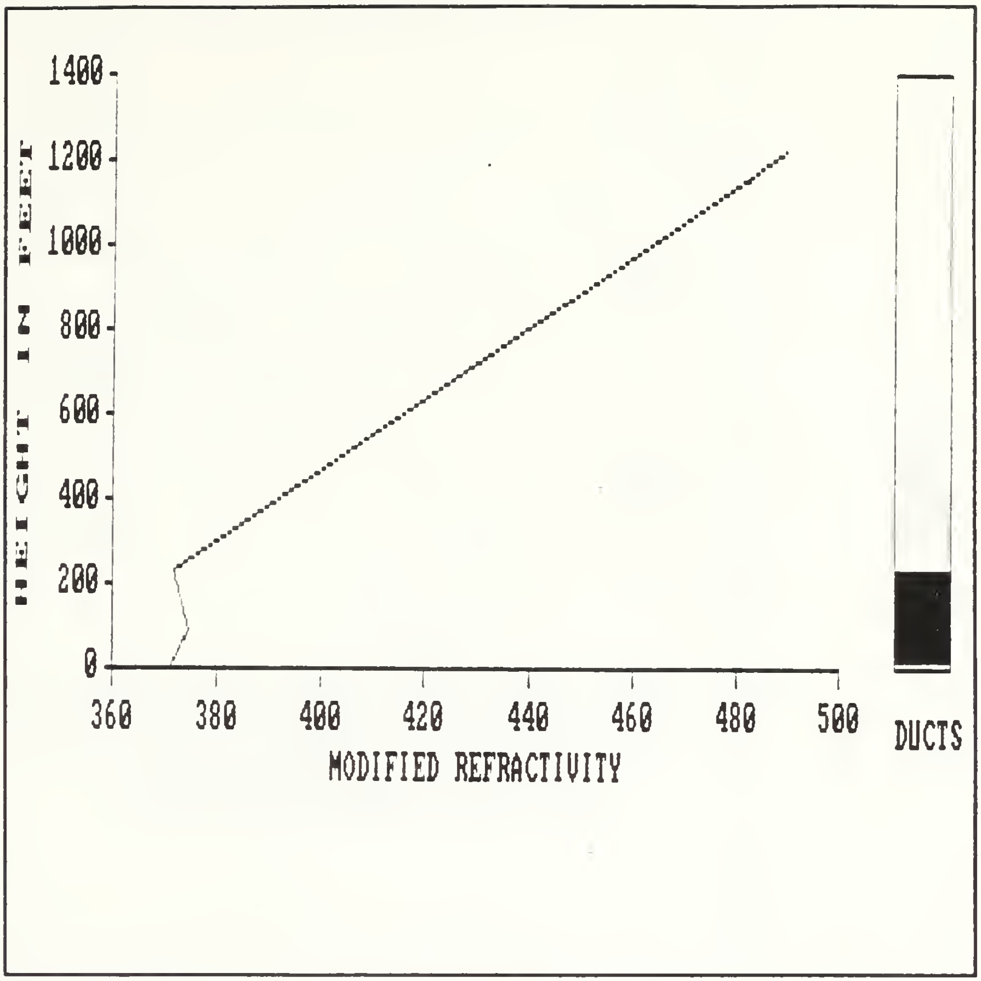

Figure 42 Refractivity Profile For Bandar Abbas.

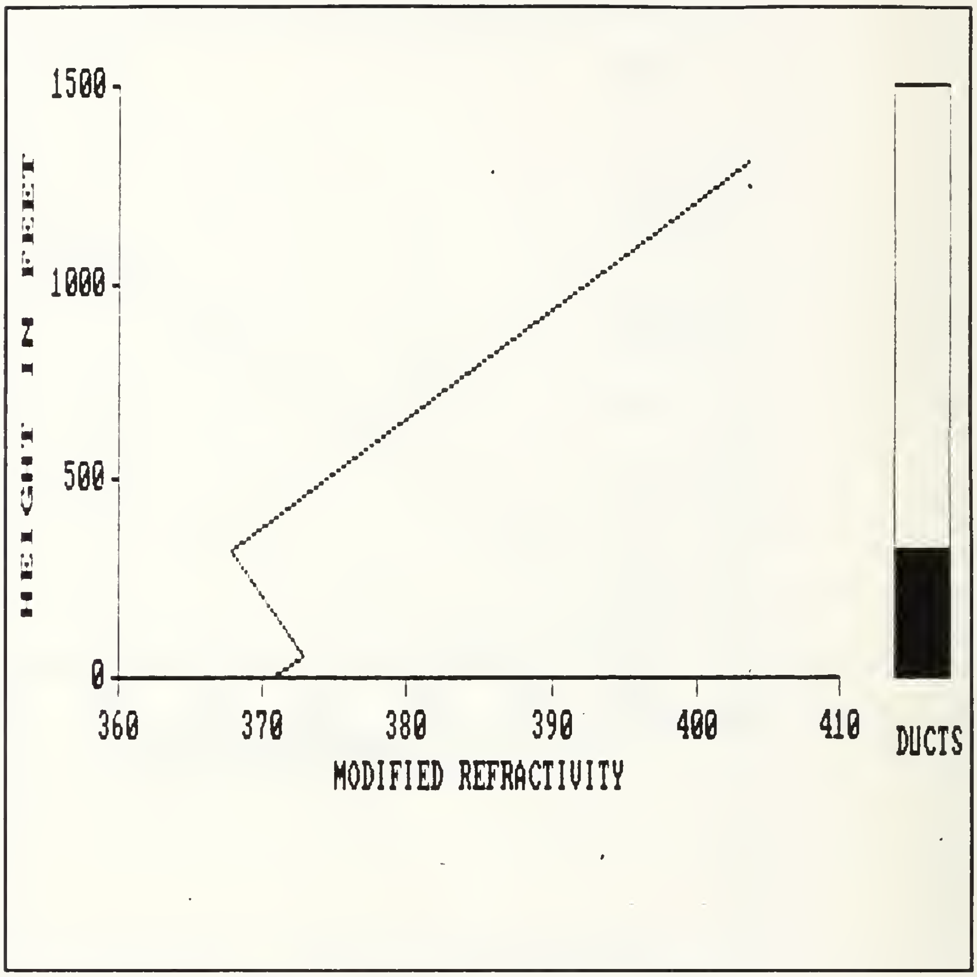

Figure 43 Refractivity Profile Of Diego Garcia.

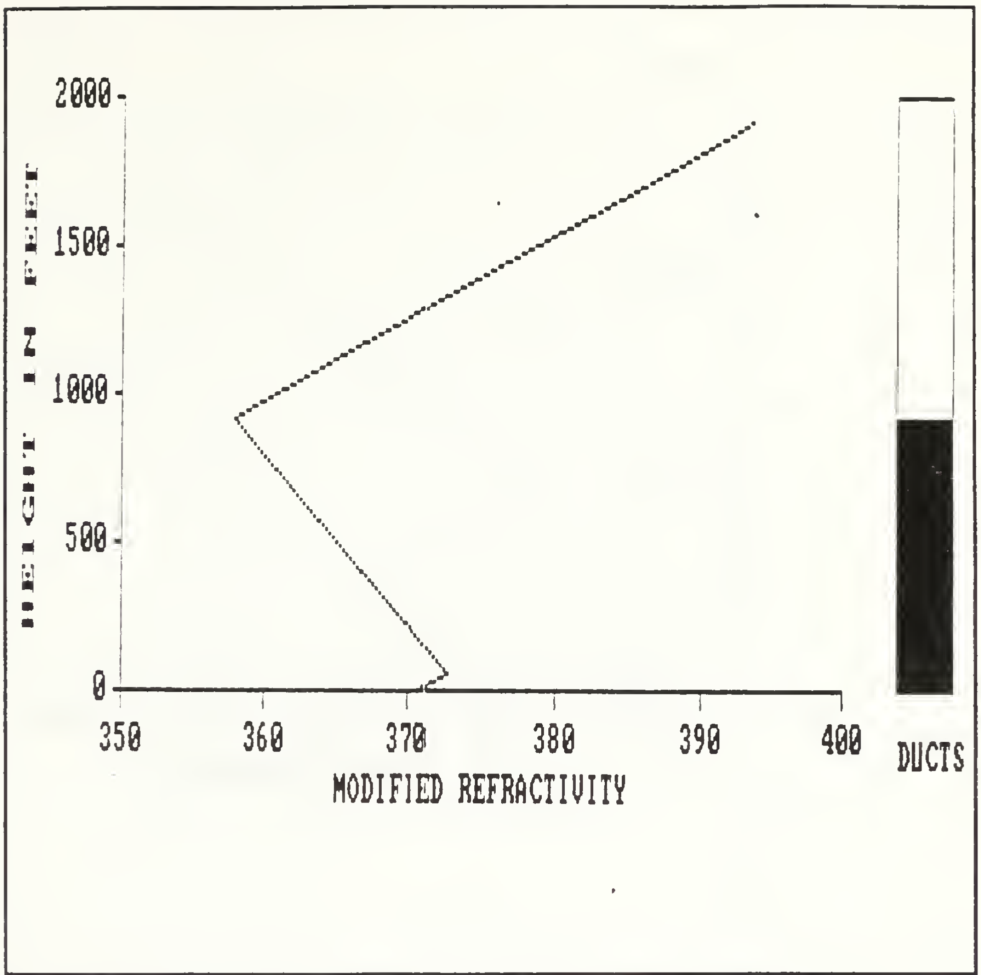

Figure 44 Refractivity Profile Of Bangkok.

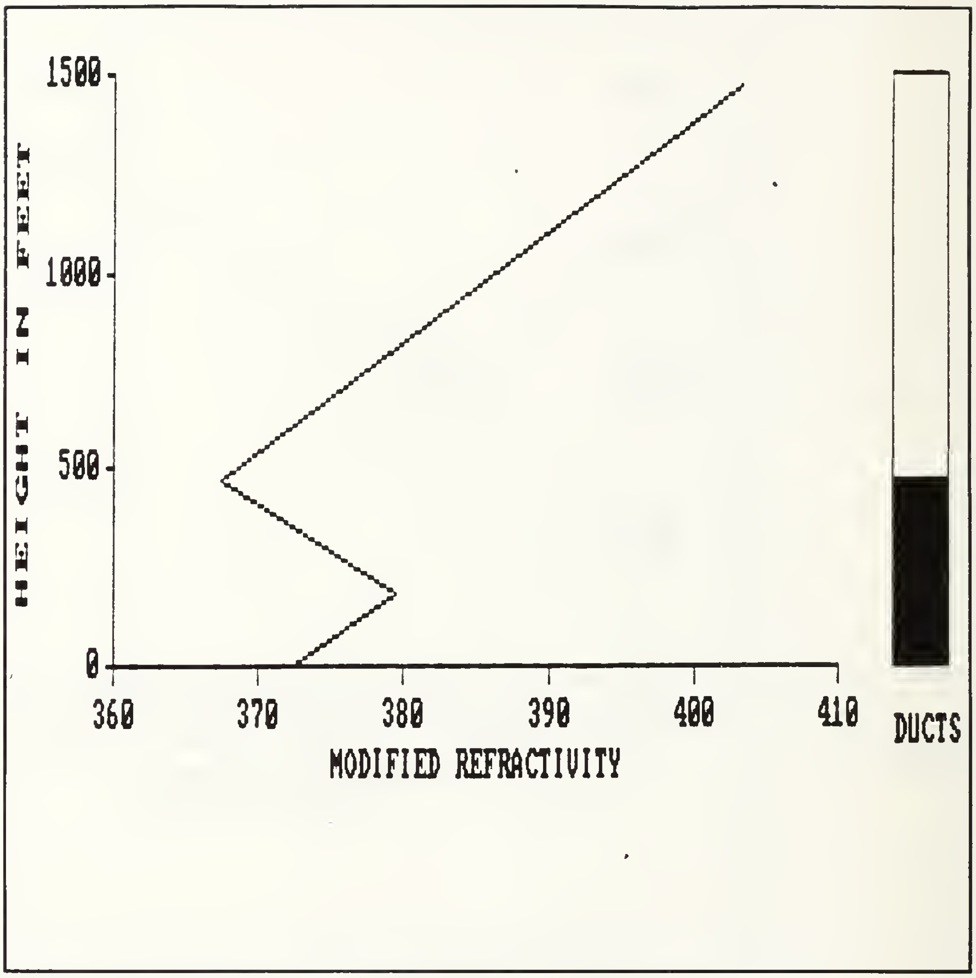

Figure 45 Refractivity Profile Of Curacao.

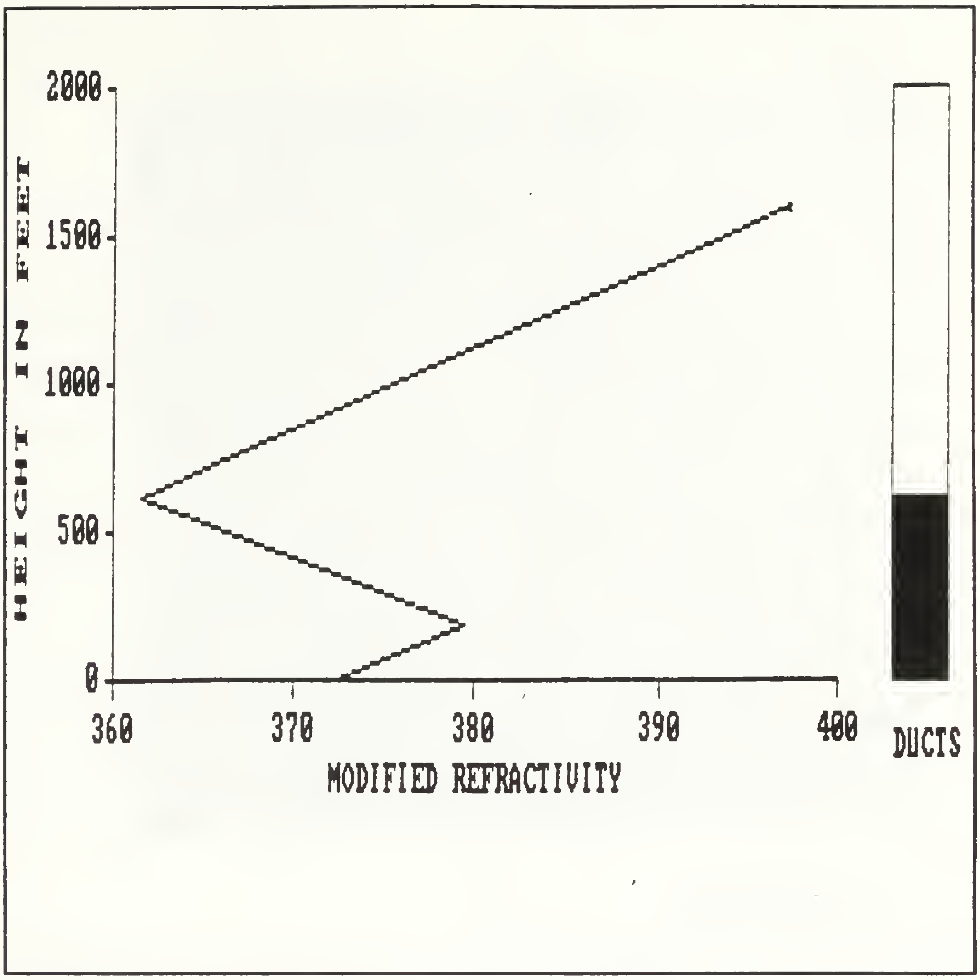

Figure 46 Refractivity Profile Of Puerto Rico.

1. Case 4 - Persian Gulf

a. Persian Gulf Profile

The inhomogeneous profile was chosen between the two sites of Abu Dhabi and Bandar Abbas (going from Abu Dhabi to Bandar Abbas). The cases considered are as follows:

- CASE 4A (Figure 47): Inhomogeneous profile for system ESM-a. This case can be compared to Case 1A of the previous chapter.

- CASE 4B (Figure 48): Inhomogeneous profile for system ESM-b. This case can be compared to Case 1B of the previous chapter.

b. Case 4 Results

(1) Signal Strength Results. Figure 47 (Case 4A) illustrates how this particular inhomogeneous region was conducive to extended ranges and is an ideal operating environment for a ESM system or any communications system desiring either to intercept or maintain communications at long ranges. A comparison of Figure 47 to the homogeneous environment (Figure 9) reveals various skip zones throughout the scene in both; however, Figure 47 displays an additional skip zone from approximately 220 nmi out to the end of the graph.

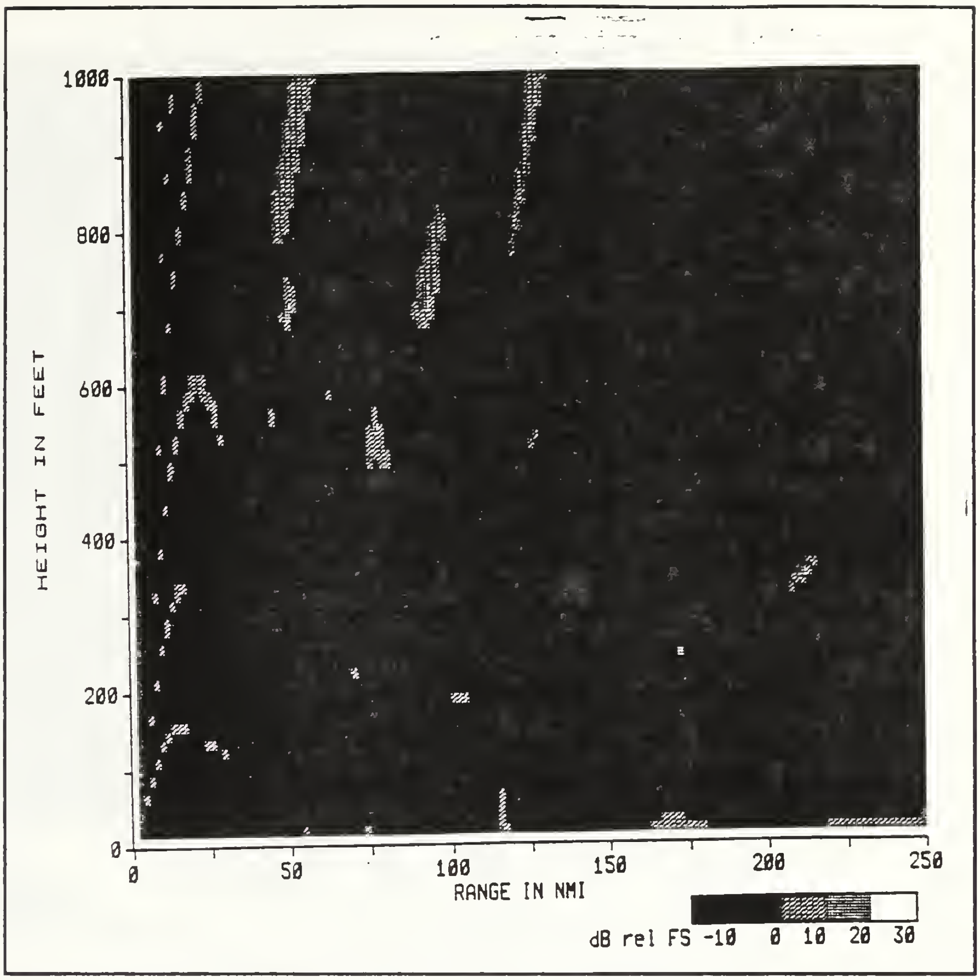

Figure 47 EMPE Signal Strength Prediction For The Persian Gulf (System ESM-a, 600 MHZ At 300 Feet), dB is relative to FS.

Figure 48 for Case 4B, depicts the ESM system's ability to detect strong signals out to a range of at least 250 nmi, the maximum distance on the graph. When compared to Figure 10 of the homogeneous environment, Figure 48 displays another skip zone region from approximately 200 nmi out to at least 250 nmi.

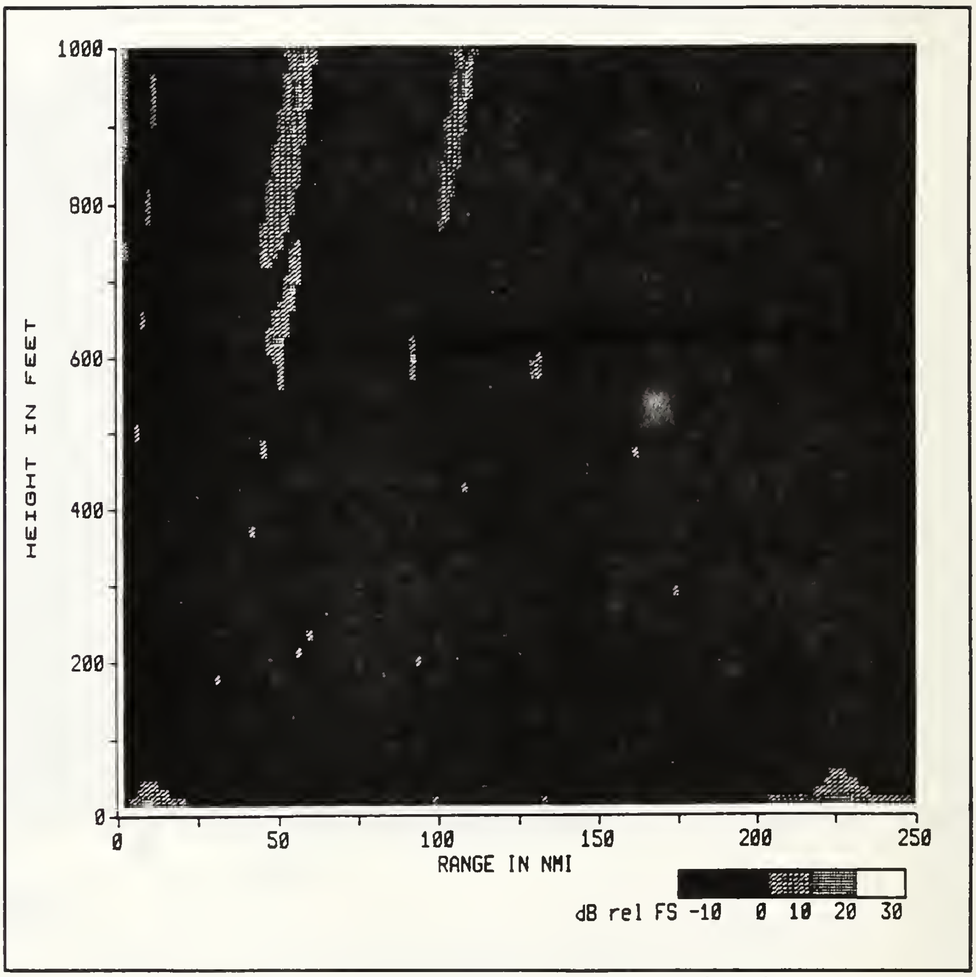

Figure 48 EMPE Signal Strength Prediction For The Persian Gulf (System ESM-b, 600 MHZ At 50 Feet), dB is relative to FS.

(2) EMPE Loss Predictions. Figure 49 displays various minima, which indicate significant signal fluctuations. Compared to the homogeneous environment of Figure 16, both indicate severe dropouts. Figure 49 reveals some greater loss (approximately 137 dB) around 50 nmi; whereas, Figure 16 indicates greater loss (approximately 168 dB) at a range of 200 nmi.

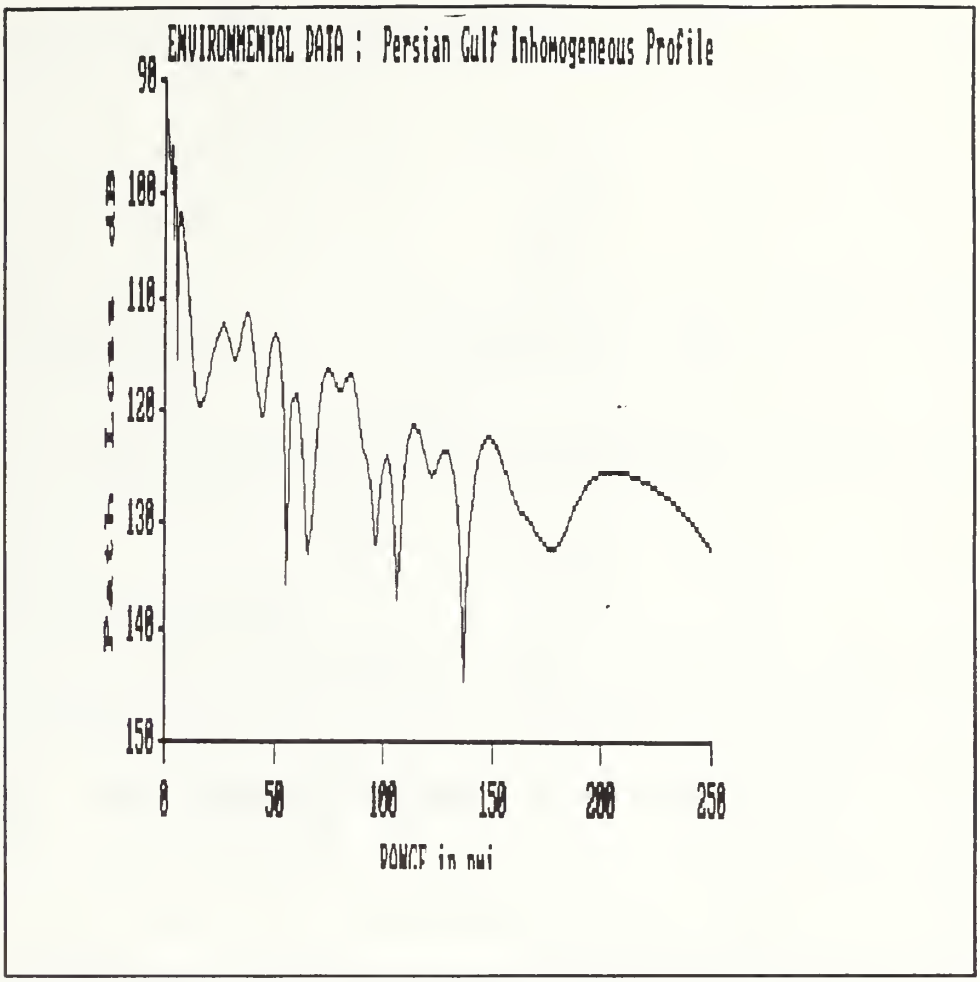

Figure 49 EMPE Transmission Loss Prediction For The Persian Gulf (System ESM-a operating).

Figure 50 indicates once again an ever changing signal strength. Comparing Figure 50 to Figure 17 for the homogeneous environment, a larger number of dropouts are present for the latter case, indicating greater signal loss for the homogeneous condition. At one point, however, Figure 50 indicates a loss of approximately 145 dB around 75 nmi.

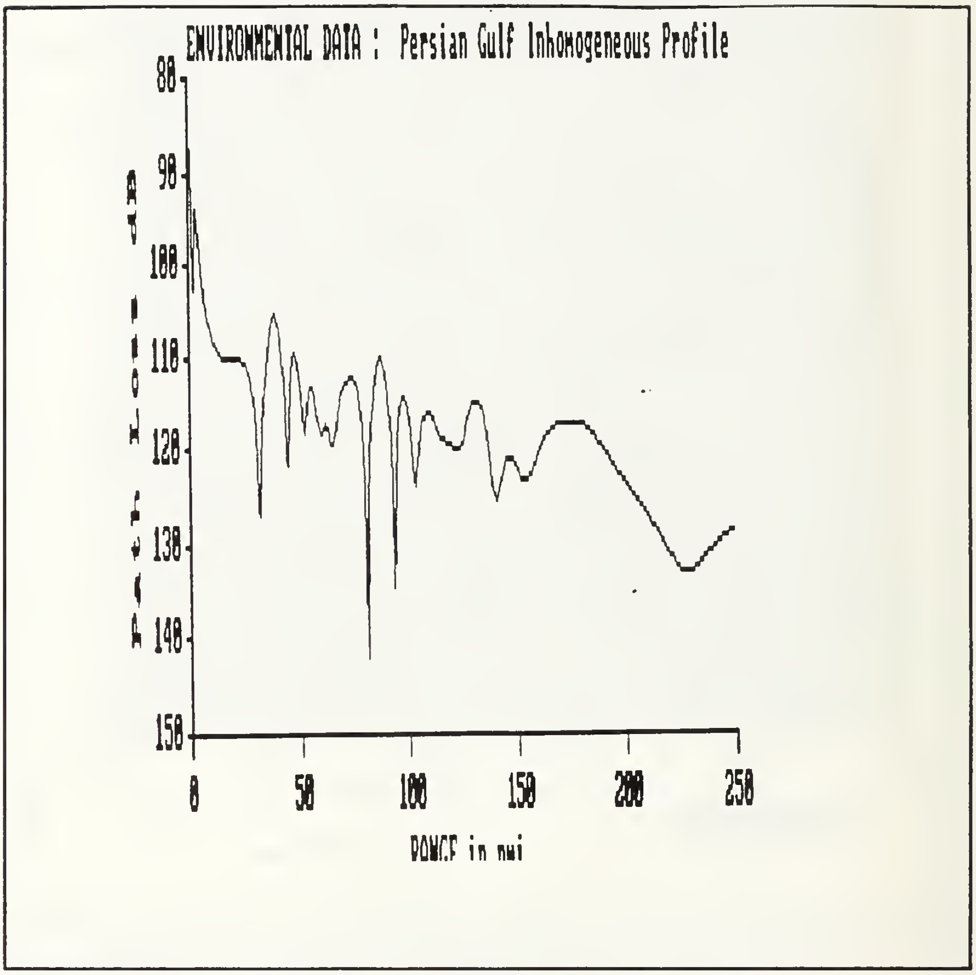

Figure 50 EMPE Transmission Loss Prediction For The Persian Gulf (System ESM-b operating).

2. Case 5 - Indian Ocean

a. Indian Ocean Profile

The two sites chosen for this study were Diego Garcia and Bangkok. Although the sites are at a distance greater than 250 nmi, the maximum range on the graphs, these were chosen to represent variations that could occur across a large land mass/ocean boundary. It was necessary to include this area because of the number of Naval deployments around the Indian Ocean, and the need to alert tactical commanders of the existence of inhomogeneous conditions. The following cases are considered:

- CASE 5A (Figure 51): Inhomogeneous profile for system ESM-a. This case can be compared to Case 2A of the previous chapter.
- CASE 5B (Figure 52): Inhomogeneous profile for system ESM- b. This case can be compared to Case 2B of the previous chapter.

b. Case 5 Results

(1) Signal Strength Results. Figure 51 (Case 5A) indicates a very suitable area for a passive ESM system to operate, due to minimal signal loss and extended range of the emitter. A comparison of Figure 51 to the homogeneous environment of Figure 20 illustrates how the signal is very strong out to at least the maximum range on the graph, 250 nmi, for Figure 51. Figure 20 indicates a large skip zone region extending from 100 nmi out to at least 250 nmi.

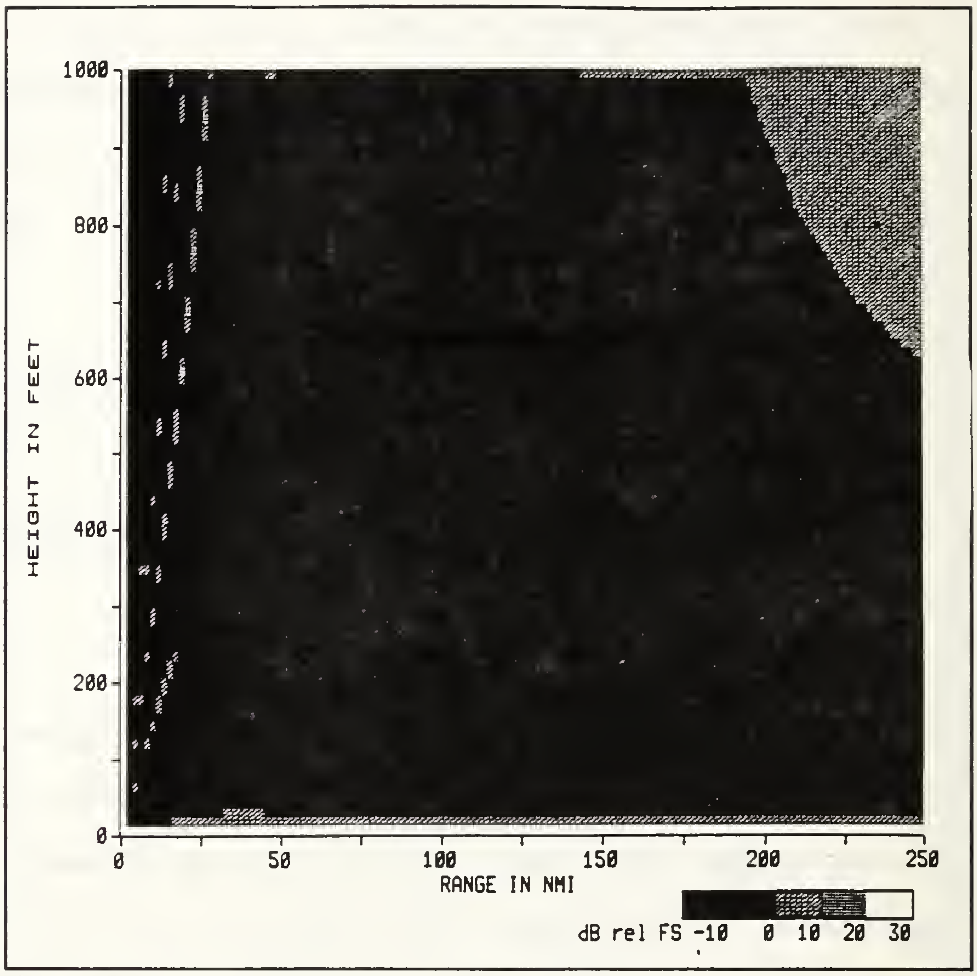

Figure 51 EMPE Signal Strength Prediction For The Indian Ocean (System ESM-a, 600 MHZ At 300 Feet), dB is relative to FS.

Figure 52 for Case 5B once again reveals the ability of a transmitting system to be detected at greater ranges with relatively small signal loss. Figure 21, the homogeneous environment, does not reveal that large of a signal strength out beyond 100 nmi. Also, a very large skip zone starts to form around 120 nmi and is present out to the maximum distance on the graph in Figure 21.

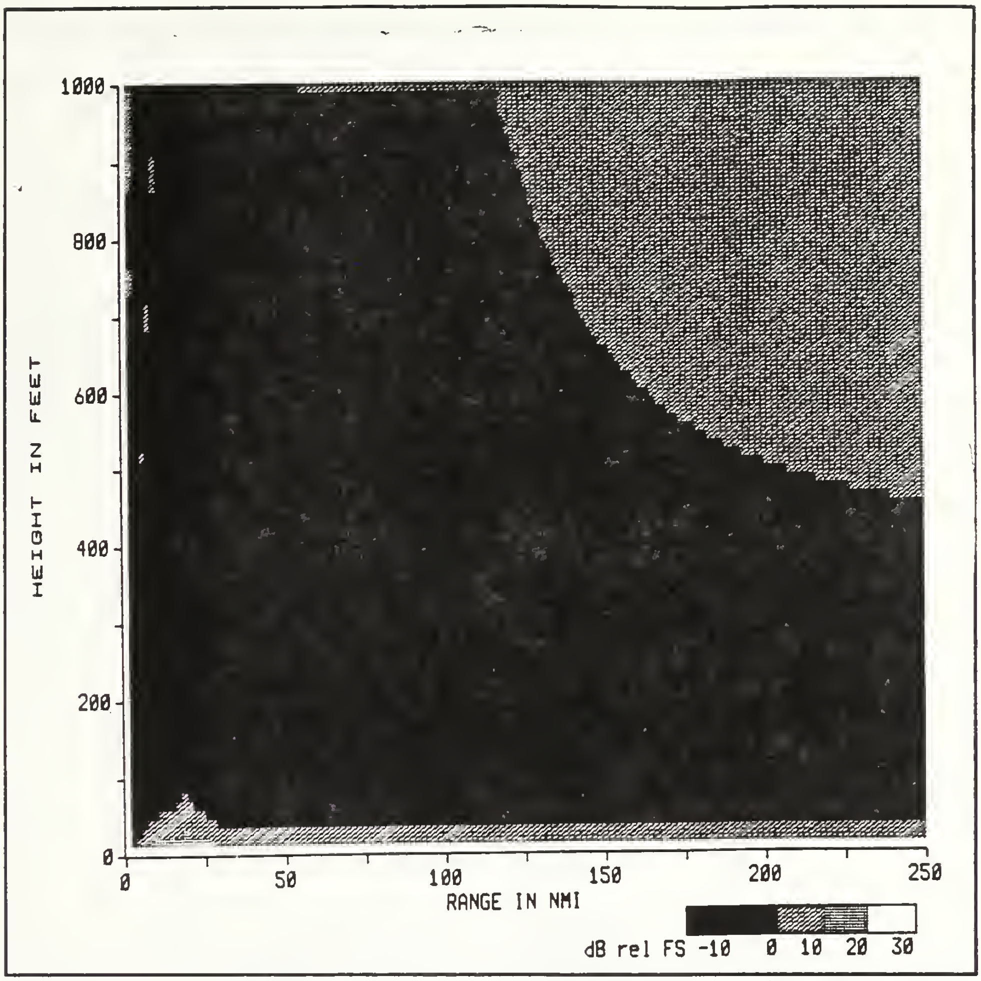

Figure 52 EMPE Signal Strength Prediction For The Indian Ocean (System ESM-b, 600 MHZ At 50 Feet), dB is relative to FS.

(2) EMPE Loss Predictions. Figure 53 reveals a loss in signal strength from approximately 50 nmi out to 250 nmi, the same signal loss for the homogeneous environment in Figure 25.

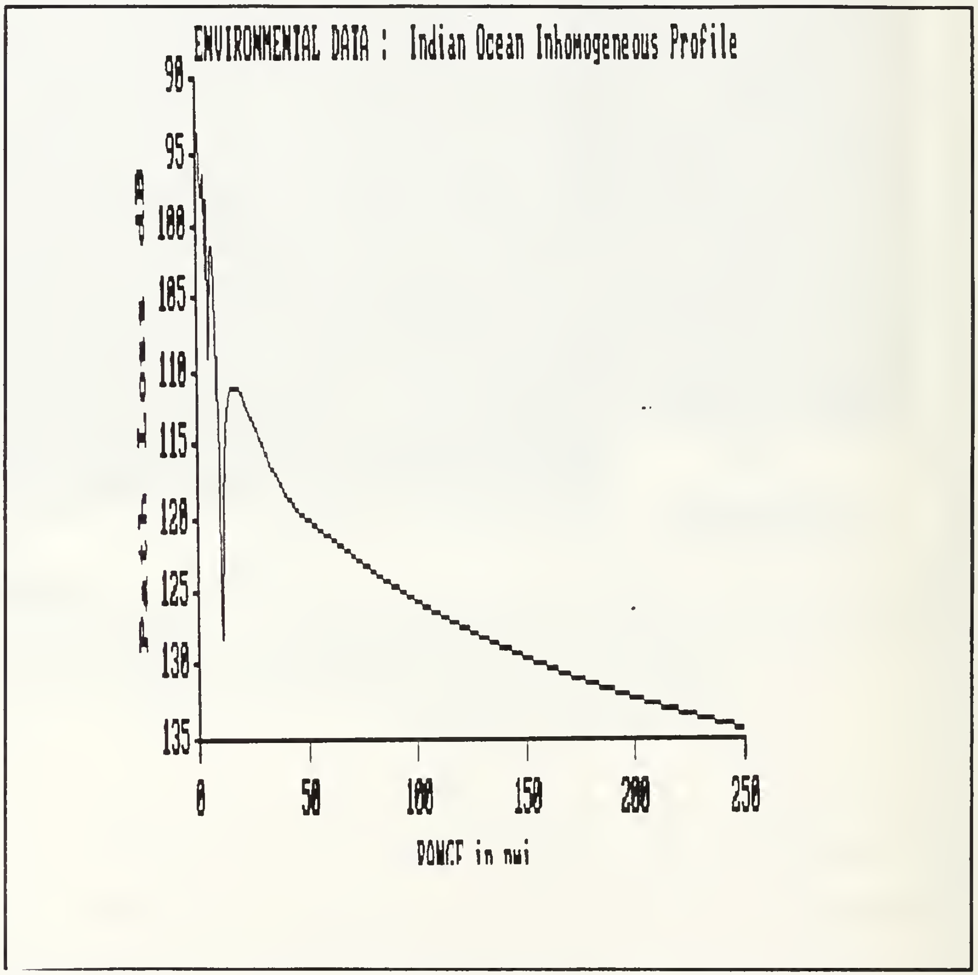

Figure 53 EMPE Transmission Loss Prediction For The Indian Ocean (System ESM-a operating).

Figure 54 reveals the same type of signal loss in the area from 10 nmi to 50 nmi as for the homogeneous case in Figure 27.

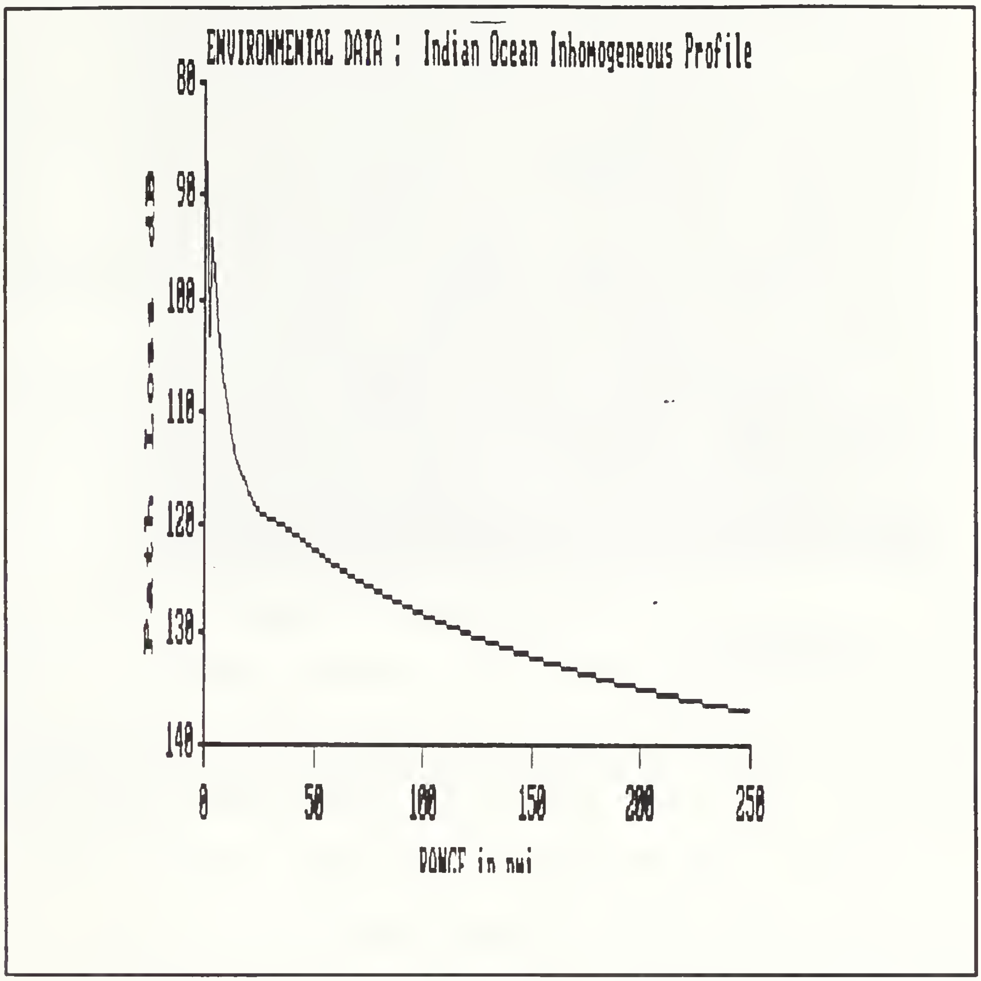

Figure 54 EMPE Transmission Loss Prediciton For The Indian Ocean (System ESM-b operating).

3. Case 6 - Caribbean

a. Caribbean Profile

The two sites chosen to represent this area went from Curacao to Puerto Rico. Once again these sites were not used to represent a 250 nmi separation as shown on the graphs, but to represent the variations that exist near small land masses. The following cases are considered:

- CASE 6A (Figure 55): Inhomogeneous profile for system ESM- a. This can be compared to Case 3A in the previous chapter.
- CASE 6B (Figure 56): Inhomogeneous profile for system ESM- b. This case can be compared to Case 3B in the previous chapter.

b. Case 6 Results

(1) Signal Strength Results. Figure 55 (Case 6A) indicates the ability of the ESM system to detect strong signals out to at least 250 nmi, the maximum range on the graph. A similar type of diplay is shown in Figure 31 for the homogeneous environment. A number of skip zone regions are revealed throughout these graphs.

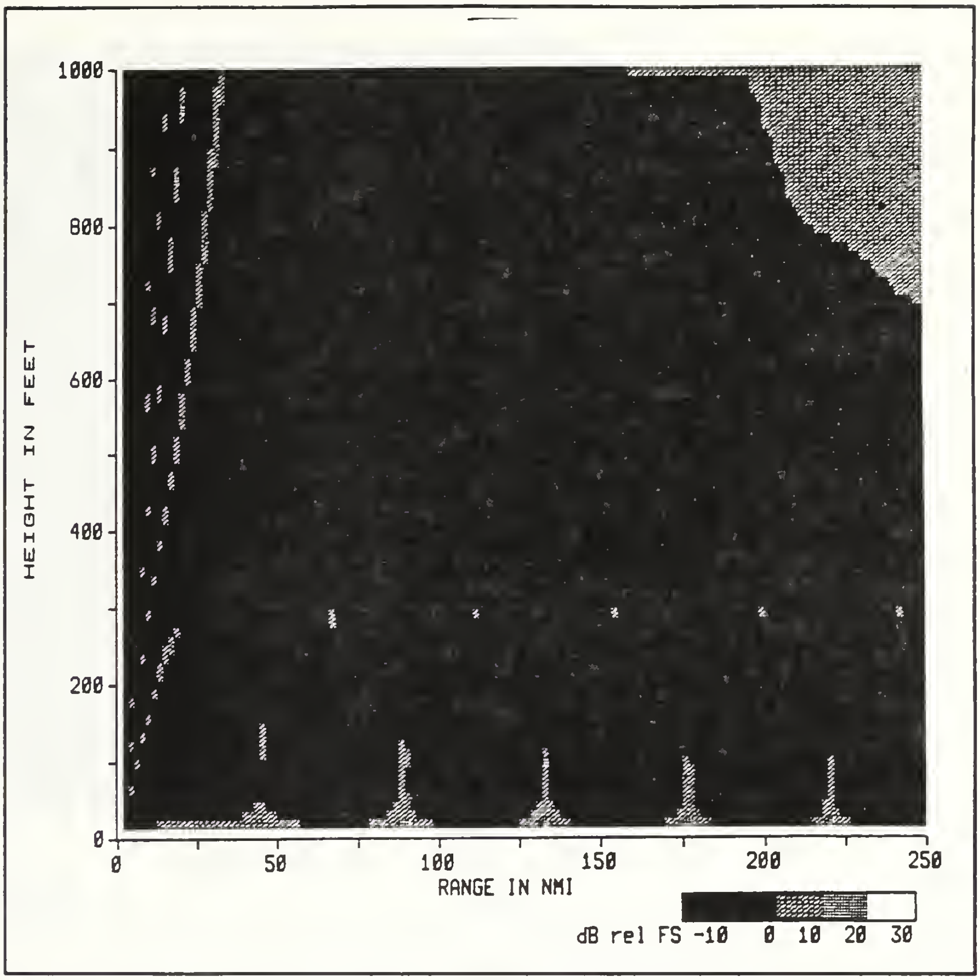

Figure 55 EMPE Signal Strength Prediction For The Caribbean (System ESM-a, 600 MHZ At 300 Feet), dB is relative to FS.

Figure 56 (Case 6B) reveals how the transmitted signal is extended out to at least 250 nmi, giving the ESM system perfect opportunity to detect the operating system. Figure 32, the homogeneous environment, reveals the same results. Both figures have some strong skip zone regions present, although the skip zone heights are greater for the inhomogeneous than the homogeneous.

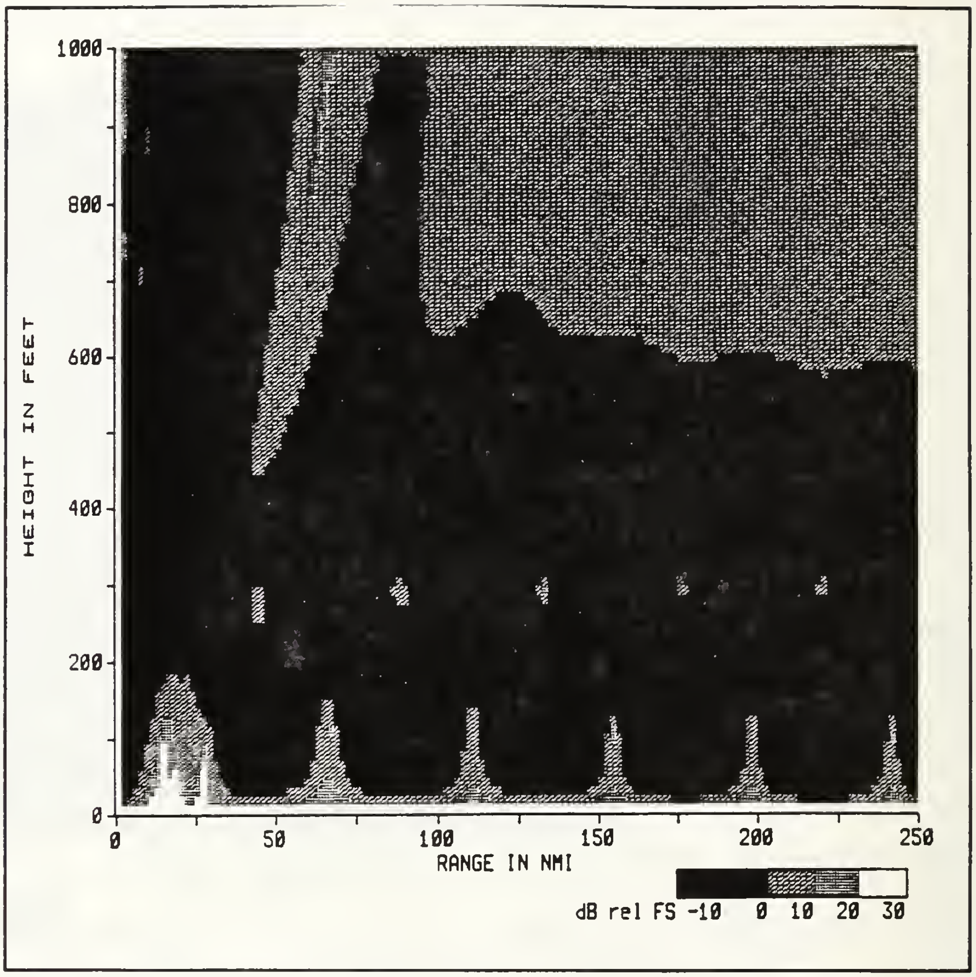

Figure 56 EMPE Signal Strength Prediction For The Caribbean (System ESM-b, 600 MHZ At 50 Feet), dB is relative to FS.

(2) EMPE Loss Predictions. Figure 57 reveals various dropouts from 10 nmi out to approximately 225 nmi. A comparison to Figure 36 for the homogeneous environment reveals similar results with less dB losses shown in Figure 36 around 175 nmi and 225 nmi.

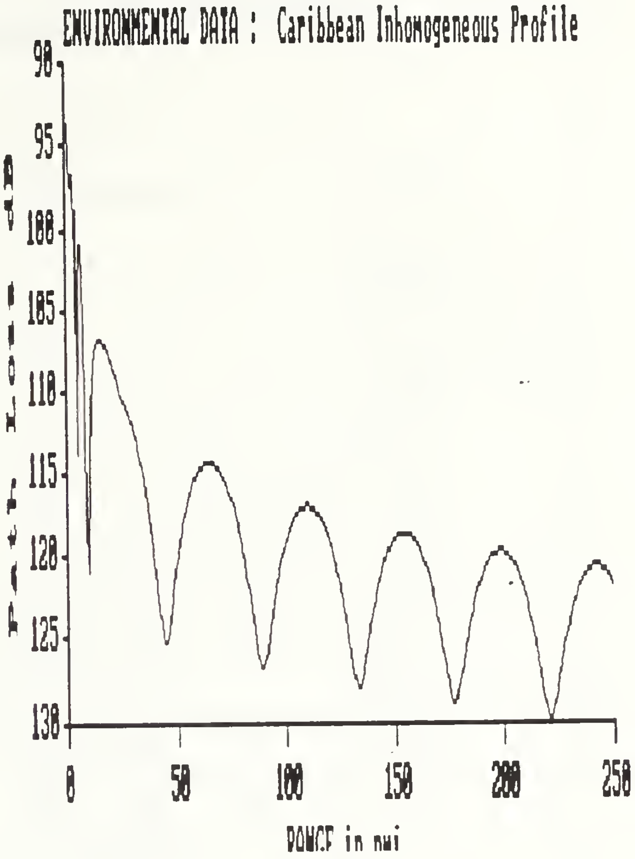

Figure 57 EMPE Transmission Loss Prediction For The Caribbean (System ESM-a operating).

Figure 58 reveals a small skip zone present around 10 nmi to 30 nmi, with little fluctuations present within the skip zone region. Numerous drop out areas were also shown to exist where signal loss was quite high. Figure 38, the homogeneous environment, reveals a similar situation, but less dB losses are present, as compared to Figure 58.

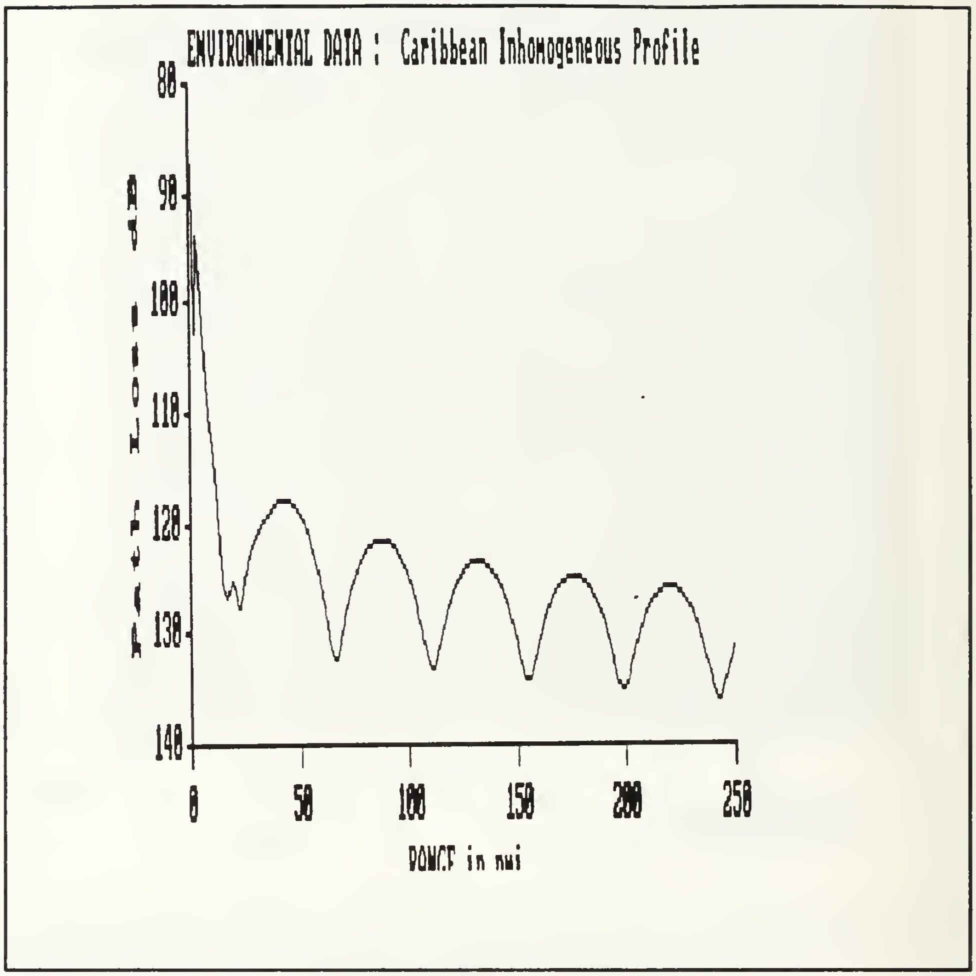

Figure 58 EMPE Transmission Loss Prediction For The Caribbean (System ESM-b operating).

C. SUMMARY

Because the U. S. Navy often operates in regions where horizontal homogeneity is not a valid assumption, it is important to make the existence of horizontally inhomogeneous conditions known. This must be taken into account for planning purposes, or prediction errors can occur if horizontal homogeneity is assumed while operating near a coastal region, or in a horizontally inhomogeneous type environment.

A coastal transition introduces an inhomogeneous atmosphere. These inhomogeneous profiles do not reveal any significant variations when compared to homogeneous profiles. As shown in the displays, some of the inhomogeneous cases had more loss of signal strength than the homogeneous, but with less skip zones present in some situations.

The objective of this chapter was to examine the similarities and differences that exist between horizontally homogeneous and inhomogeneous environments.

The first profile entered into EMPE is located at the source; follow-on profiles entered are located at different ranges from the source, as determined by the user/operator. A linear interpolation is then performed between the different profiles for each case.

VII. SUMMARY

This thesis examined the impact of anomalous propagation effects that exist, and their impact on operational EM systems.

The two systems examined were chosen to demonstrate how anomalous propagation in the atmosphere can affect an active radar fire control/guidance system with a frequency of 13 GHZ and a passive ESM CM system that acquires and DFs signals operating at 600 MHZ. Three operating regions of the world were chosen to illustrate how prevalent ducting conditions are and the type of environments in which they can exist.

It has been stressed throughout this study how important it is to know and understand how influential anomalous propagation can be on the performance of operational systems. For the horizontally homogeneous conditions, comparisons were made with a standard atmosphere to demonstrate the significant changes that occur. No typical "rules of thumb" were found. It appears that EM propagation models, i.e., EMPE and EREPS, are required to optimize system performance in the presence of such environments. A comparison was also conducted between horizontally homogeneous and inhomogeneous cases, to emphasize the importance of similarities and differences between the two, and to also illustrate how a horizontally homogeneous assumption could lead to planning errors if a horizontally inhomogeneous condition exists. Again, a reliance on EM propagation prediction systems is needed if the tactical commander is to optimize the performance of his operational EM systems.

Many of these refractivity conditions can be detected by the use of AMRs, LIDARs, or radiosondes. Propagation algorithms such as EMPE and EREPS can also be employed to accurately assess the environmental situation. With the use of these current systems, an up-to-date profile can be computed, and tactical advantages over potential threats can be experienced.

To conclude, it has been demonstrated that any type of EM propagation through the atmosphere becomes affected. Depending upon the atmospheric properties, EM energy can be reflected, refracted, scattered, or absorbed. The frequency of the signal, geometry, and the electrical properties of the atmosphere determine these propagation effects.

APPENDIX A

EM WAVE PROPAGATION IN A WAVEGUIDE TYPE MEDIUM

Surface based ducts and evaporation ducts can be compared to a leaky waveguide, with no side boundaries but consisting of an upper and lower boundary. An effect similar to a waveguide is produced by the combination of the atmosphere's refractivity and the sea surface reflection called ducting. The atmosphere, consisting of electrical properties that affect EM waves, can be described as a dielectric medium due to its make up of gases, of which 99% is nitrogen and oxygen; but water vapor being a critical trace gas. The parameters that have an affect on refractivity comprise of atmospheric pressure, air temperature, and humidity; the latter being the most influential. The top of the boundary is the duct height, defined as the height where the modified refractivity gradient changes sign; the lower boundary being that of the conductive rough sea surface. Propagation within a surface or evaporation duct is similar to propagation within a waveguide. Modes of propagation are called leaky when high leakage of energy occurs, and are called trapped modes when low leakage occurs. A EM wave will become trapped within these boundaries and will continue propagating down this path. Travelling like this, the EM wave will cover a greater distance than the standard atmosphere diffraction propagation limit. If no losses in signal strength are experienced at the boundary, and no molecular absorption is present in the duct, then the wave will theoretically travel indefinitely, or until the duct reaches land and breaks down. This is due to the changes in the parameters affecting refractivity. (Hoipkemeier, 1980, p. 61)

As waves propagate between two boundaries, certain angles of incidence at the earth give way to constructive or destructive interference. The angles of constructive interference are not a problem in the guide. Non-perfectly reflecting boundaries and discontinuities between heights of the duct and the resonant frequencies that are trapped give way to energy leaking through the duct and becoming lost, because energy cannot be completely trapped in the duct. (Hoipkemeier, 1980, p. 64)

Because of a surface duct's and evaporation duct's similar characteristics of a waveguide, a transmitter or receiver placed in these ducts will experience significant signal enhancement, and long detection ranges. Omni-directional sources will experience cylindrical spreading losses, and narrow radar beams will view the duct as basically a waveguide.

A. INDEX OF REFRACTION PROPERTIES

The index of refraction, n, is represented as the ratio of the speed of propagation of a EM wave in free space to the speed of propagation of a EM wave through a particular medium, such as air. The equation form of this ratio is given as:

$$n=\frac{c}{v} \tag{8}$$

where

n = index of refraction,

c = speed of EM wave in free space, and

v = speed of EM wave in a medium.

For air, n typically varies between 1.000250 and 1.000400; since EM waves travel at a slower speed in air than in a vacuum, the ratio will always be larger than 1, except on a free electron region.

For calculating the velocity of the EM wave travelling through free space, the following equation is used:

$$c=\frac{1}{\sqrt{\mu_o \epsilon_o}} \tag{9}$$

where

μ_o = free space permeability (12.566 x 10^7 h/m), and

ϵ_o = free space permittivity (8.854 x 10^{-12} f/m).

The propagating EM wave travels through a varying atmosphere, and along with this is also experiencing an associated change in its permeability and permittivity. A change in the propagating wave's velocity in the atmosphere then arises.

A critical angle (θ_c) is encountered when the angle of incidence for which the EM wave will not transmit, but will be reflected along the two regions' boundary, or will reflect back into the region from which it was transmitted. It is the angle that causes the angle of refraction, θ_2, to equal 90 degrees, or the ray to travel horizontal relative to the layer. According to Snell's Law, $n_1 \text{ Sin } \theta_c = n_2 \text{ Sin } 90$; $\text{Sin } 90 = 1$, so this can be reduced to: $n_1 \text{ Sin } \theta_c = n_2$ or, $\text{Sin } \theta_c = n_2/n_1$. Thus solving, $\theta_c = \text{Arcsin } (n_2/n_1)$.

Since the refractive index in the atmosphere varies from roughly 1.0003 to 1.0005, a minimum critical angle of incidence of nearly 89 degrees results. Therefore, a maximum critical angle of acceptance (θ_a) of 1 degree is needed. The EM wave must than be transmitted within 1 degree of a boundary with a lower refractive index in order for it to be refracted back into the same layer. (Stevens, 1983, p. 19)

The index of refraction usually decreases with altitude. Rays, therefore, are normally bent towards the earth's surface, due to higher n values there. With n changing rapidly with height, rays continuously bend toward and reflect off the sea surface.

In order for energy to propagate within the duct, the angle that the radar ray makes with the duct is required to be small. Rays from a radar that are nearly parallel to the duct will get trapped. Placement of a transmitter at the top of the guide will give way to leakage out of the top of the duct, because less main beam energy will be able to make the critical angle required for reflection.

APPENDIX B

Modified Refractivity

As stated earlier, modified refractivity, M, is useful in identifying conditions appropriate for trapping. M is defined as, $M = N + 157\ z$, where z = height in kilometers and N = refractivity at that height.

To quickly review, the index of refraction, $n = 1.000250$ to 1.000400 near the surface of the sea, so using the equation $r/a = 1 + h/a$, or $r/a = a/a + h/a$, where a = radius of the earth, we obtain the following:

$$\frac{h}{a} = \frac{h}{6370\times10^{3}} = 0.157h\times10^{-6}\ (h{=}meters) \quad \textbf{(10)}$$

Next refractivity, N, is included and the equation $n = 1 + N \times 10^{-6}$, where N = 250 to 400 on the surface; so, $r/a\ n = (1 + N \times 10^{-6})\ (1 + h/a)$, which approximately results in, $1 + (N + 0.157\ h) \times 10^{-6}$ and when substitutions are made, the equation becomes

$$1 + M \times 10^{-6} = m \qquad \textbf{(11)}$$

where, m (modified index of refraction) = $n + h/a$, and M (modified refractivity) = $N + h/a \times 10^{-6}$. Therefore, from Snell's Law, $r/a\ n \sin\theta = \text{constant} = m \sin\theta$, where both θ_s are the same.

The plot of the height of a certain value of refractivity versus M reveals a positive slope for a EM wave curvature less than the earth's, a vertical slope where parallel propagation exists, and a negative slope when trapping occurs (refer to Figure 59).

On a plot of M, the place where the M gradient goes from negative to positive is where the top of the duct is located. Trapping does not occur above this point. The region which contains a negative M gradient is known as the trapping layer.

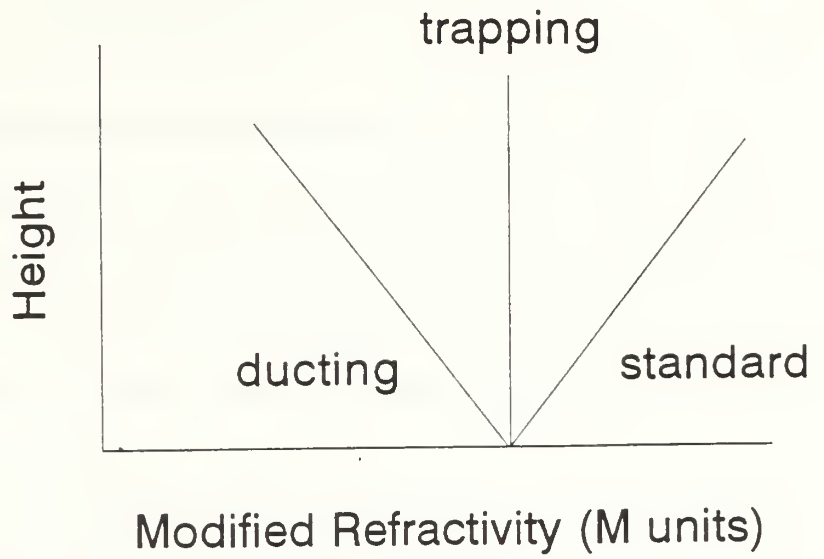

Figure 59 Atmospheric Refraction Based on M Scaling Representation (From Hoipkemeier, 1980, p. 23).

APPENDIX C

Atmospheric Measuring Devices

A. RADIOSONDE

A radiosonde is a balloon-borne device used for measuring, recording, and transmitting pressure, temperature, relative humidity, and wind speed and direction, as a function of altitude, in order to assess conditions appropriate for anomalous propagation. Radiosondes consist of transducers for pressure, humidity, and temperature measurements, a modulator responsible for converting the transducer's output to a quantitiy that controls a property of the radio frequency signal, a selector switch that determines the sequence the above parameters will be transmitted, and a transmitter. These balloons are launched from stations twice a day, across the world, as coordinated by the World Meteorological Organization (WMO). The N profile can then be calculated, and from this any problems for propagation can be identified.

Radiosondes cannot be used to obtain the height of the evaporation duct, because the heights of the gradients are too small for it to measure. Also, radiosondes are slow-response instruments, and are not always able to detect significant refractive index gradients with the accuracy needed for describing ray paths. Other limitations are that radiosondes are useful for indicating the atmospheric structure above the release point but not accurate enough for indicating conditions 1 km away; sensitivity of the humidity element is inadequate once saturated because of the long recovery time; the humidity and temperature sensors response times to temperature changes, thermal lag, hysteresis and contamination of the humidity sensor lead to inaccuracies; and the sonde can ascend through thin layers without detecting them due to the sampling rate, this can lead to an underestimation of a duct presence (which is most important in the first 200 m of an ascent).

B. LIDAR (Light Detection and Ranging)

An ever present need of radar, surveillance, and tracking systems is the ability to have updated information on the atmospheric condition and how it will impact propagation. Another means to accomplish this measurement is with the use of a ship-based LIDAR remote sensing system.

The refractive index is complex and depends a great deal upon the atmospheric temperature and water vapor partial pressure, which both vary in time and position (Thomas/Duncan, 1990). Radiosondes and aircraft-based sensors currently do not perform three-dimensional characterization effectively or with accuracy. A real-time three-dimensional ability to monitor could be done with a LIDAR system.

A basic system consists of a transmitting laser and a detector (receiver), which is similar to a radar. It operates much like a radar in that a short laser light pulse is transmitted through the atmosphere, the light becomes attenuated (forward and backward) when it encounters gas molecules, particles, and droplets, because of absorption by the gas molecules, and by light scattering due to aerosols, out of the forward-propagating direction. Some of the backscattered light is detected as a function of time, and gathered into a receiver using a telescope, then transferred to a photodetector, converted into an electrical signal, and recorded (Zysnarski, 1991). Using a range resolved fashion, information about the atmospheric extinction and backscattering properties are obtained from the magnitude of the received signal. Therefore, information on transmission properties of the atmosphere may be obtained as a function of the distance to the LIDAR. LIDAR systems that are well-calibrated may be a very reliable way to measure backscattering coefficients. With LIDAR's ability to remotely sense backscattering coefficients, it becomes very valuable in obtaining information on the vertical structure of the atmosphere and the mixed layer's dynamic behavior. LIDAR is therefore extremely sensitive to assumptions on the composition of the atmosphere.

Atmospheric LIDAR applications of laser-remote sensing techniques can substantially increase an understanding of the environment and have an impact on atmospheric investigations. A significant factor is atmospheric laser Doppler velocimetry, that includes measurements of wind shear, clear-air turbulence, aircraft wake vortices, tornadoes, storms, and wind patterns globally (Measures, 1984, p. 320).

A great benefit of LIDAR use is its diversity; it can provide local or global meteorological information on cloud structures and humidity and temperature profiles, as well as provide a means to probe the stratosphere and the mesosphere, and even the ocean floor. LIDAR is able to be mounted aboard ships, vans, helicopters, aircraft, and even space platforms.

C. AMR (Airborne Microwave Refractometer)

This system provides an accurate assessment of a refractivity versus altitude profile. It is the most accurate method to gather information on the atmospheric profile of the index of refraction. The AMR measures refractivity directly; as was stated earlier, knowledge of refractive conditions is important when performance of weapon and surveillance systems need to be determined. The AMR has the ability to detect the existence of ducting layers and collect refractive data.

It is currently used by the U. S. Navy onboard its E-2C aircraft and is scheduled for installation on the EA-6B aircraft. The AMR determines the refractive index of air as a function of altitude of the airplane.

Using a tuned cavity group that contains a sampling cavity whose resonant frequency is directly a function of the atmosphere's refractive index, the AMR samples the atmosphere. The cavity is contained in an aerodynamic faring with a temperature sensor and hardware required for passing the RF signal through the cavity to the detector hardware on top. (Khan, 1990, pp. 60-61)

A real time, as well as recorded, assessment of meteorological profiles at various altitudes along the flight path is provided by the AMR; this information can either be linked or transmitted to ships at sea if the radiosondes have not been launched. Super refractive and subrefractive layers that are believed to affect surveillance and communication systems are located and identified.

The atmosphere is sampled by the AMR to obtain refractivity information, and to also record it for post-flight processing. M is calculated as a function of altitude during processing, in order to determine the vertical extent of the duct. Raw real time recorded data is made up of static pressure, pitot pressure, temperature, and the refractive index. (Khan, 1990, p. 61)

Duct thickness that is greater than 500 feet, is considered strong; if it is between 200 feet to 500 feet, it is considered weak by the AMR. A duct thickness that is less than 200 feet is too weak to be declared. (Khan, 1990, p. 62)

As with radiosondes, AMRs are also unable to determine the height of the evaporation duct because of its small gradients.

LIST OF REFERENCES

Applied Technology Institute, Columbia, Maryland, Personal Computer Electromagnetic Parabolic Equation (PCEMPE) Revision 2.1 User's Manual, July 1991.

Bowen, E. G., A Textbook of Radar, Cambridge The University Press, 1954.

Cook, J. et al, Summary of Environmental Effects on Sensors and Communications Systems, Naval Environmental Prediction Research Facility Technical Report TR 87-02, August 1987.

Dockery, G. D., and Konstanzer, G. C., Recent Advances in Prediction of Tropospheric Propagation Using the Parabolic Equation, Johns Hopkins APL Technical Digest, Volume 8, Number 4, 1987.

Geernaert, G. L., Remote Sensing of Evaporation Ducts for Naval Warfare, Naval Research Laboratory NRL Report 9228, 14 November 1989.

Hitney, H. V. et al, Engineer's Refractive Effects Prediction System (EREPS) Revision 1.00, Naval Ocean Systems Center, San Diego, California, July 1988.

Hitney, H. V., Evaporation Duct Effects on Low-Altitude Target Detection, Naval Ocean Systems Center, 23 June 1987.

Hitney, H. V., Evaporation Duct Effects on Low-Altitude Propagation: Guidelines for the NATO AAW System Project, Naval Ocean Systems Center Technical Report 1304, June 1988.

Hoipkemeier, S. F., ESM Detection Above the Evaporation Duct, Master's Thesis, Naval Postgraduate School, Monterey, California, March 1980.

Khan, K., Refractive Conditions in Arabian Sea and their effects on ESM and Airborne Radar Operations, Master's Thesis, Naval Postgraduate School, Monterey, California, September 1990.

Ko, H. W. et al, An Analysis of EMPE Code Performance in a Selection of Laterally Inhomogeneous Atmospheric-Duct Environments, Johns Hopkins APL Technical Digest, Volume 9, Number 2, 1988.

Marom, M., Effects of Irregular Sea Surface and Evaporation Duct on Radar Detection Performance, Master's Thesis, Naval Postgraduate School, Monterey, California, June 1988.

Measures, R. M., Laser Remote Sensing, Krieger Publishing Company, 1984.

Sakkas, C. I., Information Analysis of Anomalous Propagation Phenomena and their effects on EW Systems, Master's Thesis, Naval Postgraduate School, Monterey, California, June 1984.

Sari, J. W. et al, Anomalous Microwave Propagation Through Atmospheric Ducts, Analysis and Technology Microwave Propagation, 1986.

Schemm C. E. et al, A Predictive System for Estimating the Effects of Range-and Time-Dependent Anomalous Refraction on Electromagnetic Wave Propagation, Johns Hopkins APL Technical Digest, Volume 8, Number 4, 1987.

Schleher, D. C., Introduction to Electronic Warfare, Artech House Inc., 1986.

Skura, J. P., Worldwide Anomalous Refraction and its Effects on Electromagnetic Wave Propagation, Johns Hopkins APL Technical Digest, Volume 8, Number 4, 1987.

Smith, W. L. et al, GAPEX: A Ground-Based Atmospheric Profiling Experiment, American Meteorological Society, Volume 71, Number 3, March 1990.

Stevens, W. R., Tactical Aid For Radio Wave Propagation Assessment in the Arabian Sea, Master's Thesis, Naval Postgraduate School, Monterey, California, September 1983.

Thomas, M. E. and Duncan, D. D., "Ship Based Remote Sensing of the Atmosphere in Support of AEGIS," paper presented to D. P. Serpico at Johns Hopkins APL, Laurel, Maryland, 12 October 1990.

Wiseman, C. H., Microwave Ducting's Relationship to Electronic Warfare, Analysis and Technology Microwave Propagation, 1986.

Zysnarski, A. H., "Remote Sensing of the Atmospheric State Using Differential Absorption Lidar (DIAL) Techniques," paper presented to D. D. Duncan at Johns Hopkins APL, Laurel, Maryland, 30 September 1991.

INITIAL DISTRIBUTION LIST

1. Defense Technical Information Center 2
   Cameron Station
   Alexandria, Virginia 22304-6145

2. Library, Code 52 2
   Naval Postgraduate School
   Monterey, California 93943-5002

3. Johns Hopkins University 3
   Applied Physics Laboratory
   Johns Hopkins Road
   Laurel, Maryland 20723-6099
   ATTN: Dr. Harvey Ko, Group ST2

4. Naval Research Laboratory 1
   Naval Postgraduate School Annex
   Monterey, California 93940-5006
   ATTN: M. Pastore, Code 400

5. Naval Research Laboratory 1
   Naval Postgraduate School Annex
   Monterey, California 93940-5006
   ATTN: J. Cook, Code 400

6. Naval Research Laboratory 1
   Naval Postgraduate School Annex
   Monterey, California 93940-5006
   ATTN: G. Love, Code 400

7. Library, Code FNOC 2
   Naval Postgraduate School Annex
   Monterey, California 93940-5006

8. Professor K. Davidson 1
   Meteorology Department, Code MR/DS
   Naval Postgraduate School
   Monterey, California 93943-5002

9. LT Gina Cairns-McFeeters 1
   c/o Commanding Officer
   Naval Security Group Activity
   Unit 6000
   FPO AA 34060-9998

Thesis
C1833
c.1

Cairns-McFeeters
Effects of surface-based
ducts on electromagnetic
systems.

DUDLEY KNOX LIBRARY
3 2768 00033073 2